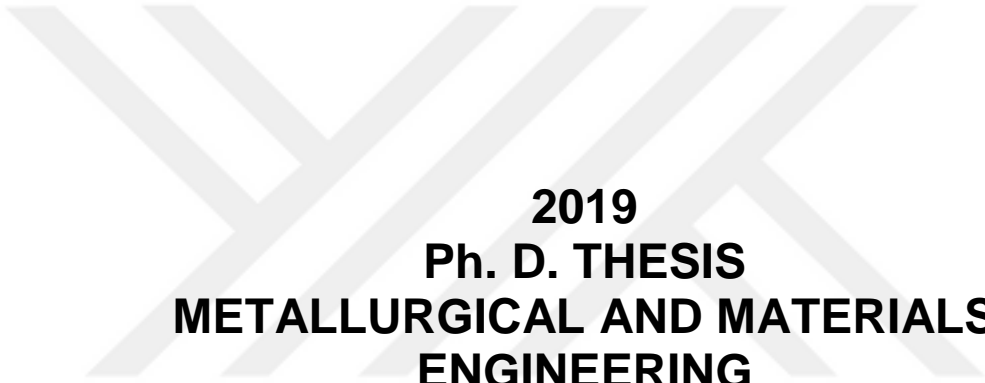


**A NOVEL SMART FATIGUE U-NOTCH SENSOR  
FOR STRUCTURAL HEALTH MONITORING OF  
DANGEROUS MODULES**



**2019  
Ph. D. THESIS  
METALLURGICAL AND MATERIALS  
ENGINEERING**

**TARIQ SALEM K. ALSHAHBOUNI**

**A NOVEL SMART FATIGUE U-NOTCH SENSOR FOR STRUCTURAL  
HEALTH MONITORING OF DANGEROUS MODULES**

**BY**

**A THESIS SUBMITTED TO  
THE GRADUATE SCHOOL OF NATURAL AND APPLIED SCIENCES OF  
KARABUK UNIVERSITY**

**TARIQ SALEM K. ALSHAHBOUNI**

**IN PARTIAL FULFILLMENT OF THE REQUIREMENTS FOR  
THE DEGREE OF DOCTOR OF PHILOSOPHY OF SCIENCE IN  
DEPARTMENT OF  
METALLURGICAL AND MATERIALS ENGINEERING**

**February 2019**

I certify that in my opinion the thesis submitted by Tariq Salem K. ALSHAHBOUNI titled "A NOVEL SMART FATIGUE U-NOTCH SENSOR FOR STRUCTURAL HEALTH MONITORING OF DANGEROUS MODULES" is fully adequate in scope and quality as a thesis for the degree of Doctor of Philosophy.

Prof. Dr. Ali GÜNGÖR

Thesis Advisor, Department of Metallurgical and Material Engineering

This thesis is accepted by the examining committee with a unanimous vote in the Department of Metallurgical and Material Engineering as a Doctor of Philosophy thesis. 11/02/2019

Examining Committee Members (Institutions)

Signature

Chairman : Prof. Dr. Hakan ATEŞ (GU))

Member : Prof. Dr. Ali GÜNGÖR (KBU)

Member : Prof. Dr. Hasan GÖKKAYA (KBU)

Member : Prof. Dr. Hayrettin AHLATÇI (KBU)

Member : Assist. Prof. Dr. Javad RAHEBI (THKU)

..... / ..... / 2019

The degree of Doctor of Philosophy by the thesis submitted is approved by the Administrative Board of the Graduate School Natural and Applied Sciences, Karabük University.

Prof. Dr. Filiz ERSÖZ

Head of Graduate School Natural and Applied Sciences



*“All information in this thesis is obtained and presented in accordance with academic rules and ethical principles; I also declare that I have made all the references that do not originate from this study as required by these rules and principles.”*

Tariq Salem K.ALSHAHBOUNI

## **ABSTRACT**

**Ph. D. Thesis**

### **A NOVEL SMART FATIGUE U-NOTCH SENSOR FOR STRUCTURAL HEALTH MONITORING OF DANGEROUS MODULES**

**Tariq Salem K. ALSHAHBOUNI**

**Karabük University**

**Graduate School of Natural and Applied Sciences**

**The Department of Metallurgical and Material Engineering**

**Thesis Advisor:**

**Prof. Dr. Ali GÜNGÖR**

**February 2019, 123 pages**

Fatigue is the most widely recognized failure in all structural components which are subjected to cycling loads. In recent years, impressive efforts have been made for the development of analytical and additionally numerical models for the better estimation of fatigue life for critical components of structures. The application of fatigue sensors for Structural Health Monitoring (SHM) aims the evaluation of weakness and damage keeping in view the structural life of a component.

The main goal of this study is to design and analyze a U-notched fatigue sensor to predict the fatigue life, to provide an indication for maintenance and to have sufficient time for the replacement of parts before any catastrophic failure could occur.

In this study, ANSYS Workbench software was used to design, implementation and analysis of the fatigue sensor. The sensor model consists of four beams with U-notch

geometry that has been designed parallel to the applied tension load on the structure. The magnitudes of the width, length and thickness of the sensor are  $305 \times 76.2 \times 1.6$  mm, respectively. In addition, aluminum alloys (7075-T6, 2024-T4 and 6061-T6) were used as sensor materials.

In order to ensure that the stress concentration is independent of element size, a mesh sensitivity study was performed. The mesh sensitivity study was carried for five element sizes (11717, 21095, 39367, 55222, 121561). The equivalent stresses were considered for the mesh sensitivity. In addition, the mesh sensitivity analysis was carried out for the critical location ( $r = 6.4$  mm) of the high stress regions obtained during the first iterative analysis of the sensor model.

The results showed the maximum equivalent stress (90.815 MPa) at a U-notch radius of 6.4 mm and the minimum equivalent stress (68.715 MPa) at a U-notch radius of 25.4 mm. It has been shown that the beam with a U-notch radius of 25.4 mm had a better fatigue life than the beam with U-notch radius of 6.4 mm. This implies that fatigue life of the sensor increases with increasing U-notch radius. Based on the results it can be said that the maximum equivalent stress decreases with increasing notch radius and that this provides us information that fatigue life depends on U notch radius of the sensor, applied forces and specifically tension at the end of the sensor. Finally, analyses showed that 7075-T6 alloy has better fatigue life than 2024-T4 and 6061-T6 alloys.

**Keywords** : Fatigue sensor, damage monitoring, U-notch sensor.

**Science Code** : 915.1.092

## **ÖZET**

**Doktora Tezi**

### **TEHLİKELİ MODÜLLERİN HASAR TESPİTİNİN İZLENMESİ İÇİN U- ÇENTİKLİ YENİ BİR AKILLI SENSÖR**

**Tariq Salem K. ALSHAHBOUNI**

**Karabük Üniversitesi**

**Fen Bilimleri Enstitüsü**

**Metalurji ve Malzeme Mühendisliği Anabilim Dalı**

**Tez Danışmanı:**

**Prof. Dr. Ali GÜNGÖR**

**Şubat 2019, 123 sayfa**

Yorulma çevrimsel yüklere maruz kalan tüm yapısal bileşenlerde en yaygın olarak görülen hasar türüdür. Son yıllarda, yapıların kritik bileşenleri için yorulma ömrünün daha iyi tahmin edilmesi için analitik ve ek olarak sayısal modellerin geliştirilmesi için etkileyici çabalar sarf edilmiştir. Yapısal hasar izleme için yorulma sensörlerinin uygulanması, bir bileşenin yapısal ömrünü dikkate alarak zayıflık ve hasarın değerlendirilmesini amaçlamaktadır.

Bu çalışmanın temel amacı, yorulma ömrünü tahmin etmek için çentikli bir yorulma sensörü tasarlamak ve analiz etmek, bakım için bir gösterge sağlamak ve herhangi bir büyük hasar oluşmadan önce parçaların değiştirilmesi için yeterli zamana sahip olmaktır.

Bu çalışmada, yorulma sensörünün tasarımı, uygulaması ve analizi için ANSYS Workbench yazılımı kullanılmıştır. Sensör modeli, yapı üzerine uygulanan gerilim

yüküne paralel olarak tasarlanmış U çentik geometrisine sahip dört kirişten oluşur. Sensörün genişliğinin, uzunluğunun ve kalınlığının büyüklüğü sırasıyla,  $305 \times 76.2 \times 1.6$  mm'dir. Ayrıca, sensör malzemesi olarak alüminyum alaşımları (7075 T6, 2024-T4 ve 6061-T6) kullanılmıştır.

Gerilme konsantrasyonunun, eleman boyutundan bağımsız olmasını sağlamak için bir meş hassasiyeti çalışması yapılmıştır. Mesh hassasiyet çalışması beş eleman boyutu için yapılmıştır (11717, 21095, 39367, 55222, 121561). Meş hassasiyeti için eşdeğer gerilmeler dikkate alınmıştır. Ayrıca, sensör modelinin ilk tekrarlamalı analizi sırasında elde edilen yüksek stres bölgelerinin kritik yerleri ( $r = 6,4$  mm) için mesh duyarlılık analizi yapılmıştır.

Sonuçlar 6,4 mm'lik yarıçapa sahip bir U çentikte maksimum eşdeğer gerilmenin (90,815 MPa) ve 25,4 mm'lik yarıçapa sahip bir U çentikte minimum eşdeğer gerilmenin (68,715 MPa) oluştuğunu göstermiştir. Bu, sensörün yorulma ömrünün artan U-çentik yarıçapı ile arttığını gösterir. Sonuçlara dayanarak, maksimum eşdeğer gerilmenin artan çentik yarıçapı ile azaldığı ve bunun bize yorulma ömrünün sensörün U çentik yarıçapına, uygulanan kuvvetlere ve özellikle sensörün ucundaki gerginliğe bağlı olduğu bilgisini sağladığı söylenebilir. Son olarak, analizler 7075-T6 alaşımının 2024-T4 ve 6061-T6 alaşımlarından daha iyi yorulma ömrüne sahip olduğunu göstermiştir.

**Anahtar Sözcükler:** Yorulma sensörü, hasar izleme, U-çentik sensörü.

**Bilim Kodu** : 915.1.092



## ACKNOWLEDGMENTS

First of all, I would like to express deepest gratitude to my supervisor Prof. Dr. Ali GÜNGÖR for his grateful motivation, guidance, support, continuous advice and constructive suggestions toward the completion of this thesis.

I would like to acknowledge my committee for their contributions in time and advice to improve this work.

To my father, I appreciate him for all those days, when he tried to instill the basics of mathematics when I was kid. (True justice took place twenty-five years later, when I try to tell the basics of Damage Tolerance to him during his retirement).

To my mother, I appreciate her for encouraging me to bring passion and love to whatever endeavor I undertake. She has been there since the beginning, supporting me throughout my degree programs, and even stayed with me to ensure the completion of this thesis – I am lucky to have such a wonderful family.

I would like to thank my family and my wife for their support, encouragement and patience throughout my studies.

If I overlooked anyone, please accept my apologies, since there are so many nice and kind people, who provided me with moral support throughout this endeavor.

## CONTENTS

	<b><u>Page</u></b>
APPROVAL .....	ii
ABSTRACT.....	iv
ÖZET .....	vi
ACKNOWLEDGMENTS .....	viii
CONTENTS.....	ix
LIST OF FIGURES .....	xiii
LIST OF TABLES .....	xvii
SYMBOLS AND ABBREVIATIONS INDEX .....	xviii
PART 1 .....	1
INTRODUCTION .....	1
1.1. BACKGROUND.....	1
1.2. OBJECTIVE.....	4
1.3. MOTIVATION .....	5
1.4. MAIN CONTRIBUTIONS .....	5
PART 2 .....	6
LITERATURE REVIEW .....	6
PART 3 .....	21
THEORETICAL BACKGROUND.....	21
3.1. INTRODUCTION.....	21
3.2. HISTORY OF FATIGUE .....	22
3.3. FATIGUE PHENOMENON.....	23
3.4. FATIGUE LOADS .....	24
3.5. CLASSIFICATION OF FRACTURE PROCESSES .....	27
3.6. MECHANISM OF FATIGUE FAILURE .....	28
3.6.1. Crack Initiation Stage .....	29

	<u>Page</u>
3.6.2. Crack Propagation Stage .....	30
3.6.3. Rapid Fracture .....	30
3.7. CRACK PROPAGATION MODES .....	31
3.8. LOW- AND HIGH-CYCLE FATIGUE .....	31
3.9. FACTORS THAT AFFECT FATIGUE .....	32
3.9.1. Stress State.....	32
3.9.2. Geometry .....	33
3.9.3. Quality of a Surface .....	33
3.9.4. Material Type .....	33
3.9.5. Residual Stress.....	33
3.9.6. Size and Distribution of Internal Defects .....	34
3.9.7. Loading Direction.....	34
3.9.8. Grain Size .....	34
3.9.9. Environmental Conditions.....	34
3.10. NOTCHES AND THEIR EFFECTS .....	34
3.11. FACTORS AFFECTING ON FATIGUE DAMAGE .....	36
3.12. FATIGUE FAILURE MODELS .....	37
3.12.1. The Stress-Life Approach.....	38
3.12.2. The Strain-Life Approach.....	38
3.12.3. Linear Elastic Fracture-Mechanics (LEFM) Approach.....	38
3.13. FATIGUE PROPERTIES OF MATERIALS .....	38
3.14. FATIGUE LIFE PREDICTION.....	39
3.14.1. Constant Amplitude Load.....	40
3.14.2. Variable Amplitude and Complex Loads .....	40
3.15. FAILURE CRITERIA METHODS .....	41
3.15.1. Soderberg Failure Theory .....	41
3.15.2. Goodman Theory .....	41
3.15.3. Gerber Failure Theory .....	42
3.16. NOTCHES .....	43
3.17. STRESS CONCENTRATION.....	44
3.17.1. Definition of the Stress Concentration Factor .....	46
3.17.2. Effect of the Notch Geometry on the Stress Concentration Factor .....	47

	<u>Page</u>
3.18. METHODS TO REDUCE STRESS CONCENTRATION .....	49
3.19. NOTCH SENSITIVITY .....	50
3.20. OPPOSITE SINGLE U-SHAPED NOTCHES IN A FINITE-WIDTH .....	51
3.21. SENSORS .....	53
3.21.1. Definition of Sensor.....	53
3.21.2. Criteria to Choose a Sensor .....	53
3.21.3. Main Reason of Using Sensor .....	54
3.21.4. Classification of Sensors According to Energy Sources .....	54
3.21.5. Classification of Sensors According to Measured Variables .....	56
3.21.6. Fatigue Sensors.....	58
 PART 4 .....	 62
METHODOLOGY .....	62
4.1. MATERIAL .....	62
4.2. PROCEDURE FOR FATIGUE LIFE DETECTION .....	63
4.3. SENSOR DESIGN.....	70
4.3.1 Define Material Properties .....	71
4.3.2. Geometry Creation .....	72
4.3.3. Meshing of the Fatigue Sensor Model.....	77
4.3.4. Applied Loads and Boundary Conditions .....	80
4.3.5. Solving of the Fatigue Sensor Model .....	83
 PART 5 .....	 85
FINDING AND DISCUSSION .....	85
5.1 FINITE ELEMENT SOLUATION.....	85
5.2. DEFORMATION RESULTS .....	90
5.2.1. Total Deformation Result .....	90
5.2.2. Directional Deformation Results .....	92
5.3. EQUIVALENT ELASTIC STRAIN RESULTS .....	92
5.4. STRESS DISTRIBUTION RESULTS .....	93
5.4.1. Normal Stress .....	93
5.4.2. Equivalent Stress (Von- Mises).....	95

	<u>Page</u>
5.5. FATIGUE RESULTS .....	100
5.5.1 Fatigue Life .....	101
5.5.2. Fatigue Damage.....	104
5.5.3. Safety Factor.....	106
5.6. COMPARISON BETWEEN THE FATIGUE LIFE OF AL 7075 – T6, AL 2024 – T4 AND AL 6061 – T6 SENSOR.....	107
 PART 6 .....	 110
CONCLUSIONS AND RECOMMENDATIONS .....	110
6.1. CONCLUSIONS.....	110
6.2. SCOPE FOR FUTURE WORK.....	112
 REFERANCES .....	 113
APPENDIX A.DETAILED DRAWINGS OF THE FATIGUE U-NOTCH SENSOR .....	119
APPENDIX B. DEFORMATION RESULTS.....	120
RESUME .....	123

## LIST OF FIGURES

	<u>Page</u>
Figure 2.1. Sensing options for structural health monitoring .....	7
Figure 2.2. Schematic views of the electrochemical fatigue sensor . .....	8
Figure 2.3. Magnetic permeability images generated with an MWM-Array for (left) .....	8
Figure 2.4. PZTs layer designed for experiment .....	9
Figure 2.5. Diagnostics cycle of an intelligent structural health management system .....	10
Figure 2.6. Fatigue cracks forming from internal porosity in web-flange Connection.....	12
Figure 2.7. S-N curves for U-shape and V-shape notched specimens made of HS steel.....	13
Figure 2.8. Fatigue sensor type 2A geometry .....	15
Figure 2.9. Cracking in a bridge girder starting from weld defects at a weld intersection.....	16
Figure 2.10. Fatigue cracking in the riveted connection of cross-bracing elements..	16
Figure 2.11. Battery powered version of the fatigue sensor .....	17
Figure 2.12. A segment of random loading C .....	18
Figure 2.13. Definition of the used parameters .....	19
Figure 2.14. Schematic views of the ultrasonic sensor system showing selected .....	20
Figure 3.1. Schematic of fatigue fracture surface .....	22
Figure 3.2. Fully reversed stress .....	24
Figure 3.3. Repeated Stress .....	25
Figure 3.4. Fluctuating stress . .....	25
Figure 3.5. A plot of the S-N curve .....	26
Figure 3.6. Classification of fracture processes .....	28
Figure 3. 7. A schematic of the fatigue process in a specimen under cyclic loading	29
Figure 3.8. The three crack propagation modes .....	31
Figure 3.9. Low- and high-cycle fatigue .....	32
Figure 3.10. Elastic stress concentration factor to express hole in metal sheet .....	36
Figure 3.11. S-N curve of a ferrous and non-ferrous metal .....	39

Figure 3.12. Failure criteria methods .....	43
Figure 3.13. Elementary stress cases for specimens having constant cross sections. ....	44
Figure 3.14. Tension bar having notches .....	45
Figure 3.15. Strip having central hole to represent notched part .....	46
Figure 3.16. Geometrically similar specimens having similar $K_t$ but different stress.....	49
Figure 3.17. The stress concentration factor for a specimen with a central hole and .....	49
Figure 3.18. Notch sensitivity curves .....	51
Figure 3.19. Stress concentration factors $K_{tg}$ and $K_{tn}$ for tension strip having opposite.....	52
Figure 3.20. Stress concentration factor $K_{tn}$ showing flat tension bar having opposite.....	52
Figure 3.21. The side view and plan view of the remote and powerless miniature fatigue .....	60
Figure 4.1. ANSYS steps for fatigue. ....	69
Figure 4.2. Fatigue tool information using ANSYS. ....	70
Figure 4.3. Steps for aluminum alloy 7075-T6 mechanical properties in ANSYS.. ....	71
Figure 4.4. Dimensions of the sensor model.....	72
Figure 4.5. Fatigue life percentage of the sensor model. ....	73
Figure 4.6. Static structural analysis procedure. ....	74
Figure 4.7. Setting the units in ANSYS design modeler.....	74
Figure 4.8. The sketch of body sensor .....	75
Figure 4.9. Extruding the body sensor. ....	75
Figure 4.10. Sketch of U-notch beams.....	76
Figure 4.11. Extruding the U-notch beams. ....	76
Figure 4.12. Fatigue sensor geometry in ANSYS software.....	77
Figure 4.13. Automatic mesh method.....	78
Figure 4.14. Fine mesh of the sensor model. ....	79
Figure 4.15. Mesh refinement steps.....	80
Figure 4.16. Refinement of the mesh in a sensor model.....	80
Figure 4.17. Fixed boundary condition in a fatigue sensor model.....	81
Figure 4.18. Displacement boundary conditions of the fatigue sensor model.....	82
Figure 4.19. Applied load of the fatigue sensor model.....	82
Figure 4.20. Solution steps analyzing the fatigue sensor model.....	84
Figure 5.1. Meshing model implemented in ANSYS.....	86

	<u>Page</u>
Figure 5.2. A fine mesh is used around the U-notch of the model. ....	87
Figure 5.3. Simulation results of the Fatigue Sensor Model.....	87
Figure 5.4. Variation of equivalent stresses as a function of the number of elements .....	89
Figure 5.5. The total deformation behavior of the fatigue sensor model. ....	90
Figure 5.6. Total deformation of the fatigue sensor model at r = 6.4 mm. ....	91
Figure 5.7. Total deformation of the fatigue sensor model at r = 25.4 mm. ....	91
Figure 5.8. Directional deformation along the y-axis of the fatigue sensor model..	92
Figure 5.9. Equivalent elastic strain of the fatigue sensor model in ANSYS. ....	93
Figure 5.10. Normal stress ( $\sigma_y$ ) distribution in y-direction. ....	94
Figure 5.11. Maximum normal stress in the y direction ( $\sigma_y$ ) around the U-notch radius.....	94
Figure 5.12. Maximum normal stresses with different U-notch radii.....	95
Figure 5.13. Equivalent stresses (Von Mises) distribution around the U-notch. ....	96
Figure 5.14. Equivalent stress distribution at r = 6.4 mm.....	96
Figure 5.15. Equivalent stress distribution at r = 12.7 mm.....	97
Figure 5.16. Equivalent stress distribution at r = 19 mm.....	97
Figure 5.17. Equivalent stress distribution at r = 25.4 mm.....	97
Figure 5.18. Equivalent stress distribution around the notches. ....	98
Figure 5.19. Maximum equivalent stress with different U-notch radii.....	99
Figure 5.20. Equivalent stress distributions vs. U-notch radius sensor. ....	100
Figure 5.21. Fatigue life of the fatigue-notch sensor model. ....	101
Figure 5.22. Fatigue life vs. radius for U-notch fatigue sensor model. ....	102
Figure 5.23. Fatigue life of fatigue sensor for different U-notch radii. ....	102
Figure 5.24. Alternating stress vs. number of cycles (S-N curve).....	104
Figure 5.25. Alternating stress vs. number of cycles. ....	105
Figure 5.26. Fatigue damage for different U-notch radii.....	105
Figure 5.27. Safety factor for different U-notch radii with loading (4000 N).....	106
Figure 5.28. Safety factor for different U-notch radii with loading (3500 N).....	107
Figure 5.29. Comparison between the fatigue life of aluminum alloy 7075-T6, alu- minum alloy 2024 T4 and aluminum alloy 6160-T6.....	108
Figure 5.30. Fatigue life vs. U-notch radius of aluminum alloy 7075-T6, aluminum alloy 2024-T4 and aluminum alloy 6061-T6.....	109



Figure A.1. Detail drawing of U-notched sensor structure. .... 119



## LIST OF TABLES

	<u>Page</u>
Table 3.1. The summary of recently developed fatigue sensors .....	61
Table 4.1. Chemical composition of Aluminum alloy 7075-T6 .....	62
Table 4.2. Common properties of Aluminum alloy 7075-T6 .....	63
Table 4.3. Dimensions of the sensor model.....	72
Table 4.4. Magnitudes of tension loads. ....	83
Table 5.1. The mesh sensitivity analysis.....	88
Table 5.2. Magnitudes of the fatigue notch factor ( $K_f$ ).....	89
Table 5.3. Maximum normal stress with respect to U-notch radius. ....	95
Table 5.4. Maximum equivalent stress with respect to U-notch radii .....	98
Table 5.5. Maximum equivalent stress with respect to the path of the beam sensor. ....	99
Table 5.6. Comparison between the theoretical and numerical fatigue life of the sensor .....	103
Table 5.7. Fatigue life of AL-7075-T6, AL-2024-4 and AL-6061-T6. ....	109
Table B.1. The total deformation of the U-notch sensor .....	120
Table B.2. The directional deformation y- Axis of the U-notch sensor.....	121

## SYMBOLS AND ABBREVIATIONS INDEX

$\sigma$	: The Stress
$\varepsilon$	: The Strain
E	: The Modules of Elasticity
$\Sigma_x$	: The Stress in X-Direction
$\Sigma_y$	: The Stress in Y-Direction
$\Sigma_z$	: The Stress in Z-Direction
$\sigma_{\max}$	: The Maximum Tensile Stress
$\sigma_{\min}$	: The Minimum Compressive Stress
$\Delta\sigma$	: The Stress Range
$\sigma_a$ or $S_a$	: The Alternating Component
$\sigma_m$ or $S_m$	: The Mean Stress
$S_e$	: The Endurance Limit
$S_u$	: The Tensile Strength
$S_{ut}$	: The Ultimate Tensile Strength
S	: The Gross Stress
R	: The Stress Ratio
A	: The Amplitude Ratio.
b	: The Fatigue Strength Exponent
a	: The coefficients represent Stress-Life curve intercept
$\sigma_f$	: The Fatigue Strength Coefficient
$N_f$	: Number of Cycles or Fatigue Life
$K_t$	: The Stress Concentration
w	: The Width
t	: The Thickness
D	: Hole Diameter
R	: Notch Radius
L	: The Specimen Length
Ka	: Surface Condition

K <sub>b</sub>	: Crack Size
K <sub>c</sub>	: Style of Magnitude of Loading
k <sub>f</sub> :	: Miscellaneous
S <sub>y</sub>	: The Yield Strength
N	: The Factor of Safety,
K <sub>tg</sub>	: The Ratio between the Peak Stress and the Gross stress
q	: The Notch Sensitivity
K <sub>f</sub>	: Fatigue concentration factor
SHM	: Structural Health Monitoring
MEMS	: Micro Electro Mechanical Systems
FCG	: Fatigue Crack Growth
FEA	: Finite Element Analysis
NDT	: Non-Destructive Testing
CVM	: Comparative Vacuum Monitoring
FBG	: Fiber Bragg Grating
EFS	: Electrochemical Fatigue Sensor
VHCF	: Very High Cycle Fatigue
HS-Steel	: High Strength of Steel
LS-Steel	: Low Strength of Steel
PVDF	: Polyvinylidene Fluoride
PSB	: Persistent Slip Bands
LCF	: Low-Cycle Fatigue
HCF	: High-Cycle Fatigue
LEFM	: Linear Elastic Fracture-Mechanics
CDM	: Continuum Damage Mechanics
PVT	: Piezo Velocity Transducers

## **PART 1**

### **INTRODUCTION**

#### **1.1. BACKGROUND**

The American Society for Testing and Materials (ASTM) has defined fatigue as progressive localized procedures, which occur because of fluctuating stresses and strains. The fatigue process occurs after some time in a component or structure. Fatigue failure occurs often suddenly without any indication that the component is going to fail. The mechanisms that cause fatigue failure may start when the part is put into service [1].

However, fatigue is the most widely recognized reason behind structural failure. It is not a new process and it has perplexed specialists for two centuries. The fatigue issue relates to the utilization of metallic substances in different structures. In fact, some mechanical components and systems experience static loads; for the most part however, they experience dynamic loads that create stress which may be repetitive, fluctuating or alternating.

A material might fracture if it experiences various stresses above the material strength with some breaking down despite experiencing stresses below yield strength levels. It is a simple fact that these products and materials should have boundaries between satisfactory static stresses and static forces. This notwithstanding, repeating stresses lower than the yield/fracture-causing stress results in progressive failure because it limits the resistance that leads to failure as fatigue failure.

Generally, fatigue stands out as one of the most frequent issues in engineering design, reaching out from the disappointment of rotating shafts or responding parts to even ship and aircraft failures, and occasionally, failures of structures such as buildings and bridges [2].

To understand fatigue, the process should involve several technicalities that affect fatigue cracking and fatigue life, including residual stresses, material surface quality or impact of the environment. Fatigue failure is a common occurrence pertaining to metallic structures. For an entire century, attempts were made to fix such failures. The first examinations on fatigue were completed when August Wohler finished dynamic design explorations on fatigue. He believed that single load applications were lower relative to structural static strength, so they could not cause any damage; however, when a pressure is repeatedly applied, it results in complete failure. Earlier, it was believed that fatigue was a mystery as research had not been conducted on fatigue damage. Failure would occur without any warning being given.

Now, we have learned about repeated load applications that trigger fatigue in materials and lead to micro-crack nucleation, growth, and finally structural failure. The recent history of engineering has witnessed endless mechanical failure, weld structure failure and other failures. Some failures have resulted in major catastrophes and tragic accidents, such as bridge or ship failure. In general, people remain unaware of this issue as fatigue failures are not reported by newspapers or TV channels despite their economic and social significance [3].

In the last twenty years, networks have changed the manner in which people and organizations exchange information and coordinate their activities. In the next several years, we will witness another revolution as new technology increasingly observes and controls the physical world. The latest technological advances have enabled the development of distributed processing using very small, low cost and low power processors that are able to process information and transmit it wirelessly. The availability of micro sensors and wireless communications help in the development of sensor networks for many applications rather than the limited applications of sensor networks today.

Structural sensors monitor the health of structures and observe their performance. Moreover, they conduct health prognoses of significant modern engineering components. Because of a number of extraordinary developments and inventions in sensing, communications and signal-processing technologies, experts can easily

assess the structural health of structures and predict any loss and reduce damage. Therefore, SHM (structural health monitoring) can help designers, builders and building owners to make rational decisions.

It is easy to improve structural safety through the prediction of failures and optimum utilization of repair resources. The information so obtained will undoubtedly lead to improved designs. In the aerospace industry, the benefits of SHM can appear as high up-time usage rates for aerospace systems and improved designs. Traditional SHM combines visual observations and heuristic assumptions with mathematical models of predicted behavior. More modern versions include sensors and automated reasoning techniques [2].

The outputs have an electrical amount, and measurable physical amounts, properties, or conditions. Since 1975, ANSI standards have shown that a transducer was required for a sensor. Still, logical writing has not by and large received the ANSI definitions, and therefore at present, sensor is the most generally utilized term. The electrical interfacing requirements add to the scope of a sensor because now it includes signal conditioning as well as system interfacing properties, which are essential for sensing systems. Another type of sensor has vitality transduction in the form of an optical frame. Moreover, sensors mostly have micro electro mechanical functions.

During the previous 25 years, there have been smaller scale electro mechanical systems called as MEMS which have been turned from research projects into profitable business ventures. In the meantime, a proportion of economically fruitful MEMS created during research experiments have been very limited. This low rate of return is subject to MEMS improvement, which is still in its exploratory stages; however, it deserves further investigations. The scope of MEMS devices is easily conceivable and bodes well for further research in terms of further working guidelines for comparison and contrast. This exercise is embraced in order to recognize where openings are misused and to improve our understanding of what the working standards of devices are and how appropriate it is for specific applications. To date, most MEMS either exist in the category of actuators or sensors, so they

work as an interface between the real world and a design system. For instance, displacement sensors used in electromechanical systems turn mechanical signals to electrical signals, so an analog signal shifts to a controller and amplifies, conditions, and converts in a digital format. Later, it is further changed into an analog signal. Finally, the discussed electrical signal converts in a mechanical signal with the help of force/displacement actuators. Developing MEMS processes has helped to integrate actuators by enabling signal processing through only a single chip [3]; this integration positively affects cost, reliability and performance. Moreover, the integration of actuators with chips results in better distributed controlling systems [4].

The sensor is defined in specific terms, which does not throw light on physical elements and which are used in constituting a sensor. This helps the sensing and the measuring of physical factors such as pH, temperature, speed, rate of rotation, flow and pressures. Now, sensors no longer show readings through analog scales because now they generate digital voltages or signals that contain measurements. These signals can be further received and processed using computer programs, saved and plotted for presentation. Sensors are available in many forms and types and now, they can measure any physical quantity. Some sensors give voltages as an output, which has certain implications [5].

## **1.2. OBJECTIVE**

The currently discussed invention is a fatigue sensor that has several parallel beams that sense fatigue cycles and levels. The overall function is integrated within a sensor. It is attached to certain structures likely to experience cyclical bending, such as aircraft wings or bridge beams. Normally, beams are geometrically engineered and placed in such a manner that their fatigue can be assessed with the help of a sensor. The current thesis will discuss how fatigue cycle prediction is performed for U-notched beams, and it will also highlight sensor design, ANSYS simulations and U-shaped notches and apply many parameters to estimate fatigue life using a simulation method to predict the fatigue life of sensors thereby allowing the



replacement of parts before any failure can start to occur. The main objectives are as follows:

1. Describe U-notch fatigue sensors.
2. Identify which parameters should be included in fatigue sensor systems.
3. Propose suitable fatigue sensor dimensions to measure fatigue life.
4. Use the different mechanical properties of aluminum alloys and compare them.
5. Evaluate the stress and fatigue life of U-notch fatigue sensors and measurement techniques.

### **1.3. MOTIVATION**

The main motivation is that there is plenty of research into solving the problems of fatigue failure damage of critical structures such as aircraft and bridges. To reduce these failures, it is appropriate to use good techniques of failure prediction before any damage starts. This fatigue sensor technique is used for the prediction and estimation of the fatigue life of a sensor, which is why it is necessary to develop new ideas for protection and safety precautions in all critical components of a structure.

### **1.4. MAIN CONTRIBUTIONS**

This thesis makes contributions to U-notch fatigue sensor design to help address the practical problems discussed above in Section 1.2 in the context of U-notch fatigue sensor applications. The points given below show how this thesis contributes to the overall research on sensors:

1. An analysis of reverse edge U-notch sensors for structural health monitoring of serious modules.
2. An evaluation study on the fatigue life of U-notch aluminum fatigue sensors.

## **PART 2**

### **LITERATURE REVIEW**

Fatigue is not a recent process, and researchers are trying to figure out its solution for the past two centuries. Fatigue affects almost all the metallic structures. Recently, many efforts have been done to improve the numerical as well as analytical models to predict/estimate crack growth and fatigue. The researchers have been conducting researches on the mechanical design process, which have an objective to establish more reliable structures having better crack-growth resistance. Majority of designs, which are made nowadays, help assessing fatigue crack growth (FCG), which allows a designer to make predictions about load cycles, on which, a structure is prone to fail [6].

Boller and Meyendorf analyzed many state-of-the-art sensors and their roles in monitoring structural health in an article "State of the art in structural health monitoring for aeronautics" during International NDT (non-destructive testing) Symposium in Germany. That article has listed many sensors utilized to predict/measure aircraft health and listed sensors including electrical crack wires, electrical strain gauges, laser micrometer, acoustic emission, acoustic-ultrasonic, comparative vacuum monitoring (CVM), electromagnetic foils, fiber bragg grating (FBG), and micro-electromechanical systems (MEMS). They are capable to sense cracks in a structure as show in Figure 2.1 [7].

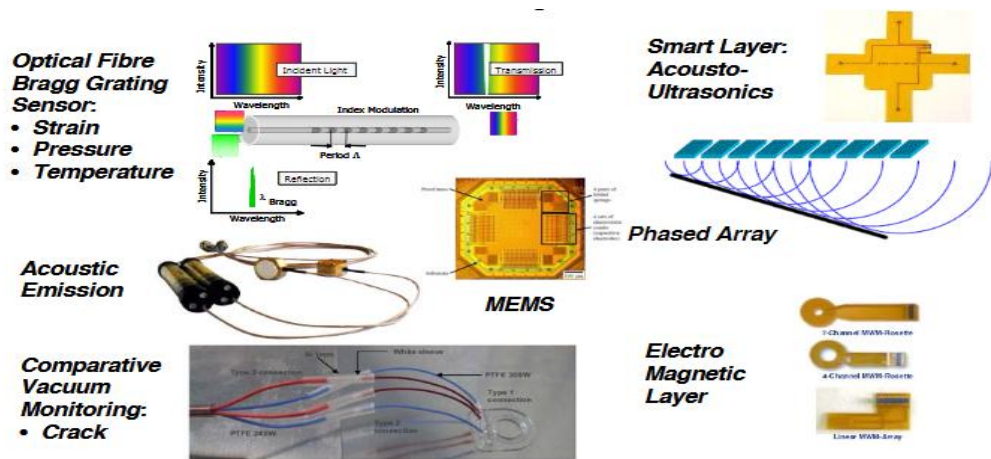


Figure 2.1. Sensing options for structural health monitoring [8].

They also find out place of a crack using EFS (electrochemical fatigue sensor) devices, which were originally meant to facilitate the U.S. Air Force for manufacturing aerospace applications. These sensors detect mainly cracks in airframes and engines. Right now, there are numerous financially accessible fatigue sensors in the market. Audits were conducted on electrochemical fatigue sensors to establish their effectiveness [9].

For many years, many researchers and organizations have filed applications for patents of those sensors, which monitor well-being of a structure. Fay et al. got patent rights of Fracture detecting structural health sensor that joins and a conductor sensing circle associated with an essential component, and it is still needs to be tested [10].

Papazian et al. published an article: "Sensors for monitoring early-stage fatigue cracking" that highlights eddy current usage, ultrasonic sensing and electro-chemical fatigue sensor (EFS). The disappointment of the primary half crushes a thin conductor-sensing circle, which uncovers the essential half frustration. It is completely different from others because it is projected to acknowledge the break once the split happens. The break on the structural surface annihilates a delicate circle, and it helps a sensor detect a crack as show in Figure 2.2 [11].

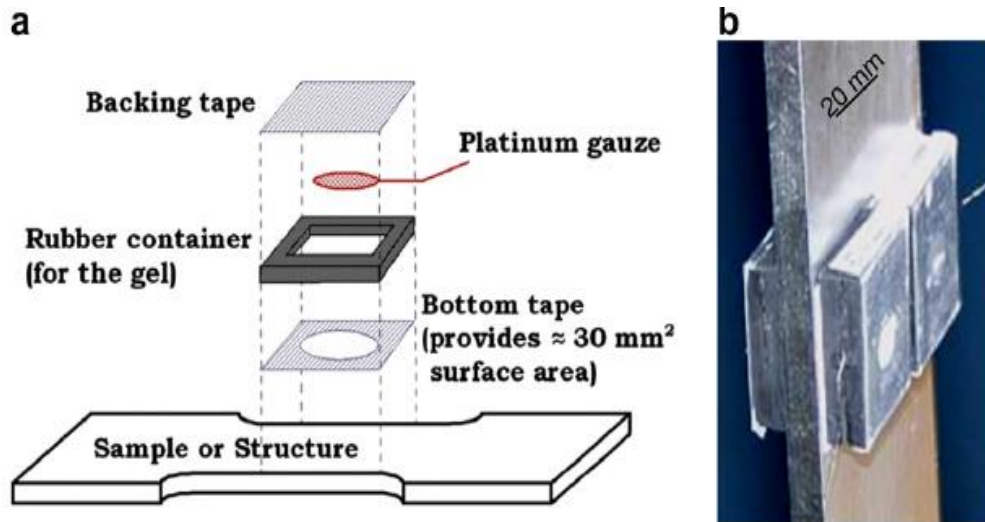


Figure 2.2. Schematic views of the electrochemical fatigue sensor [11].

Gold Fine et al. conducted another study that utilizes arrangement in an Eddy Current Sensor for distinguishing the crack presence as well as measure what lies under the sensor as illustrate in Figure 2.3 [12].

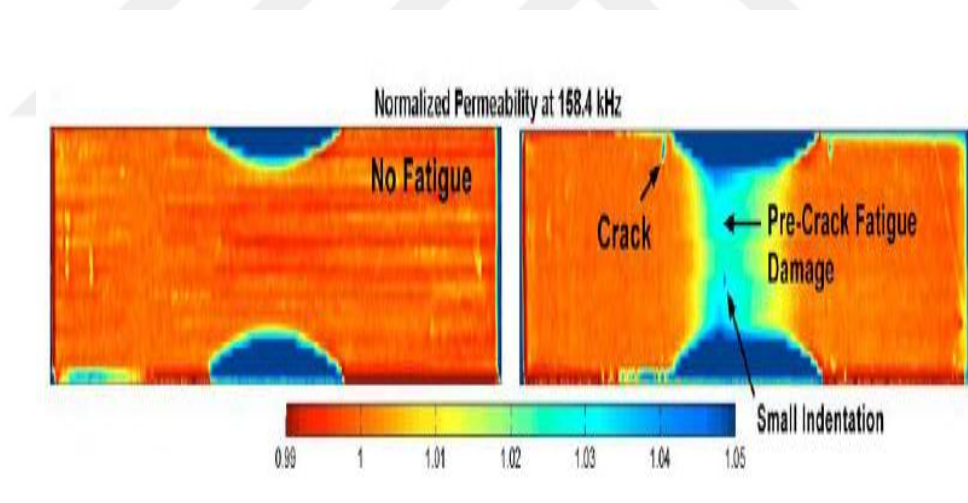


Figure 2.3. Magnetic permeability images generated with an MWM-Array for (left) a control specimen that has not been subject to fatigue testing and (right) a specimen tested to 88% of fatigue life [12].

Like the prior patent, this outline is likewise designed for distinguishing breaks after the split. When a crack becomes longer, swirl current sensors assess that circumstance and report the information. Using a sensor without physical wires is a subject of interest because its related strategies are exceptionally notable. Lei et al. have clar-

ified how to develop a wireless sensor network that works as proof in Figure 2.4 [13].

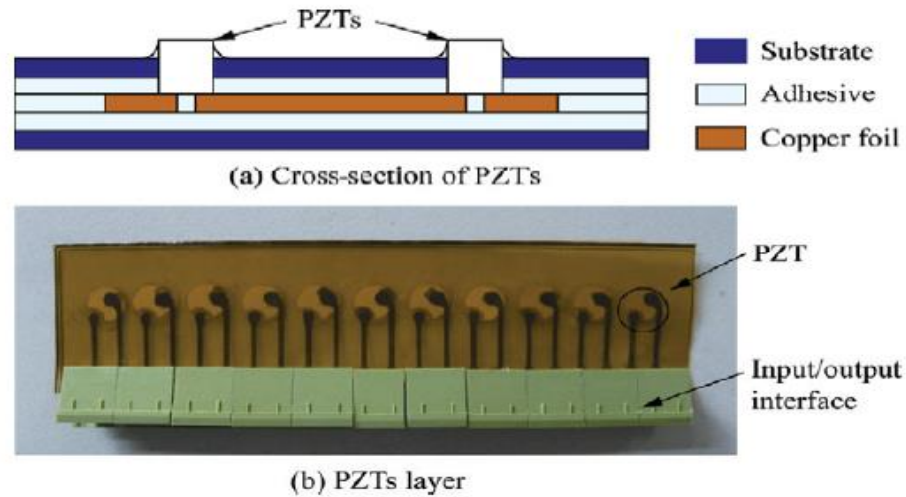


Figure 2.4. PZTs layer designed for experiment [13].

Structural health monitoring (SHM) needs reliability as well as simplicity for finding out weariness of essential components. J. D. Achenbach outlined these desires in his survey article on SHM in the following words:

A comprehensive SHM mechanism must have the following components:

1. Consists of smaller scale sensors.
2. On request or ceaseless condition, observing progressively is ought to be conceivable.
3. Wireless operations.
4. Immediately understandable sensing information.
5. Satisfactory material damage detection on primary top-stretch areas.
6. Reporting property damage mentioning its size.
7. Crack growth forecasts.
8. Adapting crack growth expectations.
9. Showing percentage/probability of harm.

Fusion of these characteristics in an SHM system is unlikely, and these components are for an ideal structural health monitoring system as show in Figure 2.5 [14].

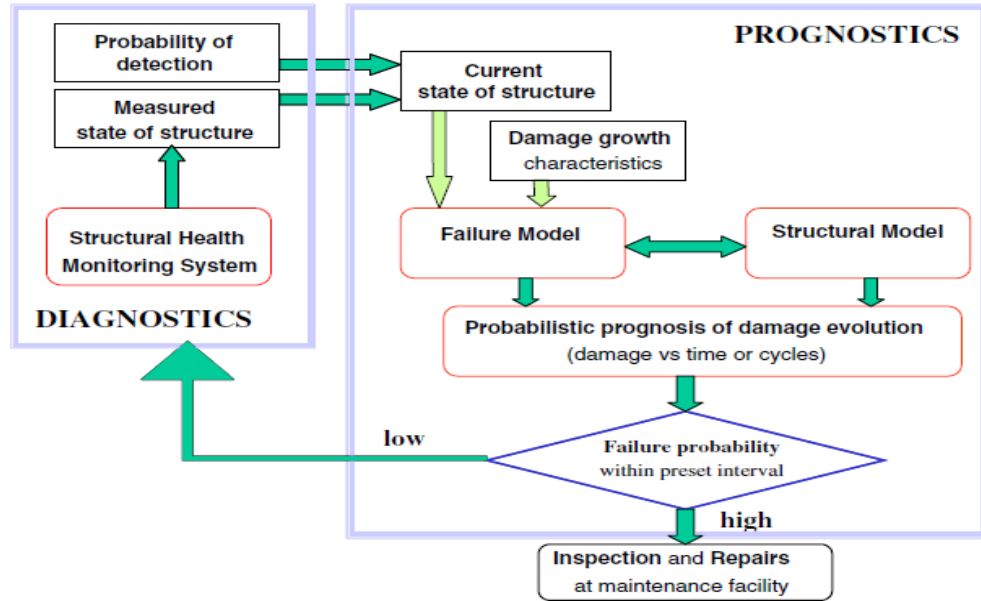


Figure 2.5. Diagnostics cycle of an intelligent structural health management system [14].

B. Pyttel, D. Schwedt and Berger, provided an overview discussing the current researches on failures and fatigue mechanisms having greater cycles ( $N_f > 10^7$ ). They have listed testing facilities in their study. Materials are classified with the help of traditional S–N curves, which has impact over other processes including residual stress, notches, and environment. Many failures are possible to occur due to very high cycle fatigue (VHCF) which is a cause of sub-surface failures. The homogeneity of microstructures as well as statistics play a significant role. Double S–N curves help describing fatigue and different other failures. Some studied materials using different metals such as steels having different strengths including tempered and quenched steel and face-centered substances such as aluminum and copper alloys. They have also given recommendations regarding the components' fatigue design [15].

Lee et al, studied 14-soldered joint fatigue models, which emphasize summarizing every fatigue model, and they are divided into five categories including plastic strain-

based, stress based, energy-based, creep-strain-based and damage-based. Out of them, every model is applicable to electronic packaging. Some categories have common dimensions and problems including coverage and solder-joint geometry. In addition, they discussed a couple of situations pertaining to fatigue model applications. According to the initial scenario, the data of current fatigue test is provided to an engineer for interpretations and finding a suitable fatigue model/s. In another case, devising a test scheme is essential for determining failure cycles [16].

G. Mesmacque et.al proposed their damage indicator model as a reaction to famous Miner's damage accumulation rule because the rule excludes loading history. When this approach was implemented to loading, damage indicator model gave higher results than Miner's for increasing loading and lower for reducing loading. For damage indicator model, damages are reported from a stress level to another, while the damage stress corresponds to residual life, and that leads to ultimate stress on last cycle prior to failure. This model only needs S-N curve. A stress field is equivalent to Von Mises stress or highest shear stress. Consequently, the presented model applies to multi-axial loading. For estimating importance of the said model to predict life of a structure, some results were obtained. The experimental literature shows that the mentioned model considers loading history, which precisely predicts fatigue life in separate loading conditions [17].

W.F. Wu et al. tested the application of different processes, which have been proposed so far to estimate fatigue damage and components' life in random loading conditions. Palmgren-Miner & Morrow's interaction rule considers the effect of stress sequence, which was verified during the strain-controlled low fatigue cycle tests of aluminum alloy 7075-T651. Results have shown that Morrow's plastic work interaction damage rule is far better as compared to commonly utilized Palmgren-Miner's linear damage principle. Morrow's rule estimated the damage, but it was a conservative method. Test results show that the specimens' fatigue life is assessed using Gaussian method [18].

Wohler one of the earliest researchers, was also an officer of German railway system in Frankfurt. He monitored railway service load on axles using zinc-plate strain gauges that he developed himself [19].

Okulove determined that a fatigue fuse having longitudinal load can be linked with a structure in vertical as compared to the connected load [20]. There was a need for accessibility arrangement and space on the structural surface. It allows visual study of a crack that was created on the corners of the notches [21].

A fatigue damage indicator is equipped with a slit, which was introduced by Smith. Normally, fatigue life can be estimated through physically monitoring the length of crack length on a sensor's notch tip. In another example, crack length had the same stacking. There is a need to regularly monitor the poorly performing components. The antecedently mentioned sensing devices are ordered for passive sensors, whereas other sensors are active having capability for piezoelectric development, engaging flux spillage, swirl current sensors, etc as illustrate in Figure 2.6 [22].

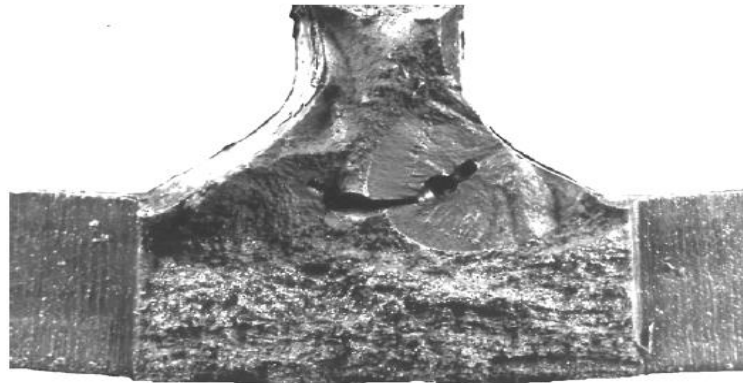


Figure 2.6. Fatigue cracks forming from internal porosity in web–flange connection [22].

Certain kinds of break recognition gages were likewise created before, nonetheless forced in an exceeding method, these crack gauges should set essential stress concentration zone wherever the cracks exist. They have many thin strands. The sensor monitors the place where a crack proliferates in the mentioned strands and cuts those [23].



Majzoobi, G., & Daemi, N. investigated the impact of notch geometry and sensitivity on fatigue life. They found that the notch sensitivity actually measures the extent to which a material is sensitive to geometric discontinuities or notches. Notch sensitivity accepts the impact of several parameters including notch geometries including U-shaped, V-shaped and II-shaped, which were observed during the study. A high-strength and low-strength steel alloys were used for investigation. It was found that the stress concentration can be achieved through numerical simulation as well as fatigue reduction factor in a bending/rotating fatigue device as show in Figure 2.7 [24].

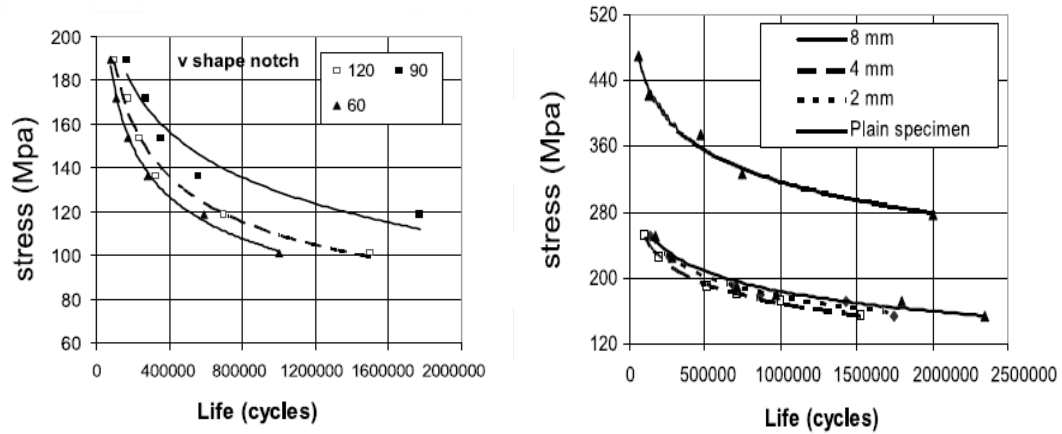


Figure 2.7. S-N curves for U-shape and V-shape notched specimens made of HS steel [24].

Gokanakonda's paper depicts the idea of devoted fatigue-monitoring sensor alongside vital plan subtle elements, reproduction information, and test outcomes that would give approval. Henceforth, the current research promotes a sensor design that can keep away previous mentioned impediments. It has particular benefits including appropriate separation far from the structure. This type of fatigue sensors is subject to an indistinguishable surrounding condition from those accomplished by the structure [25].

Tarik Ozkul, Halit Kaplan, and Melik Dolen developed a type of fatigue sensor, which has many parallel beams to detect diverse fatigue levels within a solitary sensor that is intended to attach with a structure that is likely to experience cyclical bending the way an aircraft wing or a bridge beam does [26].

Merit Enckell studied SHM as well as other sensing advancements through monitoring engineering structures including bridges. The SHM in the long haul with fiber optic sensor was analyzed along with the existing SHMSs with the end goal to create change [27].

Excellent technologies developed a device referred to as Good Layer that was made from piezoelectric sensors/actuators. They conjointly established an analytical system to sentinel multi-crack growth at riveted Lap joints. Vodicks, Lin & Chang mentioned the utilization of PVDF (polyvinylidene fluoride) electricity strain sensors in similar secured composite patches. Boeing, under USAF contract, has built up a damage securing unit called the injury dosimeter to recognize the frequency and temperature connected with the maximum strain movement to advance the damping proficiency [28].

However, the later researchers, for example, Banks et al. have demonstrated that modular techniques yield questionable harm evaluation for variable material parameters. They have proposed a non-modular NDE technique to distinguish the spatially subordinate element parameters of piezo-ceramic structures [29] Los Alamos National Laboratory published SHM literature review using vibration techniques [30].

Wijesinghe et al. published a paper on in-situ fatigue sensors for expressway scaffolds' health monitoring. The sensor was attached to the structural foundation as a part of strain-life fatigue analyses. Sensors have been developed using conductors and notched sensing arms, which help conveying anxiety focus components. The sensor works on the standard of the unsurprising dynamic disappointment of parallel arms as show in Figure 2.8 [31].

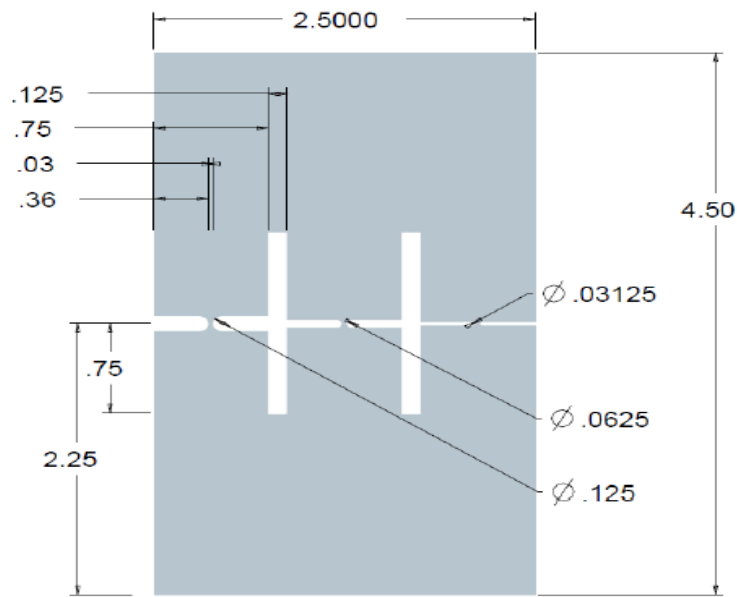


Figure 2.8. Fatigue sensor type 2A geometry [31].

Giurgiutiu et al presented a paper on active sensing use for monitoring health of old aerospace structures. A non-intrusive sensor was developed to monitor aging aerospace equipment and its structural damage [32].

Nevertheless, Aygöl, describes the influence of loading and geometrical conditions. In other words, the decks' segments that perform with each other should be accurately considered during stress estimation. The elasticity in complicated structures, for which, stress causing factors decisively impact fatigue are partially included, might result in inaccurate estimation of stress fatigue values. Applying latest life assessment procedures accurately estimates stress values, which fully include those factors, which affect stress on welded points as show in Figure 2.9 [33].



Figure 2.9. Cracking in a bridge girder starting from weld defects at a weld intersection point [33].

As far as steel bridges' fatigue performance is concerned, Haghani and Al-Emrani and Al-Emrani, which have examined. Their work showed that most fatigue damages occur on bridges on highways and railways. In the majority of issues, some unexpected, unforeseen or overlooked load interacts with load-carrying segments of a bridge, which has poor detail and finally, cracks emerge in it. A few cases were reported, which gave evidence of complicated stress within the structure as show in Figure 2.10 [34, 35].



Figure 2.10. Fatigue cracking in the riveted connection of cross-bracing elements.

A further research introduced the details of evaluating the hotspot stress, which emerges because of hotspot approach application in welded parts. It stresses that appropriate assessment procedure like FEA (finite element analysis) should be applied.

Regarding the fatigue analysis, Ramachandran et al. investigated more than 50 different cases with different behavior to reach the optimal solution for failure analysis of metal fatigue [36].

Another study was conducted by Park et al. which elaborated Lamb wave propagation measurements through PZT sensors. Furthermore, it helps quantifying influence of bonding problems in Lamb wave signal processing algorithms [37].

Lemley and Chien which offers a high sensing performance for determining the extent to fatigue damage stability caused to a structural material, based on the amount and the rate of crack propagation, developed another sensor [38].

Phares and Kaplan find out place of a crack using EFS (electrochemical fatigue sensor) devices, which were originally meant to facilitate the U.S. Air Force for manufacturing aerospace applications. These sensors detect mainly cracks in airframes and engines. Right now, there are numerous financially accessible fatigue sensors in the market. Audits were conducted on electrochemical fatigue sensors to establish their effectiveness as Figure 2.11 [9, 39].

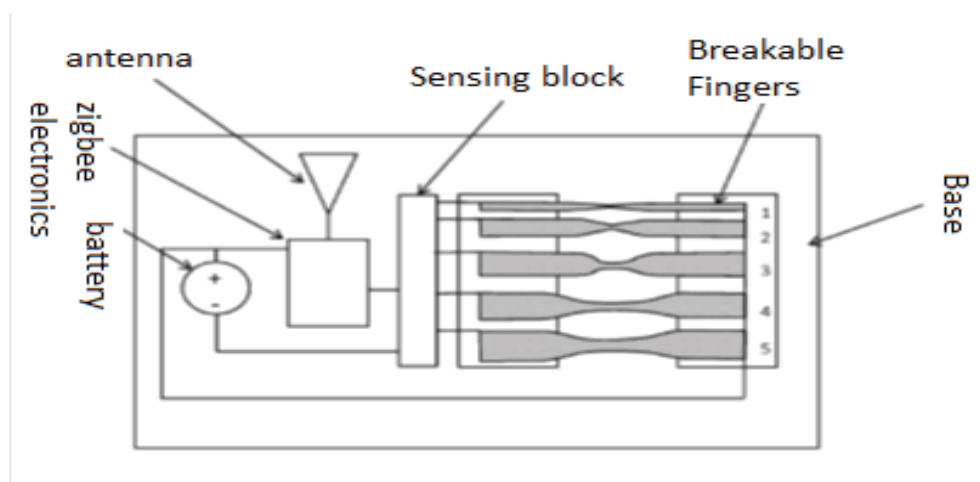


Figure 2.11. Battery powered version of the fatigue sensor [9, 39].

W.F. Wu et al. tested the application of different processes, which have been proposed so far to estimate fatigue damage and components' lives in random loading conditions. Palmgren-Miner & Morrow's interaction rule considers the effect of stress sequence, which was verified during the strain-controlled low fatigue cycle tests of aluminum alloy 7075-T651. Results have shown that Morrow's plastic work interaction damage rule is far better as compared to commonly utilized Palmgren-Miner's linear damage principle. Morrow's rule estimated the damage, but it was a conservative method. Test results show that the specimens' fatigue life is assessed using Gaussian method as show in Figure 2.12 [18].

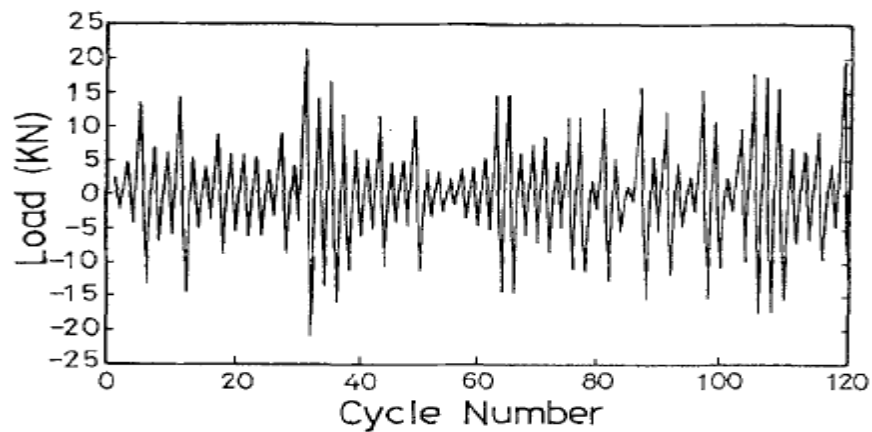


Figure 2.12. A segment of random loading C [18].

G.Mesmacque et.al proposed their damage indicator model as a reaction to famous Miner's damage accumulation rule because the rule excludes loading history. When this approach was implemented to loading, damage indicator model gave higher results than Miner is for increasing loading and lower for reducing loading. For damage indicator model, damages are reported from a stress level to another while, the damage stress corresponds to residual life, and that leads to ultimate stress on last cycle prior to failure. This model only needs S-N curve. A stress field is equivalent to Von Misses stress or highest shear stress. Consequently, the presented model applies to multi-axial loading. For estimating importance of the said model to predict life of a structure, some results were obtained. The experimental literature shows that the mentioned model considers loading history, which precisely predicts fatigue life in separate loading conditions as show in Figure 2.13. [17].

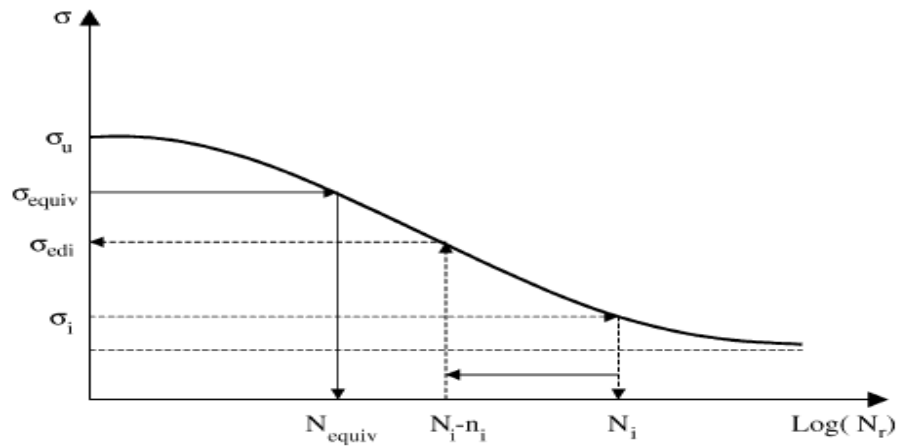


Figure 2.13. Definition of the used parameters [17].

B. Pyttel, D. Schwedt and Berger, provided an overview discussing the current researches on failures and fatigue mechanisms having greater cycles ( $N_f > 10^7$ ). They have listed testing facilities in their study. Materials are classified with the help of traditional S–N curves, which has impact over other processes including residual stress, notches, and environment. Many failures are possible to occur due to very high cycle fatigue (VHCF) which is a cause of sub-surface failures. The homogeneity of microstructures as well as statistics play a significant role. Double S–N curves help describing fatigue and different other failures. Some studied materials using different metals such as steels having different strengths including tempered and quenched steel and face-centered substances such as aluminum and copper alloys. They have also given recommendations regarding the components' fatigue design [15].

Papazian et al. published an article: "Sensors for monitoring early-stage fatigue cracking" that highlights eddy current usage, ultrasonic sensing and electro-chemical fatigue sensor (EFS). The disappointment of the primary half crushes a thin conductor-sensing circle, which uncovers the essential half frustration. It is completely different from others because it is projected to acknowledge the break once the split happens. The break on the structural surface annihilates a delicate circle, and it helps a sensor detect a crack as show Figure 2.14 [11].

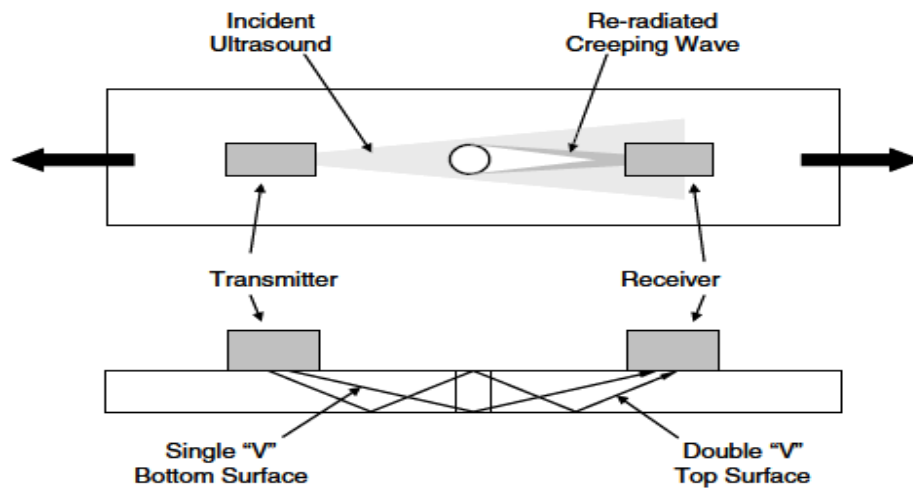


Figure 2.14. Schematic views of the ultrasonic sensor system showing selected signal paths [11].



## **PART 3**

### **THEORETICAL BACKGROUND**

#### **3.1. INTRODUCTION**

Fatigue is the most widely recognized reason for failure in metal structures. Fatigue is not a new phenomenon, it has confused researcher for more than 200 years. The issue with fatigue makes consideration with the use of metal in various structures. Commonly, fatigue failures occur in both metallic and non-metallic materials, and they are responsible for a large number fraction of identifiable service failures of metals. A typical fatigue-fracture surface looks like the one shown in Figure 3.1. In other words, the fatigue cracks nucleate on stress focal point. Normally, the surface of fatigue fractures exist perpendicular in comparison with the applied stress direction. Fatigue failures are recognizable on the surface of a fracture that may be smooth, which means crack will grow slowly. The face of a crack smoothens when the two surfaces keep on rubbing and brushing each other. If the crack surface is rough/irregular, a cracks grows fast and becomes critical because at that point, it is unable to bear the load and might result in a fracture [40].

Fatigue impact and cracks might be microscopic and need to observe using an electron microscope, so a wide striation takes place when different forms of stress are applied. On another level, maximum striations have been observed so far. The striation width equals a separation through which a crack enlarges in a cycle. A stress concentration point like a sharp corner or any other surface or shape that can initiate a fatigue crack [41].

There are three possibilities when a fatigue fracture occurs. They are given below:

High maximum tensile stresses.

1. Major fluctuation or variation in applied stress.
2. Large numbers of applied stress cycles. In fatigue studies, it was established that the stress cycles consist of many parameters like average and alternating stresses, and stress and amplitude ratios [41].

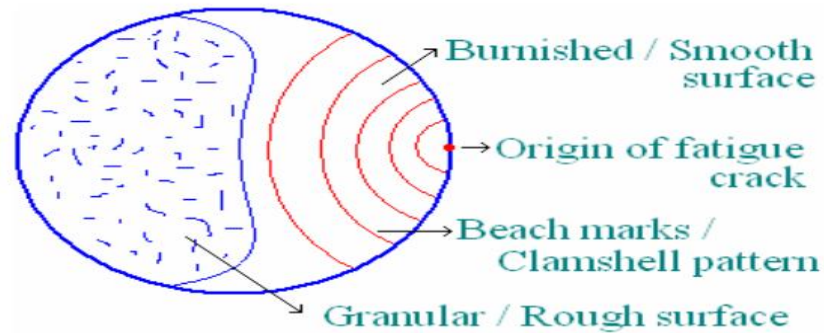


Figure 3.1. Schematic of fatigue fracture surface [40].

### 3.2. HISTORY OF FATIGUE

The word fatigue has been taken from Latin that means, To tire. Advanced engineering defines fatigue as a continuous material damage because of cyclical loading. Fatigue has many types, however, we focused on mechanical fatigue that induces damage through variations in the stress/strain levels in this study. Some other fatigue forms include creep fatigue because of cyclical loading on high-temperature thermal fatigue that takes place as a consequence of cyclical variations in temperature of a substance, thermo-mechanical fatigue, which is the consequence of mechanical as well as thermal fatigues; corrosion that takes place because of environmentally and chemically deteriorating circumstances; fretting fatigue that happens because of cyclical stress with oscillatory motion or friction among surfaces. This fatigue-devastation results in continuous deterioration and generally the last fatigue failure takes place when the stress levels are actually lower than the capacity of a substance. In the nineteenth century, it viewed as secretive because fatigue fractures didn't indicate noticeable plastic deformations, which led to wrong idea that fatigue is only an engineering issue [42].

In addition, mechanical failures take place because of fatigue, which has been the focus of engineering efforts for over one hundred and fifty years. Fatigue failures are still a primary concern in engineering. The economic prices of fracture and its bar square measure are quite important, which associate calculable prices wherever cyclic loading and fatigue square measure a minimum of a contributing factor [43].

The maintenance costs increase when a crack occurs, or investment is made on prediction of fatigue failures for heavy machinery, vehicles, trains, ships, construction machinery, oil extraction plants, bridges, and items of daily use. For example, a wind turbine generates power and it faces loads because of its rotational motion and wind turbulences that increases fatigue for its blade as well as rest of its components [44].

According to the initial investigations, Wohler (1819-1914) conducted experiments when he was serving the German Railways. He studied axles of trains and tried to figure out the reasons behind their breakage even when loads were less. He plotted his outcomes on a graph and concluded that the anxiety shifted to vertical pivot. That made it easy to identify the reason behind a fatigue failure and predict fatigue life. Created shapes should be according to the standard to anticipate a structure's fatigue life called as S-N graph or Wohler's design. Here S represents range of stress over the N cycle count [43].

### **3.3. FATIGUE PHENOMENON**

Fatigue takes place whenever a material exposes to stress cycles over a particular time. It is a function of time that begins with slip formation, which increases until reaching a critical situation/size, which might result in fracture and material failure. The slip enhances through the application of stress because of internal defects/ external holes of a plate. Since loads apply in cyclical forms, it opens the micro-cracks. When load cycles keep on increasing, crack length also increases after the load application. Fractures are a consequence of critical crack length [42]. Moreover, fatigue damages take place in components because of cyclical loads. Its consequence is total procedure with the accumulation of three important stages, which are initiation, propagation and component fracture. Amid cyclical loads, limited plastic de-

formation might take place on a top stress area. These types of plastic de-formations create damages in a component and create cracks. When the component has more load cycles, the crack-length increases. When some cycles are over, component failure finally takes place [40].

### 3.4. FATIGUE LOADS

The load, which varies, is a potential reason behind fatigue failure. These loads substantially change from function to function and situation to situation. Applied stresses can be torsional, axial or flexural. Normally, it is possible to have three different and continuously changing stress-time modes. The first can be schematically represented using sinusoidal/regular time-dependence as illustrated in Figure 3.2 and there is symmetrical amplitude having zero stress. For instance, the highest tensile stress  $\sigma_{max}$  and least compressive stress  $\sigma_{min}$  having similar magnitudes can be termed as fully reversed stress cases. Figure 3.3 Depicts repeated stress that has a waveform ranging from zero to the highest value while the mean equals and alternating component. Figure 3.4 illustrates the fluctuating stress case because all of its component values are non-zero [45].

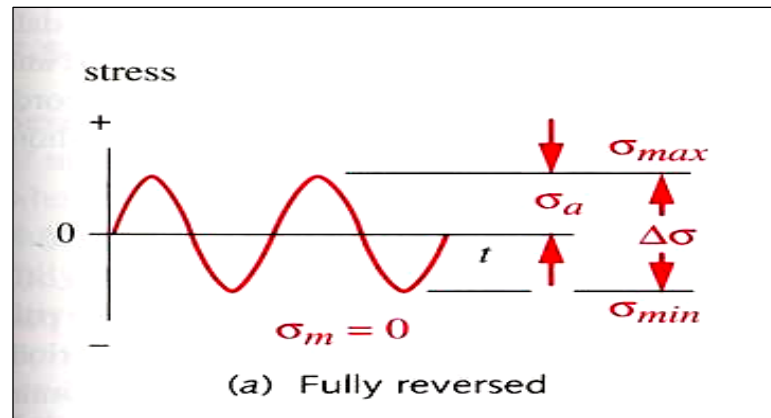


Figure 3.2. Fully reversed stress [45].

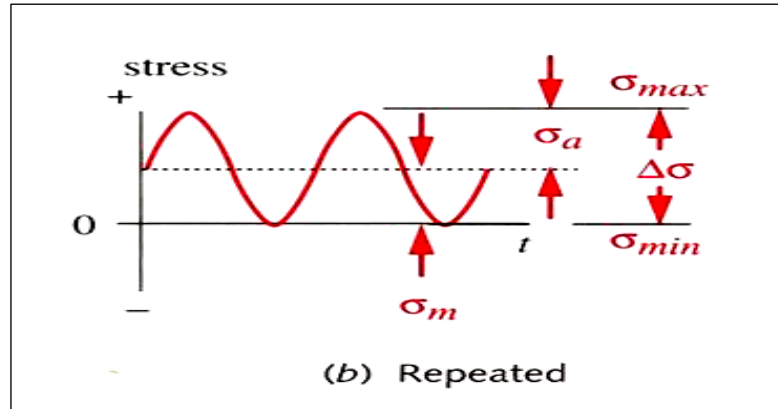


Figure 3.3. Repeated stress [45].

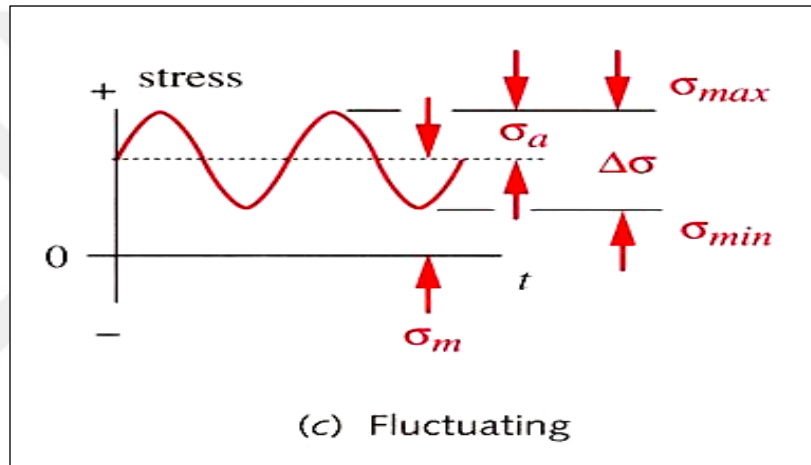


Figure 3.4. Fluctuating stress [45].

The waveforms given above are possibly characterized with two parameters, their alternating components and their mean, minimum and maximum values, and ratio between them.

$$\text{The stress range } \Delta\sigma \text{ is defined as } \Delta\sigma = \sigma_{max} - \sigma_{min} \quad (3.1a)$$

$$\text{The alternating component } \sigma_a \text{ is found form } \sigma_a = \frac{\sigma_{max} - \sigma_{min}}{2} \quad (3.1b)$$

$$\text{In addition, the mean component } \sigma_m \text{ is } \sigma_m = \frac{\sigma_{max} + \sigma_{min}}{2} \quad (3.1c)$$

$$\text{Two ratios can be found } R = \frac{\sigma_{min}}{\sigma_{max}} \quad A = \frac{\sigma_a}{\sigma_m} \quad (3.1d)$$

Here, R represents stress ratio while A means amplitude ratio. For generating useful data for fatigue design based on stress life approach, researchers conduct fatigue tests on many specimens on varying reversed stress amplitudes of identically prepared specimens' fatigue lives. The outcomes of the fatigue tests are plotted on semi-log/log-log coordinates. Figure 3.5a illustrates bending fatigue information using semi-log coordinates. This figure shows just one curve called as S-N/Wohler's curve [46].

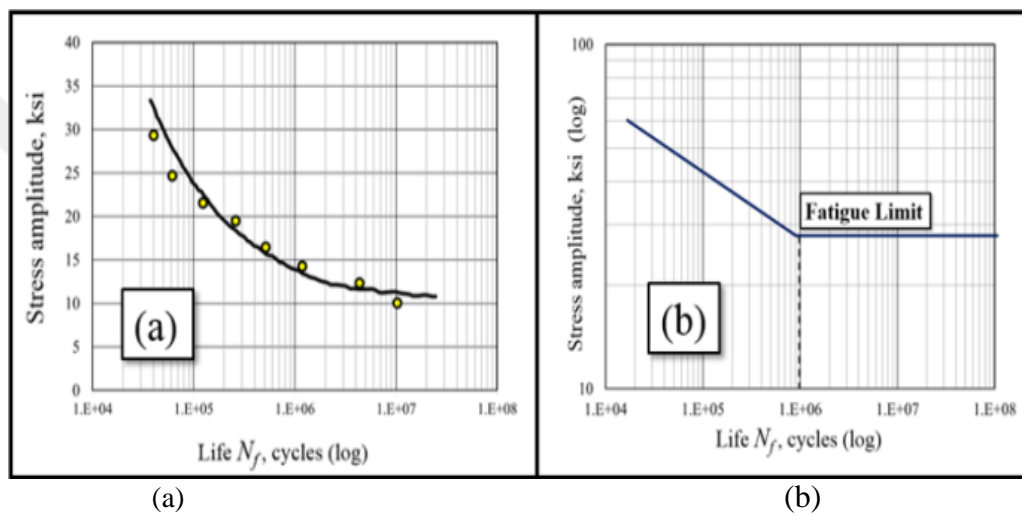


Figure 3.5. A plot of the S-N curve [46].

The plotted log-log scales are depicted in Figure 3.5 b, and here, this curve gets linear. A part of this curve is negatively sloped, which is finite life region. On the other hand, horizontal line represents infinite life region. A part of S-N curve, where the curve turns from negatively sloped line to a horizontal one is termed as knee of an S-N curve, which shows fatigue/endurance limit. Experts believe that the fatigue limit is linked with the process when crack nucleation is stopped in the first grain boundary/microstructural barrier [47].

While creating log-log plots for stress vs. fatigue life using S-N fatigue tests, the given equation shows traditional S-N curve as Equation 3.2 Shows [47].

$$\sigma_a = \sigma'_f (2N_f)^b \quad (3.2)$$

Here 'b' represents exponent of fatigue strength while  $\sigma_f$  is coefficient of fatigue strength [48].

### **3.5. CLASSIFICATION OF FRACTURE PROCESSES**

In the nutshell, we have shown the fracture process the way it is considered to take place in the current era. Figure 3.6 illustrates its formation while the next chapters highlight fracture mechanics as per the given classification [49].



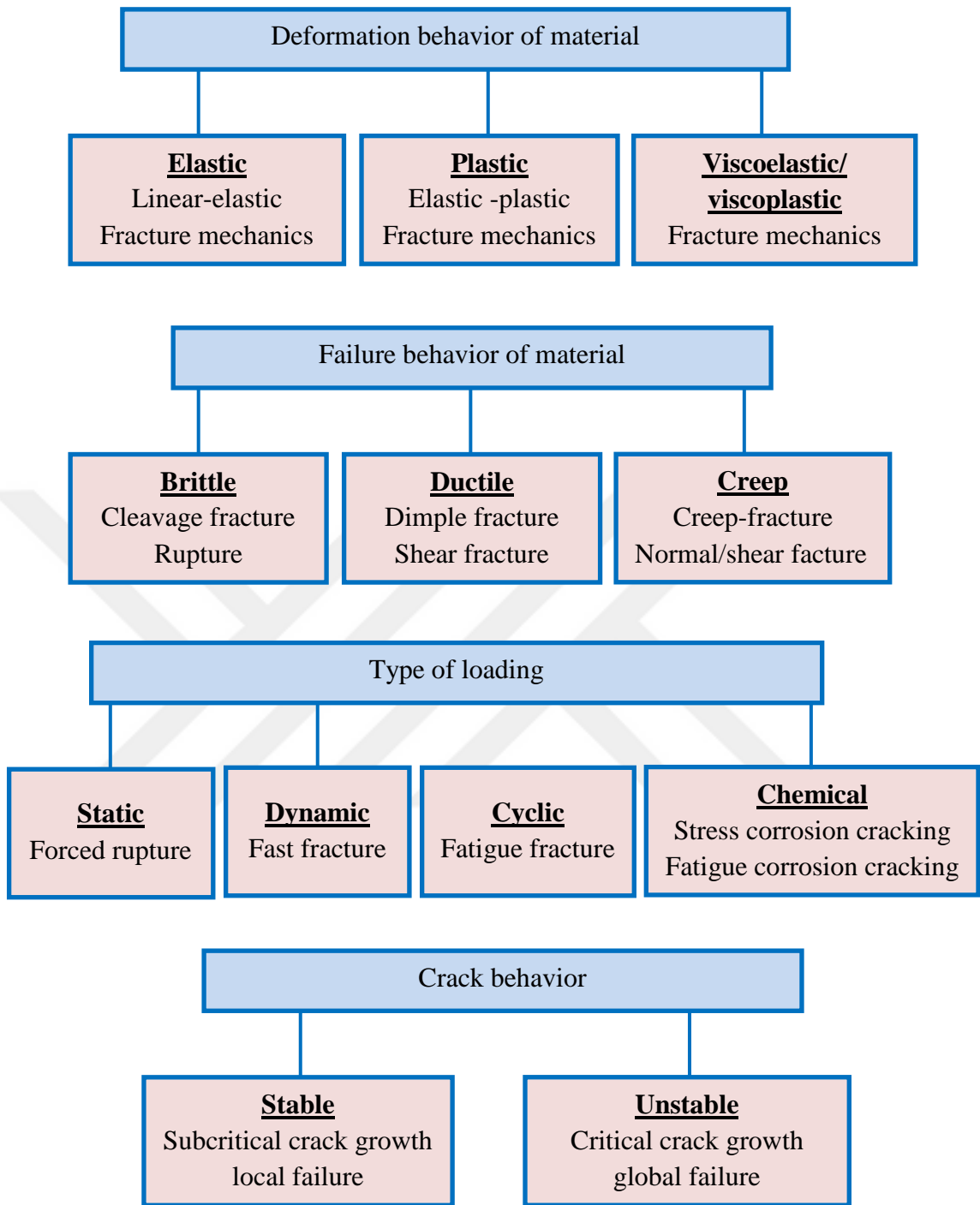


Figure 3.6. Classification of fracture processes [49].

### 3.6. MECHANISM OF FATIGUE FAILURE

It is a process, in which, components undergo some cyclical loading, which is a consequence of the culmination of three important stages including beginning, propagation and fracture. When cyclical loading causes deformation, it normally takes place



due to high stress, which results in permanent damage and cracking of a component. Whenever components experience high loading cycles, it increases the crack length. When a component is already weakened because of a crack, it only takes a few load cycles to fail. Cracks initiate on local shear planes or closer to maximum stress concentration areas including persistent slip bands (PSBs) causing discontinuity and porosity. This local shear takes place either on the surface or on grain boundaries. Micro-cracks nucleate as an initial step during fatigue damage. When nucleation takes place and cyclical loading persists, cracks increase their growth along the surface bearing high shear stress. Figure 3.7 shows the fatigue damage through crack-nucleation that initiates with maximum concentration of stress in the slip bands [47].

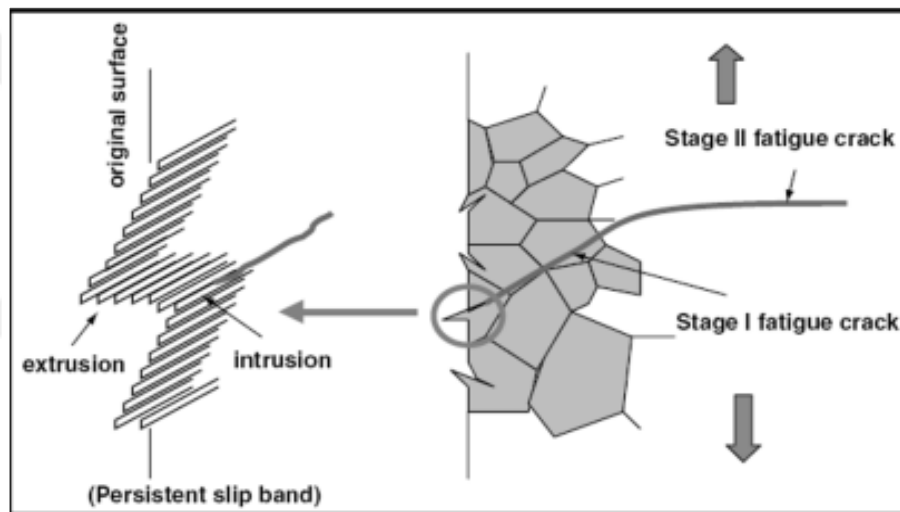


Figure 3. 7. A schematic of the fatigue process in a specimen under cyclic loading [47].

During the next step, the crack grows. This is called as crack growth stage, which is subdivided into Stage I and II cracking.

### 3.6.1. Crack Initiation Stage

During this stage, a crack emerges, which conquest upon dislocation, and creates surface irregularities such as scratches. On this stage, a material faces periodic fatigue. Keep stress concentration factor  $K_t$  is significant factor that has in mind on this stage and for predicting cracks. The growth and nucleation of a crack normally take

place during the beginning phase of crack propagation. Here, crack tip plasticity accepts the effect of slip characteristics including orientation, grain sizes, and level of stress as crack size exists in the form of a microstructure [50].

### **3.6.2. Crack Propagation Stage**

On this stage, the cycles of load increase a crack to a critical size because of high stress level and the existing vulnerability because of nucleation. Many materials have flaws, so the crack growth prediction is challenging and consequently, voraciously studied aspect. Some materials show considerable crack growth resistance, which depends on their properties. Cracking is not just a surface phenomenon. It is significant for predicting fatigue growth. When a crack becomes longer, it is globally accepted that it takes place because of principal tensile stress as well as shear stress. On this level, a crack is long but least influenced by the microstructure properties as compared to Stage I. It happens when crack tip plastic zone and front is bigger as compared to the micro-structure cracking in Stage II [51].

### **3.6.3. Rapid Fracture**

Quick crack growth takes place when a crack becomes long and critical. On that stage, a rapid fracture takes place, but in the literature, there is no regular terminology for rapid fracture. Toughness of a fracture  $K_{IC}$  is considered as a major factor behind prediction of a rapid fracture or for designing fracture-proof components [50].

For many engineering equipment's, the time taken for crack nucleation and initial growth is termed as crack initiation period while the time spent during long crack growth is termed as crack propagation period. Traditionally, high-cycle fatigue regimen (greater than  $10^5$  cycles) and crack initiation time comprise most fatigue life. Moreover, low cycle fatigue (less than  $10^5$  cycles) takes place for propagation of a crack [47].

### 3.7. CRACK PROPAGATION MODES

According to experts, three loading modes exist, involving varying crack surface displacement, which is illustrated in (Figure 3.8.). They are given below:

Mode I: Opening/tensile mode (faces of a crack faces move apart from each other)

Mode II: Sliding/in-plane shear (surfaces of a crack slide over on another)

Mode III: Tearing/anti-plane shear (surfaces of a crack go parallel towards a crack's leading edge).

This discussion is mainly about Mode I because it is a pre-dominant loading mode for majority of engineering processes. These treatments are extendible to Mode II and III [52, 53].

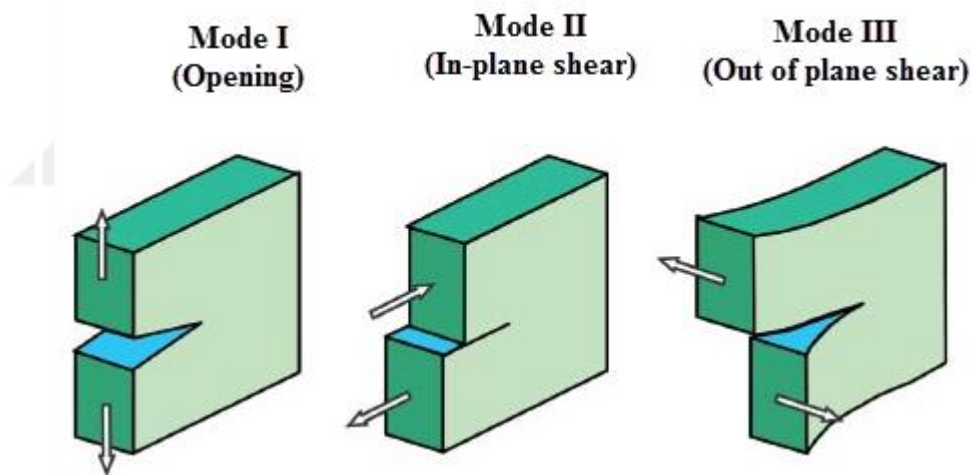


Figure 3.8. The three crack propagation modes [54].

### 3.8. LOW- AND HIGH-CYCLE FATIGUE

Analyzing fatigue not just depends on stress response. It has gained the researchers' focus because most of the research was conducted when stress-based models were applicable. Depending on load cycles required for crack creation, we should first differentiate between high- and low-cycle fatigues. There is no distinct limit between them, but they are differentiated based on 10000 cycles. The reason is that the HCF stage has low stress and elastic stress-strain relationship. In case of HCF, stress

range normally applies to describe its local state while in case of LCF, discussion centers around dissipated energy or strain range. In case of HCF, stress level is different that depends on natural state while in case of LCF, strain levels considerably vary. This is illustrated in Figure 3.9 [55].

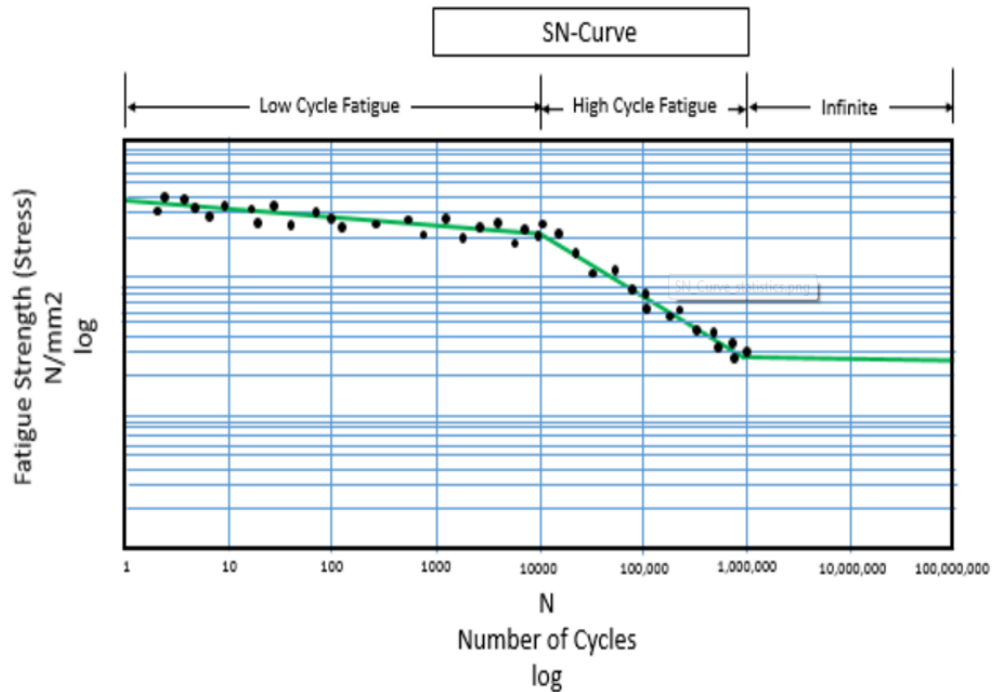


Figure 3.9. Low- and high-cycle fatigue [56].

### 3.9. FACTORS THAT AFFECT FATIGUE

Many factors influence the structural fatigue life. Some important factors are given below, which affect fatigue life of components as well as structures [57].

#### 3.9.1. Stress State

Complex geometrical loading causes immense stress, and besides, a material's stress state properties are important in this context. They include mean stress, stress amplitude, load sequence biaxiality, and shear stress.

### **3.9.2. Geometry**

A discontinuous geometrical shape greatly influences fatigue strength of a structure. Normally, a geometric discontinuity exists in the shape of cross-section variations and notches in the stress concentration area. In a majority of crack models, experts considered stress concentration as a main factor those results in crack appearance in the locations of maximum stress concentration.

### **3.9.3. Quality of a Surface**

Roughness of surface results in microscopic stress concentration, which decreases strength to bear fatigue. Compressing residual stress is possible to take place in any surface, which takes place through shot peening, which improves fatigue life of a component. Ultrasonic impact treatments and laser peening improves compressive stress on the surface, which prolongs a component's fatigue life. It is valid only in case of high cyclical fatigue.

### **3.9.4. Material Type**

Fatigue life and CL behavior is different for each material type. Many analytical possibilities exist that help dealing with many material models; therefore, material or component changes increase their fatigue life [58].

### **3.9.5. Residual Stress**

A majority of engineering materials faces residual stress, which takes place because of metal formation procedures. Cutting, welding and production/shaping procedures make use of heat/deformation that has high residual stress. When increased levels of tensile residual stress act on a component, its fatigue life reduces.

### **3.9.6. Size and Distribution of Internal Defects**

Commonly, cracks show up because of structural discontinuities on a micro level. Generally, some defects including inclusion of non-metals, gas porosity, and shrinking voids decrease its mechanical fatigue strength.

### **3.9.7. Loading Direction**

Despite the fact that the isotropic materials do not get much affected in the loading direction but certain non-isotropic materials get the impact of fatigue strength depending on the principal stress direction.

### **3.9.8. Grain Size**

It has been observed in many engineering components that the size of grain affects a component's fatigue life. For a majority of metals, small grains have more fatigue lives but still, defects on the surface or scratches reduce it in case of coarse grained alloys.

### **3.9.9. Environmental Conditions**

The environment also creates its effect, which influences large number of physical phenomena linked with a structure's surface. Environment can result in corrosion, erosion, and even gas-phase embrittlement; therefore, it strongly affects fatigue life of a material. The temperature has an important effect on fatigue strength since it was noted that high temperature reduces fatigue strength [55].

## **3.10. NOTCHES AND THEIR EFFECTS**

For over the last one and a quarter century, the effects of notches are a key issue in the fatigue studies. Since the time of Wohler (1860s), who demonstrated that additional material in railway axles could potentially weaken them? He mentioned that the radius between large and small diameters has major importance in the axles' fa-

tigue life. The emergence of fatigue cracks begin while transitioning from small to large section [59].

It is impossible to avoid notches especially in case of machinery and constructed structures. For example, a bolt contains notches in the thread root and transition between the shank and the top. Notches also include rivet holes in metal welds, sheets, and keyways. Normally, notches can be unsafe, but treatments can make them safer [60].

For understanding the outcomes of notches or what it means when they are beaten, we should consider five important parameters in the context of swish specimens:

1. Stress/strain concentrations.
2. Level of stress.
3. Average and residual stresses, and their effects.
4. Confined yield.
5. Nucleation as well as crack development.

In fact, one out of the given five parameters show a behavior difference between smooth and notched parts having equal cross-sections on the notch root. In a situation that has involvement of many parameters, using variable constants or notch factors is very much possible, which correlate with test outcomes [59].

Notches have their own stress and strain intensities/values called as concentration of stress, which is an important fatigue strength factor in the stressed parts. It is normally calculated through elastic stress concentration factor  $K_t$ , which has been outlined out of a relation that stress  $\sigma$ , and strain  $\varepsilon$  have on a notch with nominal stress ,S, or strain ,e.

$$K_t = \frac{\sigma}{S} = \frac{\varepsilon}{e} \quad \text{as long as} \quad \frac{\sigma}{\varepsilon} = \text{constant} = E \quad (3.3)$$

Here,  $\sigma$  and  $\varepsilon$  are local stress and strain respectively on a notch S. This helps us consider a metal sheet having a central round hole, therefore,  $K_t$  is dependent on the

relation between diameter of the hole and the sheet dimensions. Figure 3.10 exhibits  $K_t$  and relationship between quantitative vs. planned relationship, between the diameter of the hole and the dimensions of the sheet. The diagram shows two curved areas. As far as the higher curve is concerned, nominal stress is calculated by dividing load with total/ gross space (or simply  $w * t$ ). The lower curve has nominal stress, which can be found through dividing load by web space that is the position of the hole. We utilize a net space for outlining nominal stress [59].

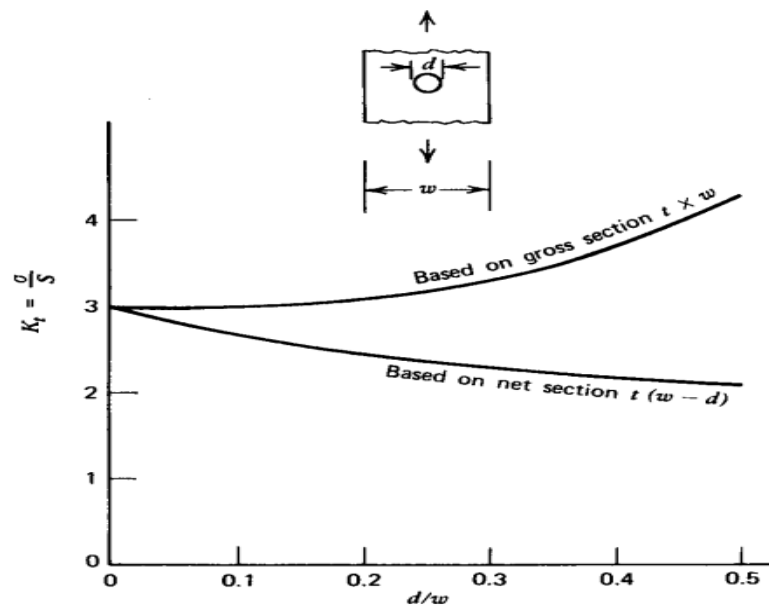


Figure 3.10. Elastic stress concentration factor to express hole in metal sheet [59].

### 3.11 FACTORS AFFECTING ON FATIGUE DAMAGE

The relationship between ultimate strength ( $S_{ut}$ ) and theoretical fatigue strength ( $S_f'$ ) can be defined as:

$$S_f' = 0.4 S_{ut} \quad \text{for } S_{ut} < 48 \text{ kpsi (330 MPa)} \quad (3.4.a)$$

$$S_f' = 19 \text{ kpsi (130 MPa)} \quad \text{for } S_{ut} \geq 48 \text{ kpsi (330 MPa)} \quad (3.4.b)$$

We know that aluminum does not have an endurance limit; thus its fatigue strength  $S_f$  is usually taken as the average failure stress at  $N = 5e+8$  cycles. Then we need to



estimate the corrected fatigue strength or endurance limit ( $S_f$ ) for our model with the aluminum material, which will be:

$$S_f = C_{\text{load}} C_{\text{size}} C_{\text{surf}} C_{\text{temp}} C_{\text{reliab}} C_{\text{miscellan}} S_f' \quad (3.5)$$

It is significant to comprehend the dissimilar factors, which can mark fatigue damage development previously and after the damage happens [45].

1. Surface condition ( $K_a$ ): It is similar to polished, ground, machined, as forged, rusted, etc. Surface may have the foremost necessary influence on fatigue life.
2. Crack size ( $K_b$ ) : This issue accounts for changes that occur once the size of the part or the crosswise differs from that of the checked specimens.
3. Style of loading magnitude ( $K_c$ ) : This issue accounts for variations in loading (bending, axial, torsional) between the parts and in the check specimens.
4. Temporary worker: This issue accounts for variations in loading (bending, axial, torsional) between the part and in the checked specimens.
5. Residual stress: This issue accounts for variations in loading (bending, axial, torsional) between the part and in the checked specimens.
6. Metal corrosion.
7. Miscellaneous ( $K_f$ ): This issue accounts for reductions from all alternative effects, and residual stress, corrosive tendencies, metal sprays, fretting or other effects [61].

### 3.12. FATIGUE FAILURE MODELS

Experts have presented three failure models, which have gained significance. They include

1. Stress-life (S-N) approach.
2. Strain-life (S-N) approach.
3. Linear elastic fracture-mechanics (LEFM) [45].

### **3.12.1. The Stress-Life Approach**

It was presented much before the rest of the two models, and it is helpful in situations having high-cycle fatigue (HCF) specifically in situations, in which assembly might last higher than  $10^3$  stress cycles. This performs well with predictable and consistent load amplitudes over the stress life of a component or structure. Since it is a stress-based concept, it tries to determine fatigue strength endurance limits of a material to keep the cyclical stresses lower than the failure, which has to be avoided for specific cycle counting. Components are designed to adjust according the needed fatigue strength/ endurance keeping in view the safety factor. As a consequence, this concept maintain local stress on notches at a lower level as compared to the level of crack formation [45].

### **3.12.2. The Strain-Life Approach**

Since crack initiation has a lot to do with yield, only stress-based approach inadequately models the situation. The strain life method commonly applies to finite-life issue and LCF, in which, cyclical stress is sufficient for causing local yield. It is very complex and needs computer operated systems for calculations [45].

### **3.12.3. Linear Elastic Fracture-Mechanics (LEFM) Approach**

Fracture mechanics concept is considered as the best to explain the crack propagation. It applies on LCF and finite-life issue that has high enough cyclic stress to initiate cracks; therefore, it is considered as appropriate for predicting residual life of cracked components [45].

## **3.13. FATIGUE PROPERTIES OF MATERIALS**

Many fatigue tests were conducted using multiple specimens having varying levels of stress. They are endured when they are plotted with sustained number of cycles. When we choose low stress, the value that is found does not cause failure, so, it has little to do with the applied cycles. The obtained stress value is actually a material's

fatigue/endurance limit. This graph has a couple of terms and it is termed as stress-cycle (S-N) diagram. Using this, it is possible to find fatigue limit of a majority of steel alloys in the range 2-10 million cycles. Some non-iron alloys and metals such as aluminum normally do not have any clear fatigue limit, which is illustrated in Figure 3.11 [62].

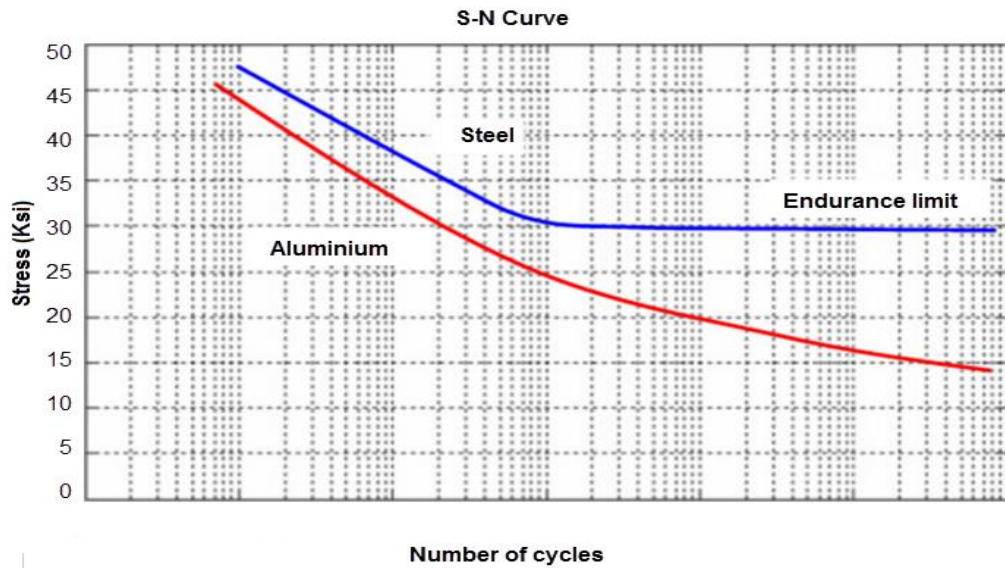


Figure 3.11. S-N curve of a ferrous and non-ferrous metal [62].

### 3.14. FATIGUE LIFE PREDICTION

The prediction process of fatigue life can be separated into two main groups according to the type of method used. The first group has prototypes established on the prediction of crack nucleation using a mixture of damage evolution rule and conditions established in the stress-strain of components. The key point of this approach is the lack of dependence on loading and specimen geometry, since the fatigue life can be estimated through the criteria based on stress and strain [63]. The approach of the second group focuses on CDM (Continuum Damage Mechanics) that predicts fatigue life through cyclical damage parameters [64]. It is possible to estimate the fatigue properties of a material through any or all of the approaches given below:

Stress-life (S-N)

Strain-life ( $\epsilon$ -N)

Crack growth rate ( $da/ (dN-\Delta K)$ )

A stress-life (S-N) curve approach is a popular technique to determine the fatigue life of different materials. A general representation of properties is accomplished through an S-N curve. In this context, special care should be given to alternating stress and its comparison with the number of cycles to failure [96].

For aluminum:

The S-N equation is [19].

$$S_n = a (N)^b \quad (3.6)$$

$$a = \frac{0.9S_{ut}}{S_f} \quad (3.7)$$

$$b = -\frac{1}{5.699} \log\left[\frac{0.9 S_{ut}}{S_f}\right] \quad (3.8)$$

Where  $S_f$  at  $N = 10^8$

### 3.14.1. Constant Amplitude Load

Wohler gave the concept of S-N curve, which works with fatigue data that was initially utilized for predicting metallic components' useful life. Rotational bending test machines are helpful for obtaining the S-N curve because number of cycles  $N_f$  is required to test the failure when a specimen undergoes alternative cycles ( $R= -1$ ) having peak stress  $\sigma_{max}$  and stress amplitude  $\sigma_a$ .

### 3.14.2. Variable Amplitude and Complex Loads

For assessing a component's safe life that operates with variable cyclical load, it is advised to take these steps:

1. Decrease the series of simple cyclical load using rain flow analysis.
2. Draw cyclical stresses on a histogram obtained through rain flow analysis to understand fatigue damage possibilities.
3. Calculate the cumulative damage degree for every level of stress with the help of S-N curves.
4. Amalgamate the individual contribution with the help of Miner's rule [65].

### 3.15. FAILURE CRITERIA METHODS

These ways are outlined and they link endurance limits on alternative stress axis with ultimate strength  $S_u$ , yield strength  $S_y$ , or real fracture stress  $\sigma_f$  [66].

#### 3.15.1. Soderberg Failure Theory

Three distinct proposed failure theories for fatigue design application will now be presented and discussed. The first is the Soderberg Theory. Using the graphic illustration Figure.3.12, this theory proposes designs for fluctuating normal stress states, which should be based on a limiting condition defined by a straight line drawn from the endurance limit on Y- axis to a yield point on X- axis in the first quadrant. This is analytically defined by the equation that ratio between alternating stress  $S_a$  and endurance limit  $S_e$ , in addition to the ratio between mean stress  $S_m$  and yield-stress  $S_y$  should be one. Safety factor  $n$  can be introduced into this equation by dividing  $n$  on the right side of the equation. This can be seen in a fairly conservative design approach [66].

Soderberg's equation is: 
$$\frac{S_a}{S_e} + \frac{S_m}{S_y} = 1 \quad (3.9)$$

With factor of safety 
$$\frac{S_a}{S_e} + \frac{S_m}{S_y} = \frac{1}{n} \quad (3.10)$$

#### 3.15.2. Goodman Theory

The second proposed failure theory for fatigue design application under a general fluctuating normal stress loading is the Goodman Theory as illustrated in Figure.

3.12. It proposes a failure line that extends from endurance limits through Y- axis to the tensile strength, which is obvious from X- axis. In effect, it discounts yielding as a failure condition and is less conservative than the Soderberg theory particularly for mean stress values in excess of the yield strength. Analytically, it is defined by the equation that the alternating stress ratio  $S_a$  to strength limit  $S_e$  plus ratio between average stresses  $S_m$  to tensile stress  $S_u$  equals one. Again a factor of safety  $n$  should be introduced through dividing the equation's right side by  $n$  [66].

$$\text{Goodman's equation is } \frac{S_a}{S_e} + \frac{S_m}{S_u} = 1 \quad (3.11)$$

$$\text{With factor of safety } \frac{S_a}{S_e} + \frac{S_m}{S_u} = \frac{1}{n} \quad (3.12)$$

### 3.15.3. Gerber Failure Theory

The Gerber Failure Theory differs from the Soderberg's and the Goodman theories because it represents the failure line as a quadratic curve that passes through the endurance limit and the tensile stress as shown in Figure 3.12. Of the three theories, it is the least conservative and is considered by many to be the more accurate about the true behavior and impact of fluctuating loads on fatigue strength. Analytically, it is represented by the equation 3.10 as ratio between alternating stress  $S_a$  to strength limit  $S_e$ , and it is added to a ratio between mean stress  $S_m$  and tensile strength  $S_u$ . The sum will be equal to one. To introduce a factor of safety into this expression,  $n$  is added to the numerator of the two stress ratios in the equation's left hand side. Out of three theories presented for design applications and analysis, generally, Goodman theory is preferred [66].

$$\text{Gerber's equation is: } \frac{S_a}{S_e} + \left(\frac{S_m}{S_u}\right)^2 = 1 \quad (3.13)$$

$$\text{With factor of safety } \frac{nS_a}{S_e} + \left(\frac{nS_m}{S_u}\right)^2 = 1$$

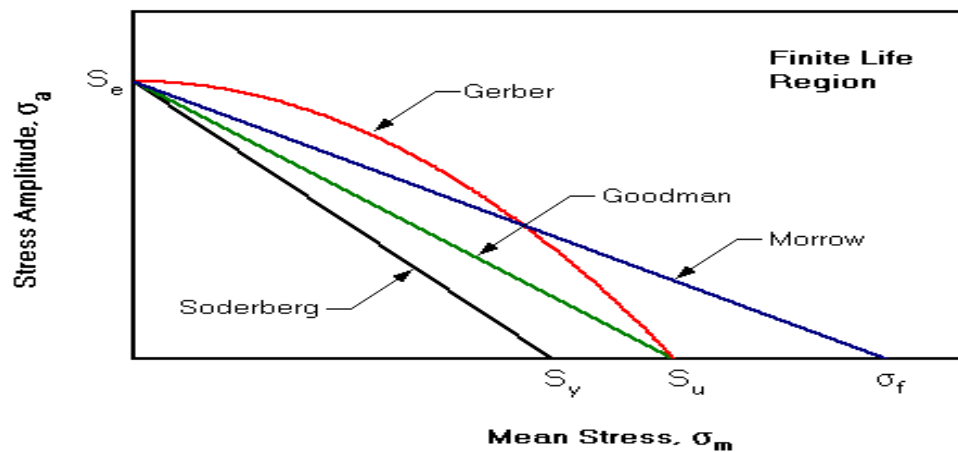


Figure 3.12. Failure criteria methods [67].

We can summarize Failure criteria strategies in these points:

1. The Goodman theory is appropriate for low-ductility metals. No correction is done for compressive mean stresses.
2. The Soderberg theory tends to be more conservative than Goodman's because it is sometimes used for brittle materials.
3. The Gerber theory provides sensible fit for ductile metals in case of tensile stress, though its prediction of harm is generally incorrect regarding mean stress, as shown on the left part of the graph [66].

### 3.16. NOTCHES

Many experts including engineers and designers have a difference about what are cracks and what are notches, so, naturally, they forget differentiating between notches and cracks particularly when the subjected structure or sample is under fatigue. Practically, notches are geometric discontinuities having definitive depths and root radius. Notches emerge in stress concentration areas of a structure machine because their surface areas are smaller as compared to the surface area of the remaining solid; therefore, in a majority of cases, these notches fail at first because they bear high stress concentration [68].

### 3.17. STRESS CONCENTRATION

Notches greatly increase the stress concentration in mechanical elements. The extreme stress leads to mechanical failures, which can be dangerous for many parts of a machine. Moreover, notches in plates cannot be avoided in design of many parts and come in non-suitable places [69].

The formula for elementary stress can be used for structural design, which is based on those parts, which have a constant section or their contour gradually changes Figure 3.13 Practically, these conditions are hard-to-attain in a maximum stress region with real mechanical parts [71].

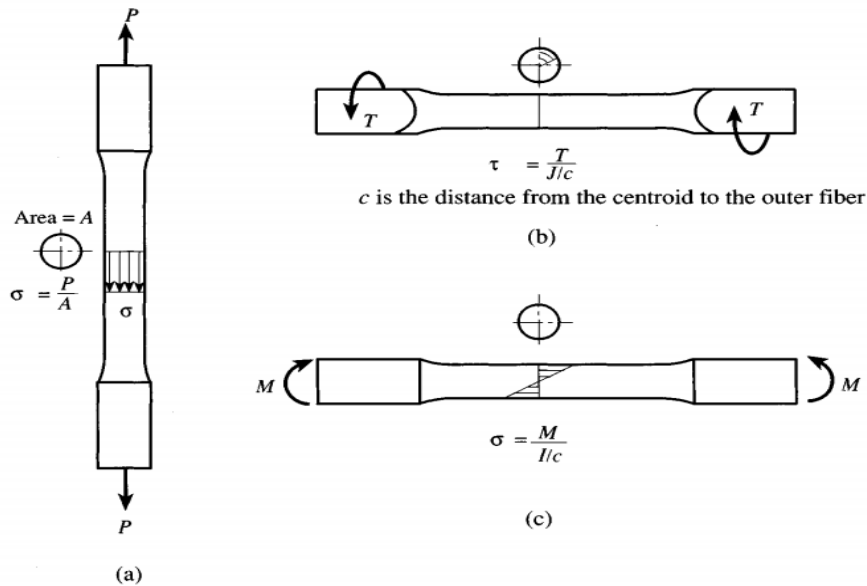


Figure 3.13. Elementary stress cases for specimens having constant cross sections or gradual cross-section [70].

Existence of grooves, keyways, threads or any other structure modifies stress distribution, which is illustrated in Figure 3.13 Local stresses are illustrated in Figure 3.14 the high-stress localization is termed as stress concentration, which can be obtained through calculating the stress concentration factor  $K_t$  that is ratio between peak stress ratio of a body and reference stress.

$$K_t = \frac{\sigma_{\max}}{\sigma_{\text{nom}}} \quad (\text{Applies in case of normal stress, tension and bending}) \quad (3.14)$$



Here, maximum stress  $\sigma_{max}$  shows highest stress that takes place in real load as well as nominal stress  $\sigma_{nom}$  that is termed as reference stress. At times,  $K_t$  becomes a form factor [70].

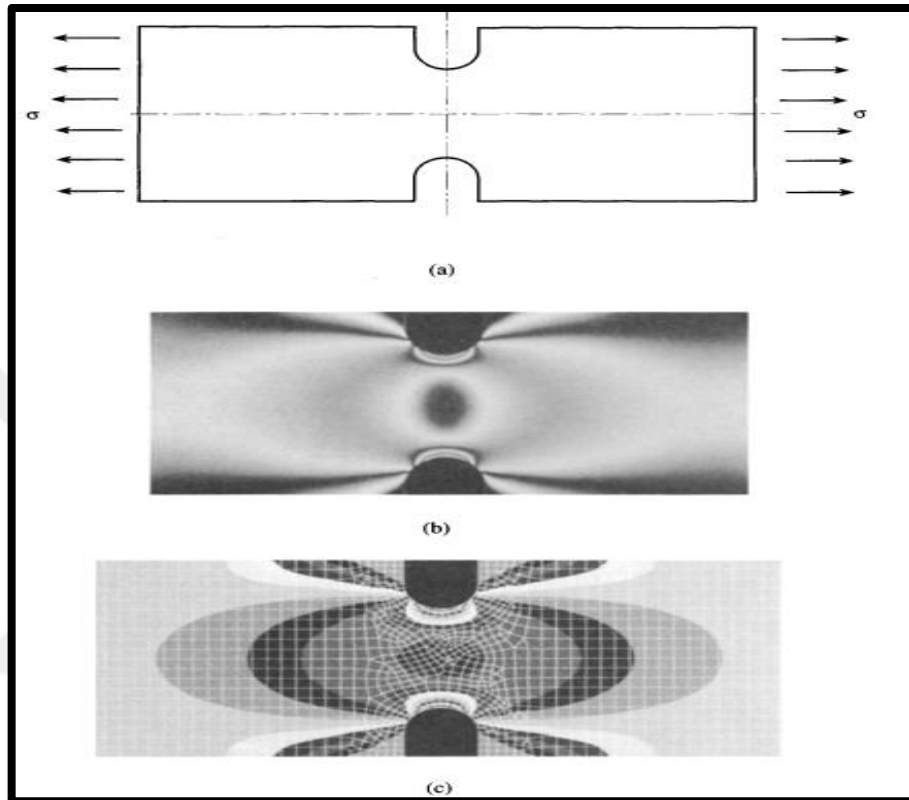


Figure 3.14. Tension bar having notches [70].

Sometimes, it is impossible to avoid holes or other geometrical notches, which cause non-homogeneous distribution of stress Figure 3.15 that has stress concentration on the notch root. That stress concentration factor  $K_t$  is a ratio between peak stress on notch root and nominal stress that exists when stress concentration doesn't take place.

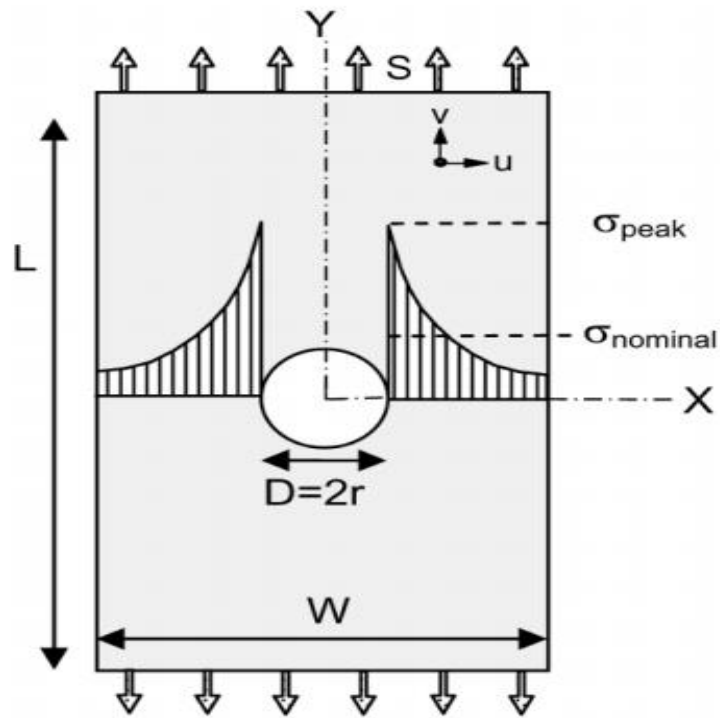


Figure 3.15. Strip having central hole to represent notched part [1].

$$K_t = \frac{\sigma_{peak}}{\sigma_{nominal}} \quad (3.15)$$

The stress concentration intensity depends on notch geometry or shape. It is imperative for designers to decrease the concentration of stress in order to avoid the issue of fatigue and consequent cracking [1].

### 3.17.1. Definition of the Stress Concentration Factor

The strip having a hole in the middle as an example of a notched material. That was used to study effects of notch on fatigue. When that strip was loaded through homogeneous stress, the hole caused inhomogeneous stress on critical area that covers very less area as compared to the remaining hole. That area possesses peak stress  $\sigma_{peak}$  on the notch root, and nominal stress  $\sigma_{nom}$ . A ratio between peak and nominal stresses shows net value according to the general definition of stress concentration as illustrated in Equation (3.16.). It must be noted that deformations are elastic.

$$\rho_{peak} = K_t \sigma_{nominal} \quad (3.16)$$

It is generally appropriate to find peak stress-gross stress  $S$  ratio that applies to a component. This ratio is represented by symbol  $K_{tg}$  and it is given by:

$$K_{tg} = \frac{\sigma_{peak}}{S} \quad (3.17a)$$

Both the concerned factors have interrelationship. These dimensions are  $W$  (width of specimen) and  $D$  (diameter of the hole):

$$K_{tg} = \frac{\sigma_{nominal}}{S} \quad K_t = \frac{W}{W-D} K_t \quad \text{hus } K_{tg} > K_t \quad (3.17b)$$

$K_t$  and as well as  $K_{tg}$  are the symbols used were presented by R.E. Peterson in his book "Stress Concentration Factors" [71].

### 3.17.2. Effect of the Notch Geometry on the Stress Concentration Factor

In case of a circular hole in infinite metallic sheet, diameter  $D$  is the only useful and significant dimension. For observing this central hole, shown in Figure 3.15, the available dimensions are mainly three including width of specimen ( $W$ ), length ( $L$ ) and diameter of hole ( $D$ ). The thickness of specimen is irrelevant until now. Figure 3.16 illustrates two geometrically similar specimens with just one difference and that is their size. Here, the Geometric similarity means that the obtainable ratios are equal such as  $D/W$  and  $L/W$  [1].

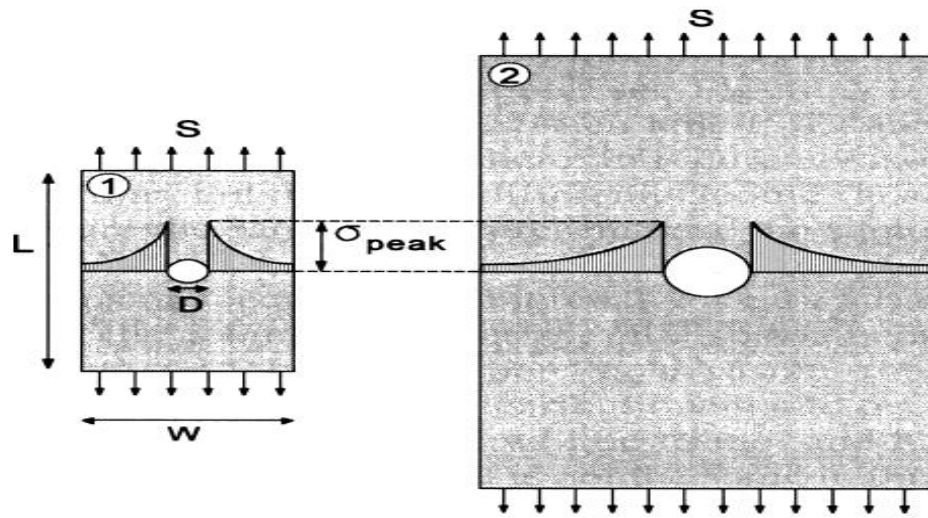


Figure 3.16. Geometrically similar specimens having similar  $K_t$  but different stress gradients [1].

Figure 3.17, exhibits  $K_t$  that represents double-edged notch and a middle hole and a double edge notch, as well as geometry that has been used to investigate fatigue in labs. When the radius of the notch ( $r$ ) increases,  $K_t$  reduces that takes place more often in edge-notched samples as compared to the samples having a hole in the middle. In case of edge-notched sample  $K_t \rightarrow 1$  for  $2r/W \rightarrow 1$  (zero ligament), and in case of middle hole sample  $K_t \rightarrow 2$  for  $D/W \rightarrow 1$  (zero ligament) [1].

$K_t(D/W)$  curve can be drawn for the specimen having a central hole but it largely depends on Howland calculations [72], was approximated by Heywood [73] by Equation 3.17 to:

$$K_t = 2 + \left(1 - \frac{D}{W}\right)^3 \quad (3.18)$$

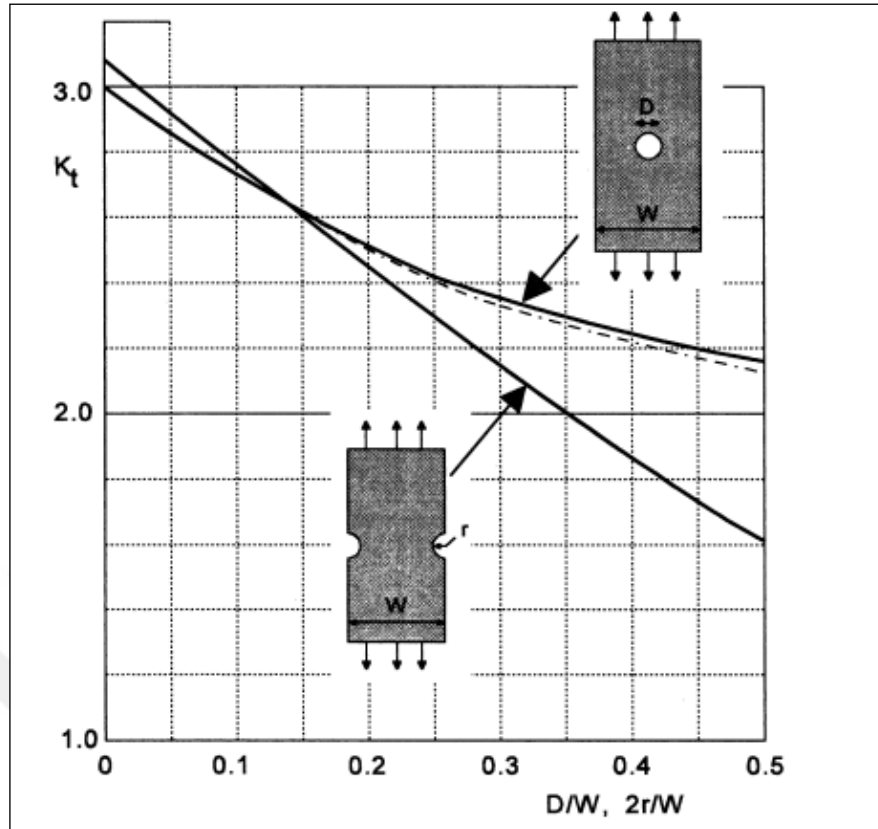


Figure 3.17. The stress concentration factor for a specimen with a central hole and a specimen with two edge notches [1].

### 3.18. METHODS TO REDUCE STRESS CONCENTRATION

Many methods are viable for reducing stress concentrations in different mechanical components [75]. They are given below:

1. Providing fillet radius to gradually change a cross-section.
2. Making use of elliptical fillet.
3. Making use of many small notches instead of one long one, if notches are inevitable.
4. Having narrow notches instead of wider ones in case if there is a requirement for projection.
5. Utilizing stress-relief grooves.

### 3.19. NOTCH SENSITIVITY

Experts have found that a few substances are less notch- sensitive when they found the stress concentration. In case of such substances, reduced less  $K_t$  value is needed.  $K_t$  has been illustrated in Figure 3.18 the maximum stress of these materials is given below [74].

Maximum Stress =  $K_f$ \* nominal stress

Notch-sensitivity q will be:

$$q = \frac{K_f - 1}{K_t - 1} \quad (3.19)$$

This q can assume values between 0 and 1, so when  $q=0$ , then  $K_f = 1$ , which shows that the material does not have notch-sensitivity. If  $q = 1$ ,  $K_f = K_t$  so the substance is completely notch-sensitive. During the design and analytical work, we first calculate  $K_t$  using the part of geometry. Later, we specify substance calculate q, and find out  $K_f$  using the given equation [70]:

$$K_f = 1 + q(K_t - 1) \quad (3.20)$$

According to the Peterson's relation, the fatigue notch factor of 7075-T6 aluminum alloys is given as [75]:

$$K_f = 1 + \frac{K_t - 1}{1 + \frac{\rho}{r}} \quad (3.21)$$

Where

$\rho$ : is a material constant and  $\rho = 0.5$  mm for aluminum alloy.

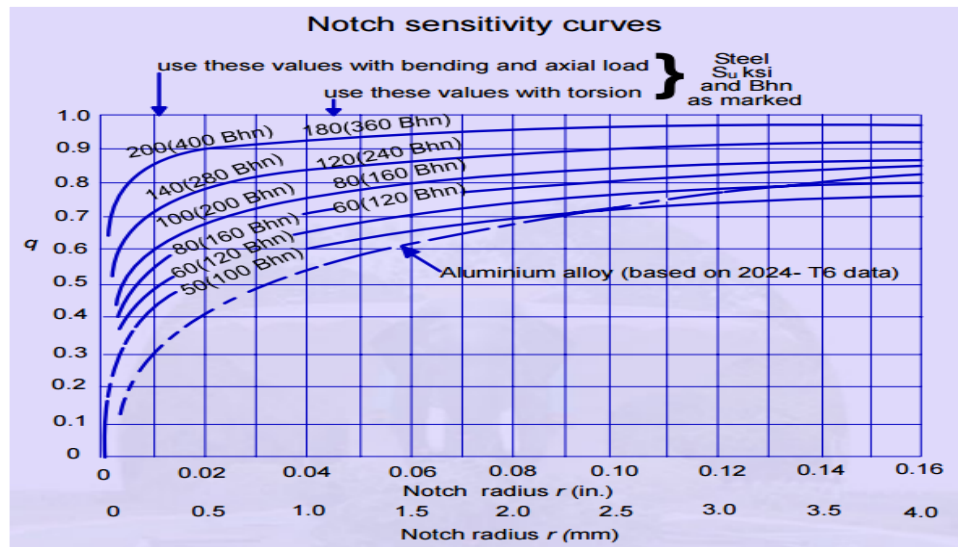


Figure 3.18. Notch sensitivity curves [74].

### 3.20. OPPOSITE SINGLE U-SHAPED NOTCHES IN A FINITE-WIDTH

Some tests including photo-elastic tests, strain-gage tests) and mathematical analyses help providing data for opposing U-shaped notches on a plain bar illustrated in Figure 3.19. it shows that a curve that represents mathematical outcomes of semi-circular notches as exhibited in Figure 3.20, which is a special U-notch case. There is an ideal agreement of values of  $H/d < 2$ . Photo-elastic outcomes for  $H/d = 1.05$  also show appropriate agreement [70].

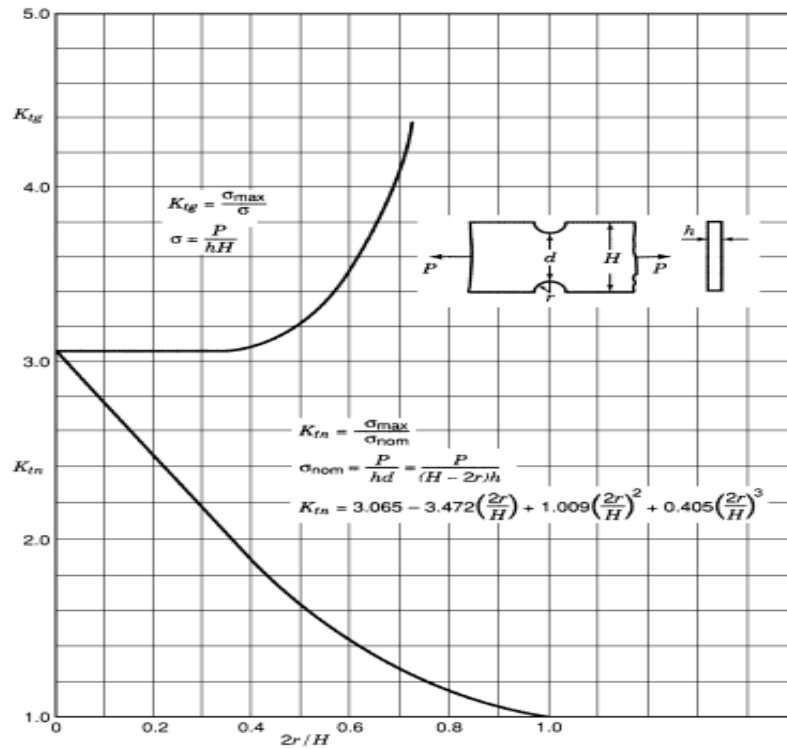


Figure 3.19. Stress concentration factors  $K_{tg}$  and  $K_{tn}$  for tension strip having opposite semi-circular edged notches [76,77].

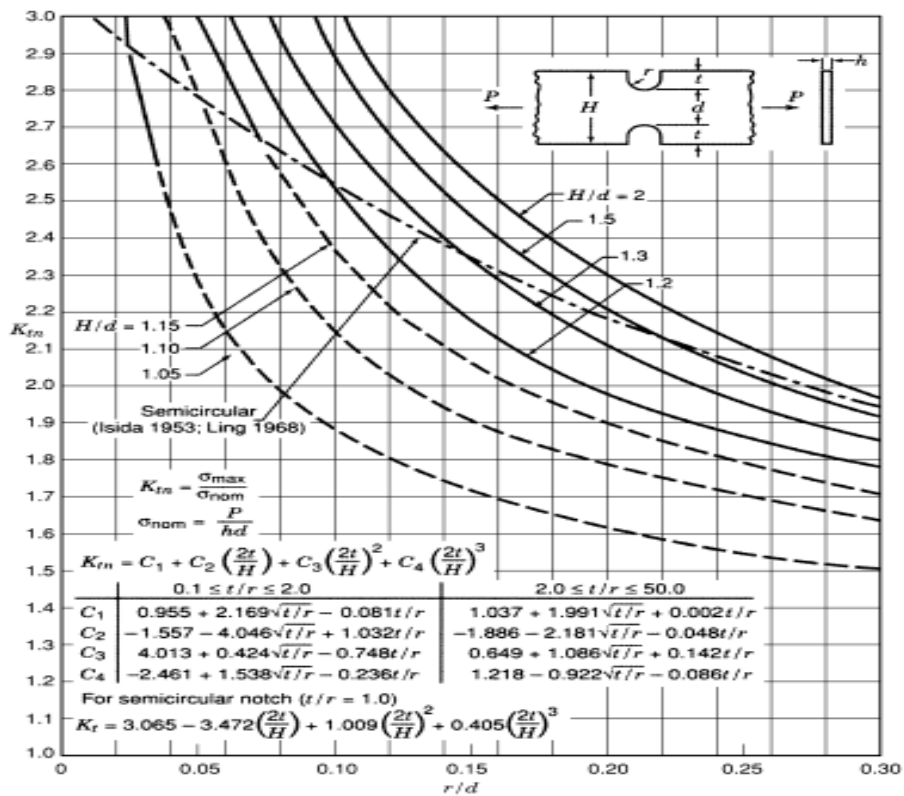


Figure 3.20. Stress concentration factor  $K_{tn}$  showing flat tension bar having opposite u-shaped notches [76-79].



### **3.21. SENSORS**

When the structures are designed, designers normally consider fatigue, which is abstruse because the history of its actual loading is unknown and consequently unpredictable. In this case, a device is needed to monitor fatigue damages, which provides reliable estimation of residual fatigue life of a structure before a fatigue failure. In order to find the fatigue damage and make prediction about the residual useful life of components and structures, testing engineers use fatigue detection systems consisting of detectors, gages and fuses. They are linked with the under-study structure for monitoring the alignment in the direction of stress/strain. Certainly, the fatigue calculating devices can monitor fatigue damage in a specific direction [80].

#### **3.21.1. Definition of Sensor**

Sensors calculate variables such as pressure, temperature, speed, rate of rotation, and other physical and chemical variables. Nowadays, sensors no longer use analog scales but sophisticated digital signals, which indicate measurement of physical variables. It is possible to gather the data of those signals using computer programs, store it, plot it and analyze it. Sensors are available in many varieties depending on the quantities or qualities they have to sense. Some sensors still use output in voltage. Certainly that is not without implications [81].

#### **3.21.2. Criteria to Choose a Sensor**

When an investor invests in any sensing system, he/she looks for certain qualities that a sensor must have in order to function appropriately. Those functions are as follows [82].

1. Precision.
2. Ability to perform in rains, snow and other environmental conditions and temperatures.
3. Appropriate range.

4. Calibration - It is necessary for almost all sensing devices because every reading changes in some time.
5. Resolution - ability to detect even a little change.
6. Cost-effectiveness.
7. Repeatability - capability to repeatedly read a measurement within the same circumstances.

### **3.21.3. Main Reason of Using Sensor**

1. Sensors help avoiding extremes and disrupting factors such as over- and under-cooling, electro-static discharges, corrosive surfaces and short-circuit.
2. They reduce operational cost of an organization on an issue, increase operational efficiency, improve capacity, and help future growth.
3. Sensors help monitoring the environment, which alerts concerned professionals to take action before emergence of an issue including fire, moisture, smoke, and safety problems.
4. Some sensors save energy costs because they notify about the temperature changes [83].

### **3.21.4. Classification of Sensors According to Energy Sources**

According to their energy source, sensors can be classified as follows:

#### **3.21.4.1. Active Sensors**

Active Sensors produce energy, which is necessary for transmission and measuring processes, for example:

1. Thermal element.
2. Induction coil.
3. Hall-effect probe.
4. PH electrode [84].

Some of the active sensors produce electrical signals, which have to be converted into voltage, for example:

1. Piezo-crystal.
2. Photo-diode.
3. Wiegand-sensor.

#### **3.21.4.2. Passive Sensors**

Energy flows through passive sensors. The sensor changes its resistance and modulates a defined variable of the flow of energy. The resistance can be resistive, capacitive or inductive, for example:

1. Potentiometer.
2. Strain gauge.
3. Piezo transducers camera / Natural transducers camera.
4. Phototransistor capacitive: by manipulation of distance of capacitor plates.
5. Di-electric medium's retraction depth [84].

Inductive:

1. Permeability.
2. Cross section.
3. Distance of air gap.

Sensors with an optical signal output and light flux can be influenced by:

1. Intensity.
2. Frequency.
3. Wave length.
4. Polarization.
5. Spectral resolution.

### **3.21.5. Classification of Sensors According to Measured Variables**

According to the measured variables, sensors can be classified as follows:

#### **3.21.5.1. Displacement sensors**

While regular sensors detect the existence of objects, displacement sensors detect the amount of displacement when objects move from one position to another. Detecting the amount of displacement allows the measurement of height and thickness of the objects.

Displacement sensors can be classified as follows:

1. Inductive.
2. Capacitive.
3. Gyroscope.
4. Magnetic.
5. Optical.
6. Ultrasonic.
7. Acoustic Emission [85].

#### **3.21.5.2. Velocity Sensors**

Piezo-velocity transducers (PVT) measure piezo-electric velocities in a solid state. PVTs are concerned with acceleration having an IC (integrated/integration circuit) that generates output in terms of velocity. Several vibration experts prefer examining vibration as velocity in inches per second. The PVT sensors reduce signals having greater frequencies, which help measuring vibrations of low frequency [85].

### **3.21.5.3 Acceleration Sensors**

They are popular and commonly used sensors called as accelerometers, which have a vast sensing range. They have capacities to measure acceleration based on 1, 2 or 3 orthogonal axes [85].

### **3.21.5.4. Strain Sensors**

They sense resistance changes in output terminals whenever there is a stretch/compression. They are installed on a solid material surface, which captures even the minutest dimensional variations during tension or compression. This kind of sensors report deformations in a specific material. This behavior also determines most of their application areas. For example, they are most often used to watch the statics of bridges, buildings, and wooden constructions. Mechanical shafts and different kinds of scales as well as cranes are also typical areas of application for strain sensors. Currently, they are made out of foils, wires or semiconductors [86].

### **3.21.5.5. Force Sensors**

They weigh luggage and freight after manufacturing as well as before transporting to any destination. They are used for monitoring load on machinery to assure compliance to the safety standards for lifts, cranes, tanks, locomotives and grain silos, and assure that they not overloaded. In case of using force sensors, load cells and transducers, force sensors help changing force into an electric output. These load cells include pneumatic, hydraulic, piezo-electric, and capacitive varieties. The strain-gage loading cells are commonly available. They consist of fine wires having approximately (0.02 mm) diameter and they may be made up of aluminum, steel, or beryllium-copper. These wires are linked with a paper plastic in zigzag formation that increases material change effects responding to external load. The wires on the two sides of the zigzag wave are linked with the circuit that amplifies and manages the signal [87].

### **3.21.5.6. Temperature Sensors**

Out of all the sensor types, temperature sensors are the most popular form that detects heat or temperature. They also assess the heat energy coolness that a system object generates, which helps sensing detecting physical changes either through digital or at least analog output system. Different forms of temperature sensors are available having different properties [88].

### **3.21.5.7. Pressure Sensors**

They help recording fluid pressure and they are helpful to manage fluid technologies. Their workability is decided according to the situations, under which, they are utilized. For fulfilling such requirements. Electronic pressure transducers measured pressure variables and convert them to an appropriate output signal. They switches pressure variables as per given pre-settings. It is very important to monitor vacuum, hydraulic, pneumatic, and other forms of liquid and gas pressures. Balluff pressure sensors perform better than the needed standards with installation ease and flexibility and have simple output configuration in a very demanding situation. Balluff focuses on quality, better sensor design, and provides more reliability, decreases down time, and improves usefulness [88].

### **3.21.6. Fatigue Sensors**

When designers design components or structures, they consider fatigue as an abstruse phenomenon because generally the real loading history of that component structure is unknown and unpredictable, so, a device is needed to observe fatigue damage and estimating residual operational life of that component structure as well as getting a warning about possibility of fatigue failure. In order to determine the fatigue damage and make other necessary estimations, engineers apply fatigue detectors, gages and fuses. They attach them to a structure to see whether the tested elements align in the stress/strain direction. As such, these fatigue measuring and monitoring devices are capable of monitoring fatigue damage in only one fixed direction. Furthermore, these fatigue gages typically contain only one test element, which ne-

cessitates multiple tests on the structure being tested or alternatively the attachment of multiple gages to obtain the desired values of fatigue damage or remaining service life. Some of these are either expensive or follow tedious measurement procedures. Some kinds of fatigue monitoring devices, which were meant for multi-directional fatigue monitoring, are limited in their operation to only measure or monitor structures with different lengths of artificial cracks or structures having welded joints. Other gages containing multiple test elements were limited because they were designed to measure compressive stress only [80].

For addressing exigency of the fatigue measurement during the initial operational phases of the structures during the span of their functional service period, a variety of methods were solicited for facilitating them in the timely actions needed to avoid any ghastly outcome. Some types of fatigue monitoring devices were recently developed, which are:

1. Fatigue fuses.
2. Piezo-electric based sensors.
3. Electro-chemical sensors.
4. Eddy current based sensors.
5. Ultrasonic based sensors.
6. Magnetic flux leakage sensors.

Fatigue fuses can also be categorized as crack gage type devices. The fatigue fuses are generally made using a sheet of metal same as that of the structure under study. The fatigue fuse comprises of a thin ribbon or strand of wires, and they are adhered to the structure generally near the site of the crack initiation. It is designed to contain a pre-crack that assists in providing a location for the striation formation. Figure 3.21 illustrates schematic side view as well as the top view to show what a fatigue fuse (A) looks like. This is linked with the structure that needs fatigue monitoring with (D).

The face (C) is not in contact with the structure. The coupon is pre-cracked (B) at the center and the operation of this device, which is based on this pre-crack that ad-

vances the fracture surface in incremental distances proportional to the applied cyclic stress. The loading experienced by the structure will be transferred to the coupon through the adhesive bonding [89].

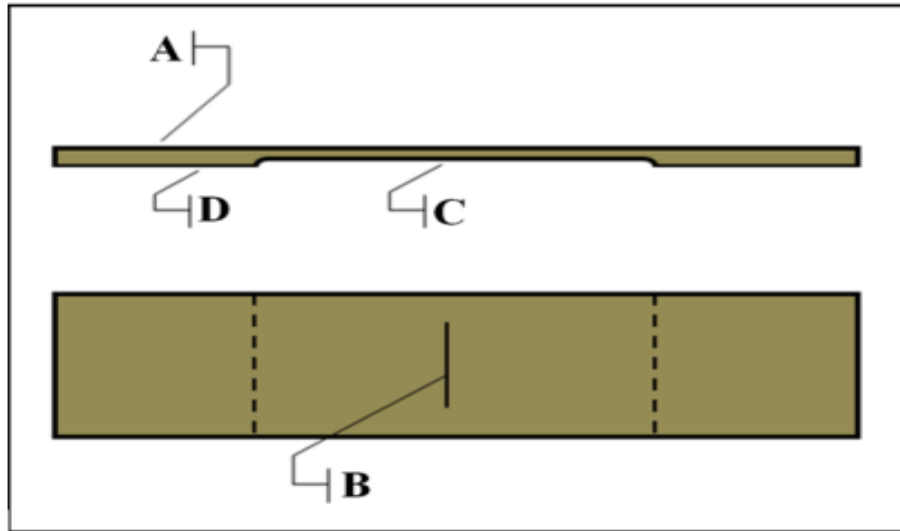


Figure 3.21. The side view and plan view of the remote and powerless miniature fatigue monitoring device [89].

According to Henkel, this device measures the stress intensity ranges because of the loading experienced by the sensor coupon, which is linked with the fatigue life. There are, however, some drawbacks of the sensor. The process of assessing fatigue life is not continuous as a sensor needs to get removed from the structure and then analyzed based on the striations formed, which includes a number of steps. Moreover, the sensor needs to be pre-cracked prior to mounting on the structure. Another aspect is the limitation of the material that is used for the sensor needs to be a cubic crystalline structure having face in the center [80].

A summary of some of the fatigue sensors developed in the past is illustrated below:



Table 3.1. The summary of recently developed fatigue sensors [48].

No.	Sensor Name	Principle of operation	Comments (Cons)
1.	Remote and powerless miniature fatigue monitoring device	Fatigue fuses (Passive Sensors) Comments (Cons),(1-4)	1. In some cases, the testing elements have to be subjected to pre-cracking. 2. The testing elements have to be subjected to artificial weakening. 3. They can measure the fatigue damage or stress in a particular direction. 4. Complex fabrications have to be employed.
2.	Fatigue indicator with slots		
3.	Longitudinal rib with notches for load counting		
4.	Fatigue monitoring coupon with notches		
5.	Fatigue-damage indicators equipped with slit		
6.	Fatigue sensor with variable slots		
7.	Fatigue sensor with slots and ligaments		
8.	A built-in piezoelectric sensor/actuator network	Active Sensors	5. Not all the sensors perform in-situ fatigue sensing. 6. They would not account/mimic for the ambient conditions
9.	Piezoelectric strain sensor array		
10.	Structural Impedance sensors		
11.	Piezoelectric paint sensor		
12.	Electro-chemical Fatigue Sensor		
13.	Eddy current sensors		
14.	Ultrasonic based sensors		
15.	Magnetic Flux Leakage sensors		

## PART 4

### METHODOLOGY

#### 4.1. MATERIAL

It is important to note that for the current study, aluminum alloy 7075-T6 was used. This alloy has been actively utilized for over 5 decades, and specifically, it has been used for aeronautical engineering purposes to produce critical components. However, nowadays, it is used in the production of mechanical components due to its mechanical strength being an established fact. It has been used for aeronautical equipment in the T6 form due to its peak yield strength. Moreover, 7075-T6 has good strength-to-weight and cost ratios in addition to its having the best machinability resulting in a very nice finish. For these reasons we used this material in our thesis.

Having mentioned that 7075-T6 has widespread application, we present its chemical composition in Table 4.1 given below and the mechanical properties which are utilized for sensors are presented in Table 4.2.

Table 4.1. Chemical composition of Aluminum alloy 7075-T6 [93].

<b>Component</b>	<b>Wt. %</b>
Aluminum	86.9-91.4%
Zinc	5.1-6.1%
Magnesium	2.1-2.9%
Copper	1.2-2.0%
Iron	0-0.5%
Chromium	0.18-0.28%
Silicon	0-0.4%
Manganese	0-0.3%
Zirconium	0-0.25%
Titanium	0-0.2%
Others	0-0.15%

Table 4.2. Common properties of Aluminum alloy 7075-T6 [94].

<b>Physical Properties</b>	<b>Metric</b>
Density	2.77 g/cm <sup>3</sup>
Young's Modulus	71 Gpa
Poisson's Ratio	0.33
Shear Modulus	27 Gpa
Fatigue Strength (Endurance Limit)	160 MPa
Yield Strength	468.8 MPa
Ultimate Strength	579 MPa
Fatigue Strength Coefficient	887.6 MPa

This thesis mainly presents the details of our investigations in the design, implementation, and analysis of the fatigue life of the sensor using a simulation on the ANSYS workbench software. Some of the important features of this sensor are its simplicity in design, ease of installation and the fact that the sensor need not be located at a critical location. The sensor can be placed in the vicinity of stress concentration zones such as holes, notches, etc. it and can mimic the stresses and strains at the critical locations in the structure.

#### **4.2. PROCEDURE FOR FATIGUE LIFE DETECTION**

ANSYS provides a comprehensive solution that allows testing possibilities over an entire range of variables applied in physics. It facilitates professionals requiring any engineering simulation, and they are needed in the design process. Professionals and organizations all over the globe trust ANSYS because it delivers reliable values against engineering simulation needs.

To predict the fatigue life of a U-notch sensor during the design stage, a simple procedure of fatigue life prediction is suggested:

1. Define the aluminum alloy 7075-T6 properties.
2. Create geometry of the sensor.
3. Define the meshing of the sensor model.
4. Apply loads and boundary conditions.
5. Make the solution.

6. Calculate fatigue life.
7. Check the accuracy of the results and find a good meshing element.
8. Obtain the fatigue life result and location of damage.
9. Produce compression between some of the aluminum alloy.

ANSYS has taken engineering product development to a different level with unequal width and depth and an unmatched engineering scalability with multi-phase foundations and architectural adaptation that sets it apart from the available CAE tools [97].

This method is basically a numeric process to solve problems that can be described using partial equations and those which can be stated in a functionally minimizable state. They are represented with the help of finite variables. The approximation function is determined for the node values. FEM turns a physical problem into a discrete and finite problem having unknown node values. In the case of linear problems, linear algebraic equations need to be solved for the values of elements.

Two FEM characteristics are worth mentioning:

1. The approximation that takes place is piece-wise pertaining to the finite elements, and this is a source of accuracy when we have a simple approximating function.
2. Approximation on a local scale results in sparse equations in cases of a discrete problem, and this helps in finding solutions even when the number of nodal unknowns is large [98].

To summarize the method through which finite elements process functions, we can list the following major steps to find the solution to finite unknowns:

1. We first need to make the continuum discrete, so initially, we should divide the solution region into finite terms. Pre-processor programs traditionally generate the mesh of finite elements. This mesh has many arrays out of which some are nodal coordinates.

2. We then select the interpolation functions. These help in interpolating field variables pertaining to an element. We may sometimes select polynomials in place of interpolation functions. The degree of the polynomial (monomial, binomial, etc.) depends on how many nodes are assigned to an element.
3. Knowing and understanding element properties: We form a matrix equation in the case of finite unknowns that links nodal values of different parameters, including unknown functions. We use multiple approaches to accomplish this task, but from these, the Galerkin method and the variation approach are the most convenient.
4. Organizing the equations for the elements: In order to find the equations, we need to organize the equations for accuracy and clarity. This means that we should combine local elements for discretizing. For assembly, inter-elemental connectivity is used. Prior to finding a solution, we should impose boundary conditions (not included in the equations).
5. Solving global equations: A set of global equations is generally symmetric, sparse, and positive. To find a solution, iterative and direct processes can be employed. The nodal values of the sought function are the outcome of the whole process.
6. Calculating further values: Sometimes we should calculate more parameters, including stress and strain values and even sometimes displacement, which is very important in certain situations [98].

Experts have attempted to determine the properties of concrete under different conditions using different methods. The classical analytical procedure was applied first; however, this procedure is almost impossible for complex structures. For this reason, empirical methods were used based on large databases of experimental outcomes. Today, experts use the finite process as it is a very useful method to conduct analytical calculations of different factors in concrete, such as stress fields in two or three dimensions, cracking parameters, interface problems, and so on. In the past, some of these effects and parameters are ignored or treated as approximations, which explains the reason for problems not having been modeled rationally. However, experimental research did not stop with finite element development

because it is still very important for comparing the outcomes of finite elements using experimental outcomes.

The finite method is based on finite elements which connect with limited joints. The following parameters must be defined for the structural analysis: structure geometry, boundary conditions, properties of materials, and loading. The results show that we should read any displacement values from the grid points and stresses.

ANSYS is a commercially used FEM package that has multiple capabilities to help in linear, simple and static analyses and complex and non-linear analyses. It contains different modules every one of which applies to certain set of problems. For instance, ANSYS civil is widely used in construction and structural analyses. In the same manner, ANSYS flow transit analyzes the levels of liquid flows. Using ANSYS is more beneficial because of its pre-processor and post-processor software.

ANSYS is generally used as an FEA (Finite Element Analysis) package. FEA is a numerical process that helps to convert a complicated process into smaller portions called elements. The software solves equations, manages the behavior of elements and solves all of them, thereby creating an idea about the overall functioning of a system. It is possible to present outcomes in graphic or tabulated form. These analyses help in the design and optimization of systems which are otherwise difficult to analyze. Such systems are very complicated because of their geometric configurations, scale and main equations.

Moreover, ANSYS is one of the most cost effective ways to assess any product and its performance because its information is readily and virtually present. Product development using ANSYS is also called virtual prototype generation.

A number of virtual prototyping options are available in which a user iterates many options that optimize a product well before beginning any kind of production. This reduces the market risk and saves on the costs of developing inappropriate products or designs. With a multi-faceted ANSYS, users are able to observe the impact of any

design and the effect of a product along with its properties, such as mechanical, electromagnetic or thermal properties.

Since ANSYS mechanical software has been a trusted brand all over the globe, it has helped to resolve complicated thermal and structural issues rapidly and with maximum convenience. It is possible to simulate a structure or component using ANSYS and it also allows complex non-linear statistical analyses regarding deformation and stress. Therefore, it virtually determines the impact of vibration or any other movement with the help of its advanced non-linear processes that have a dynamic impact.

With ANSYS, it is possible to import complex geometry and use it for assemblies, or the creation of meshes or appropriate boundaries. It also analyzes variables including motion, vibration strength, and other important variables. Many graphic design and modeling software packages can visualize a simulation and allow modification, re-modification and optimization of a design. When solving any problem analytically, it is necessary to define:

1. The possible domain of a solution or solutions.
2. A practical model.
3. The applied loads and boundary conditions.
4. The physical characteristics.

This program consists of several modules. The module primarily used in this thesis is the workbench module. This module allows the user to import geometry from other rendering programs and create a model based on this geometry. A project in ANSYS Workbench is divided into seven steps:

1. Analysis system
2. Engineering data.
3. Geometry
4. Model
5. Setup

## 6. Solution

## 7. Results

At this point, it becomes possible to solve a problem showing the desired outcomes. If we opt for a numerical method, our additional step is generally the generation of a mesh. It turns a complicated model into divisible parts to make it solvable.

Using ANSYS, it was found that fatigue was the reason behind 50% to 90% of structural failures. Therefore, experts required a high-quality, reliable fatigue design tool. No such tool has yet been available that allows productivity with flexibility in comparison with other analysis tools. Consequently, many analysts and designers had to design and invest their own fatigue assessment programs that cost financial resources and time. In the future, engineers, analysts and designers are expecting to have a complete library containing fatigue tools to fulfill their requirements. To assist designers to analyze fatigue, ANSYS provides any required information to help to assess when fatigue failure is likely to occur.

Fatigue analyses are primarily divided in three aspects: material, analytical and evolutionary, as seen in Figure 4.1 which shows each area being discussed in more detail below.



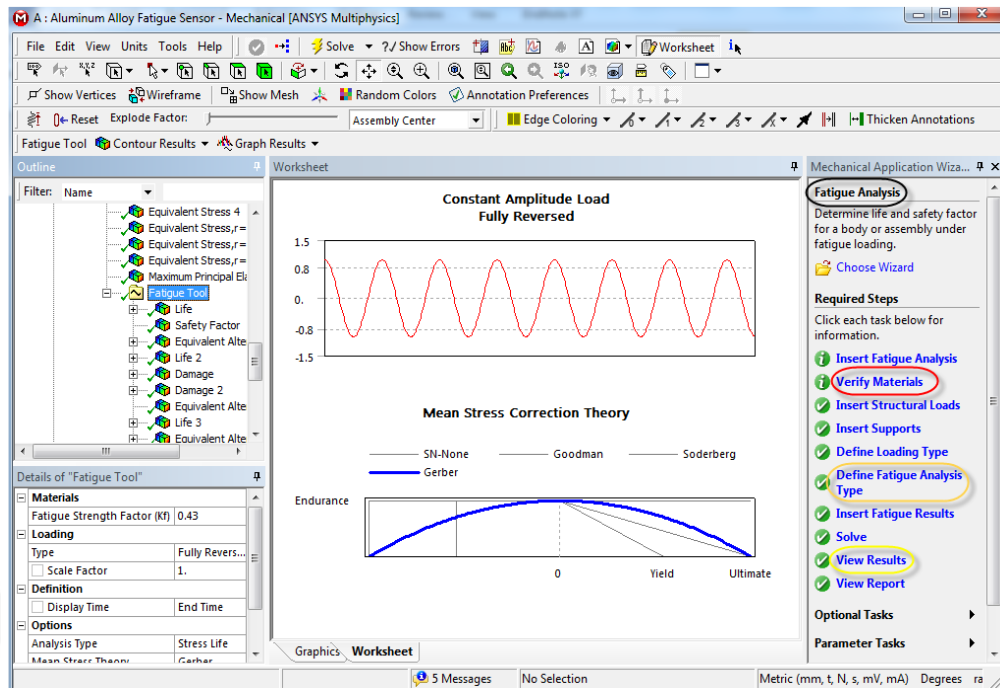


Figure 4.1. ANSYS steps for fatigue.

A major portion of fatigue analysis depends on the correct information about the material, its properties and fatigue. Certainly, fatigue is empirical; therefore, fatigue curves help to make assessments regarding aluminum alloys and steels. They are used only as guidelines directed towards users obtaining fatigue data for better analyses. For assemblies with different alloys, every one of them will have separate fatigue properties.

Some decisions regarding inputs might change and this depends on the choice as to whether a researcher conducts stress life or strain life analysis. Therefore, much actually depends on the choice of the type of fatigue analysis. The outcomes exist ranging from contour plots to particular outcomes throughout the model as information is given regarding the point of damage in a model. The following are types of results needed in the context of fatigue analyses, as in Figure 4.2:

1. Fatigue life
2. Fatigue damage at a certain point in the design life
3. Fatigue factors such as design safety
4. Stress biaxiality

5. Fatigue sensitivity diagram
6. Rain flow matrix output
7. Damage output

Available stress life results include equivalent alternating stress and available strain life results include the hysteresis.

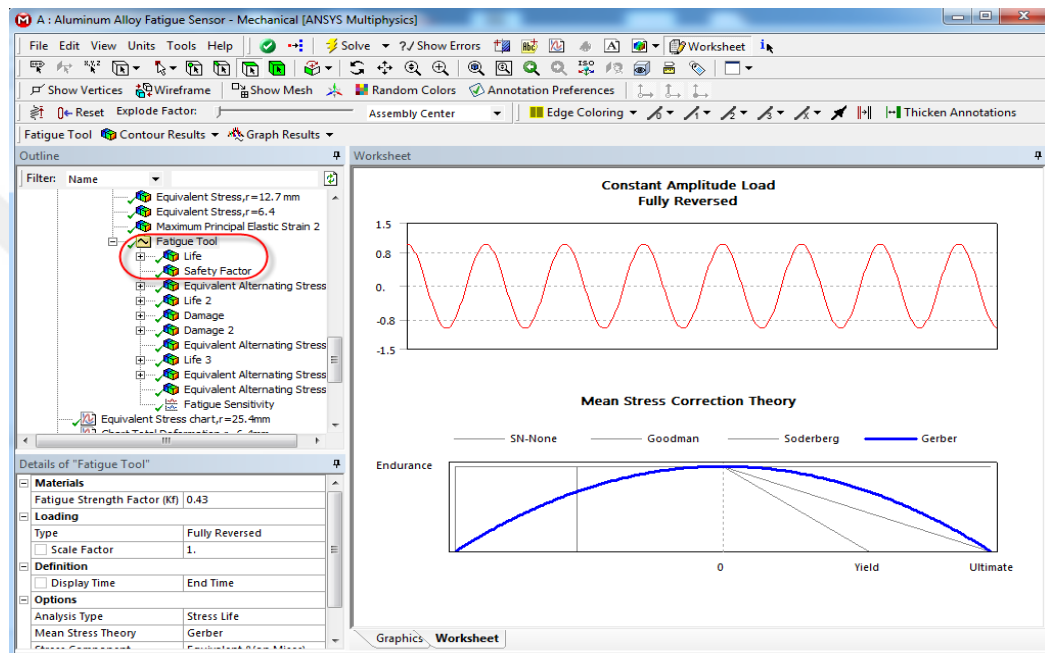


Figure 4.2. Fatigue tool information using ANSYS.

### 4.3. SENSOR DESIGN

Our goal in this project was to design, analyze and assess fatigue life in reverse-edge U-notch sensors using the original technique to solve this problem of fatigue structure that predicts fatigue life.

The sensor consists of multiple sensing arms, mounted parallel to the primary tensile axis of the monitored structure with notches of varying geometry in the arms. By closely mounting the sensor to the structure, it was anticipated that the sensor would experience the same strains as the structure, but it would accumulate fatigue damage at a much higher rate by the virtue of the notches. Carefully designed notches are expected to fail at progressively larger numbers of load cycles, and the notch failures

could be correlated with the accumulation of a known amount of fatigue damage in the monitored specimen.

### 4.3.1. Define Material Properties

The fatigue sensor material used was aluminum alloy 7075-T6. The mechanical properties of aluminum alloy 7075-T6 used for the sensor are presented in Section 4.7.2. Figure 4.3 shows the steps to obtain the mechanical properties of 7075-T6.

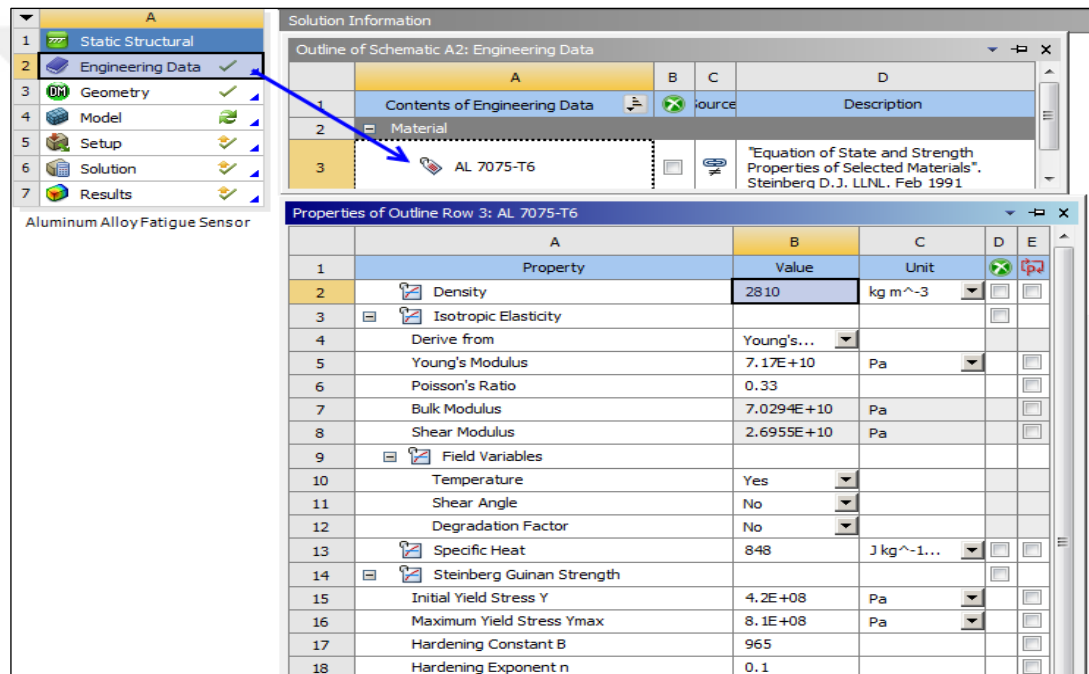


Figure 4.3. Steps for aluminum alloy 7075-T6 mechanical properties in ANSYS.

### 4.3.2. Geometry Creation

Geometric modeling is possible through ANSYS Workbench, which is an automated and flexible program for customized applications. The design modeling options in ANSYS facilitate users during simulation, which includes creation of parametrical geometry, creation of models, geometrical modifications, automation cleanups and repairs in addition to large numbers of custom tools for structural and other analyses.

The finite-element model was created on ANSYS Workbench for the geometry (Figure 4.4) performed in 2D. The sensor model consists of beams with a reverse-edge U-notch. The fatigue sensor designed in this study has an understood width and length. This geometrical configuration for width, length and thickness is shown in Table 4.3.

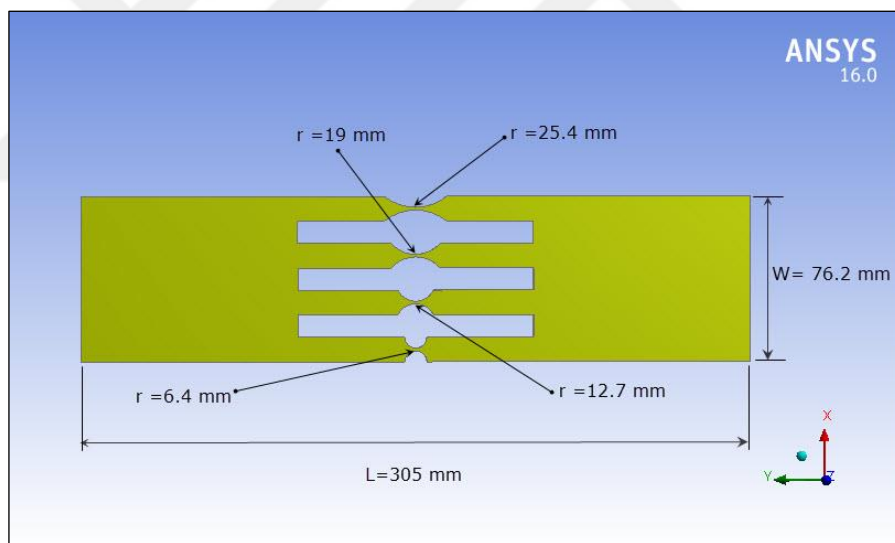


Figure 4.4. Dimensions of the sensor model.

Table 4.3. Dimensions of the sensor model.

Width	Length	Thickness
76.2 mm	305 mm	1.6 mm

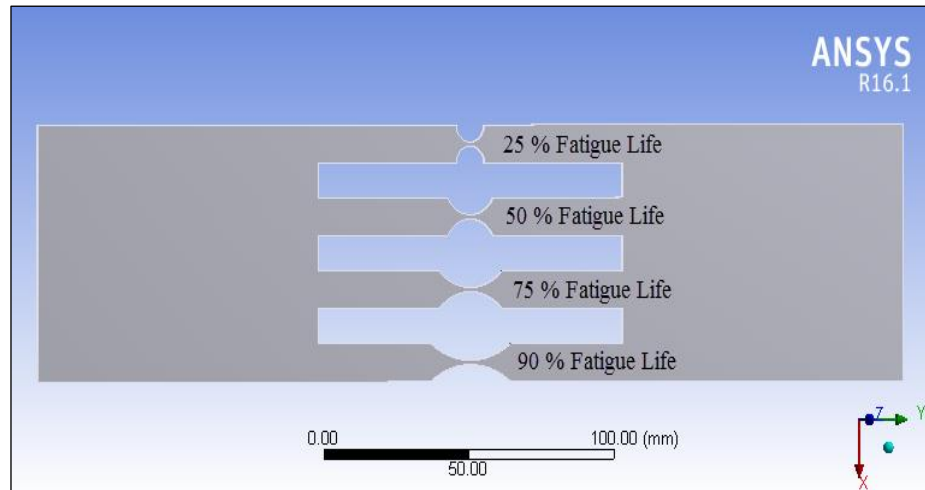


Figure 4.5. Fatigue life percentage of the sensor model.

Figure 4.5 shows the four types of percentage we used. In this model, the fourth situation with different fatigue lives is used. The sensor monitors fatigue developments by utilizing breakable fingers. Uncommon geometrical configurations were utilized to manufacture the inward fingers with guaranteed finger breaks at 25%, 50%, 75% and 90% normal component lifetime. The remote ability gains were simple to screen with the ground of the expected life time having no closeness to the sensor. The steps of “Geometry Creation” are as following:

**- Start ANSYS Design Modeler**

We open ANSYS Workbench and also open Geometry cell given in a static structural analysis system, which shows the ANSYS design modeling applications. Right-clicking Geometry cell also displays a context menu that allows a user to select *New Geometry*, as shown in Figure 4.6.

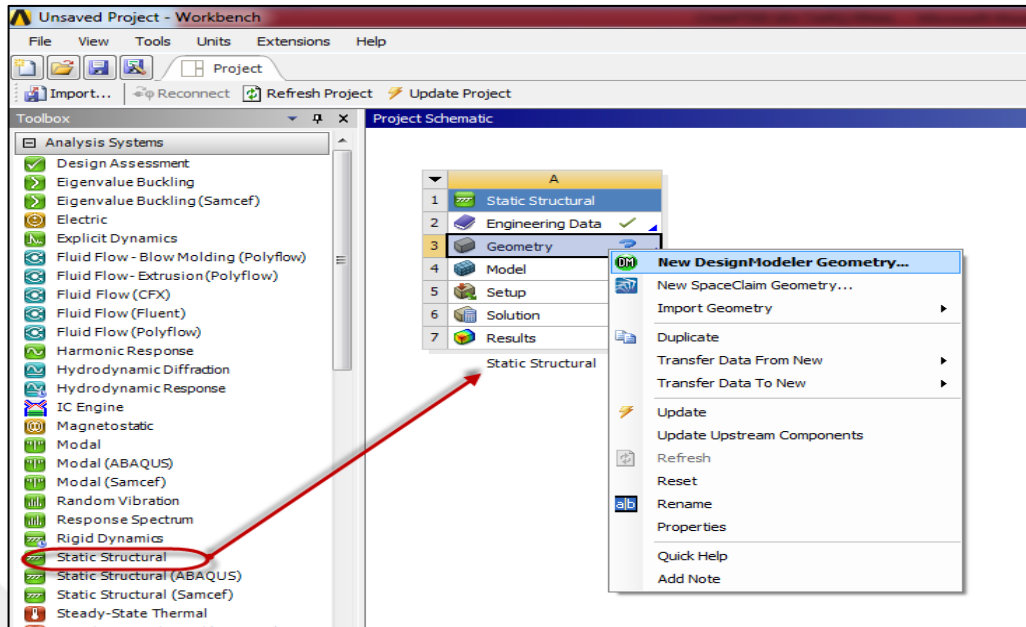


Figure 4.6. Static structural analysis procedure.

**- Enter Units in ANSYS Design Modeler.**

As soon as ANSYS Design Modeler appears, a user should choose a required system with length units. For learning, a user needs to define the geometry in millimeters before conducting static structural analyses in SI units. For details, see Figure 4.7.

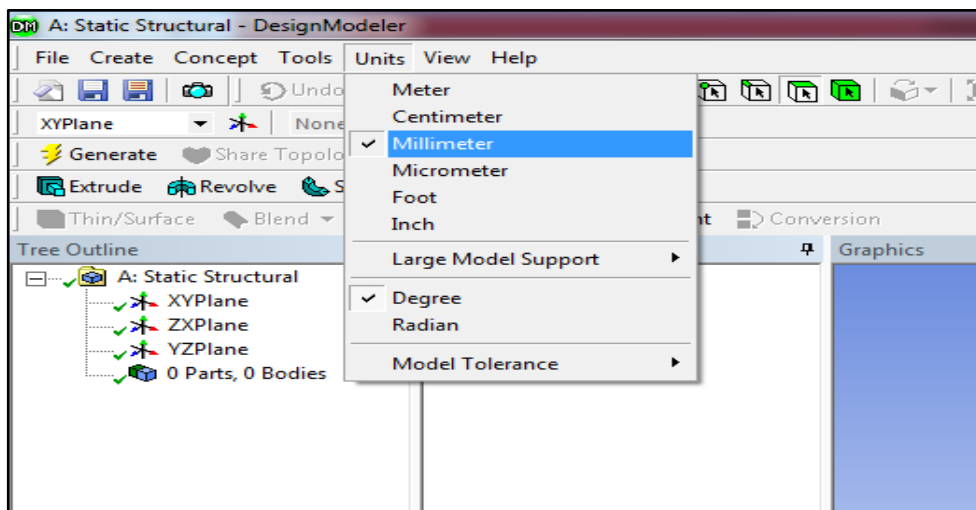


Figure 4.7. Setting the units in ANSYS design modeler.

## - Create the Geometry

The geometry for this study consists of the fatigue sensors with four beams. To create the U-notch beams, the extrude operation is used. For the extrude operation, we first define a sensor for extrusion (having a couple of half circles having symmetry with a reverse edge U-notch and generating the body sensor geometry), as illustrated in Figures 4.8, 4.9, 4.10 and 4.11.

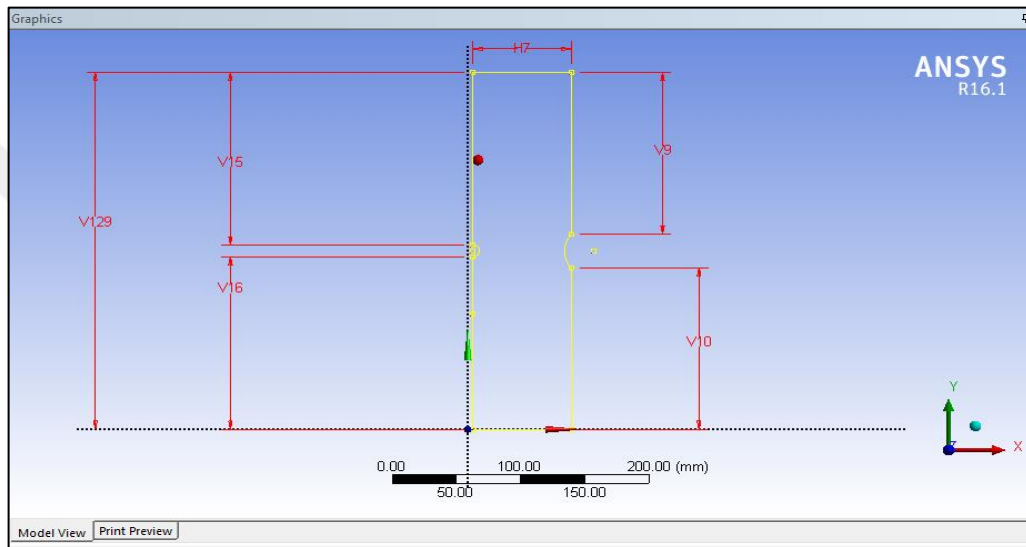


Figure 4.8. The sketch of body sensor.

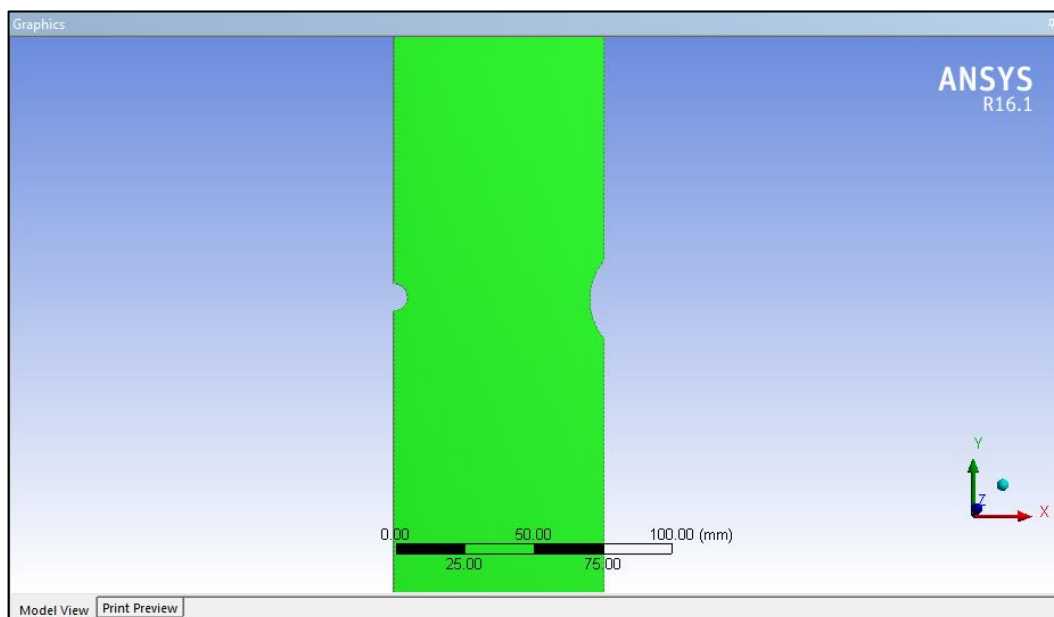


Figure 4.9. Extruding the body sensor.

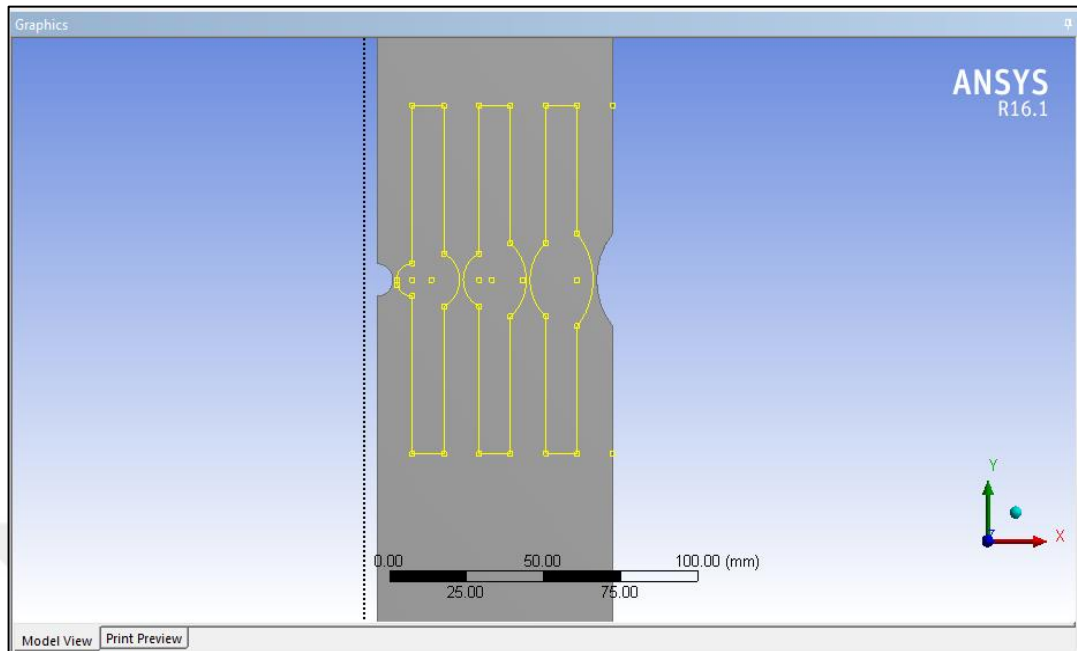


Figure 4.10. Sketch of U-notch beams.

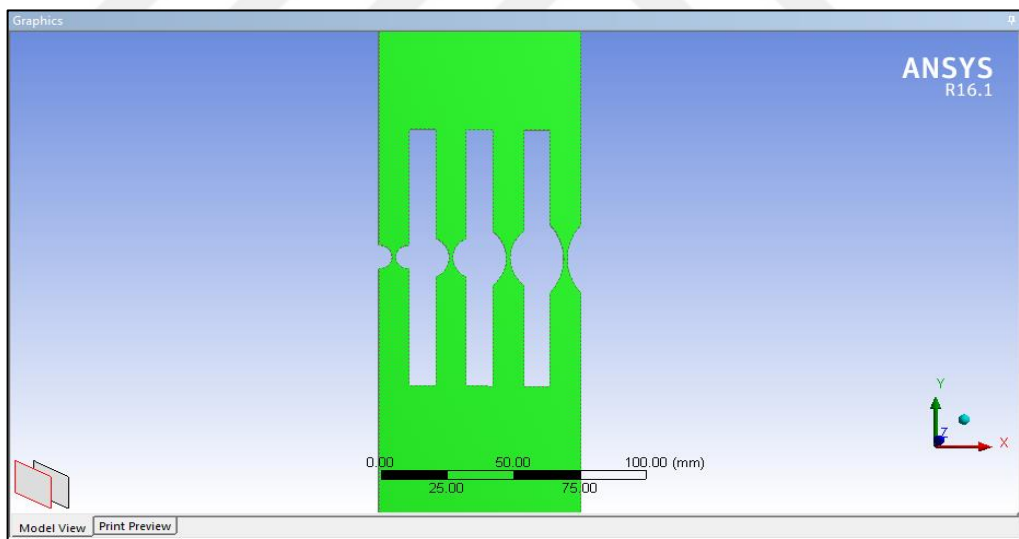


Figure 4.11. Extruding the U-notch beams.

Finally, we obtain the final shape of the fatigue sensor, as illustrated in Figure 4.12.



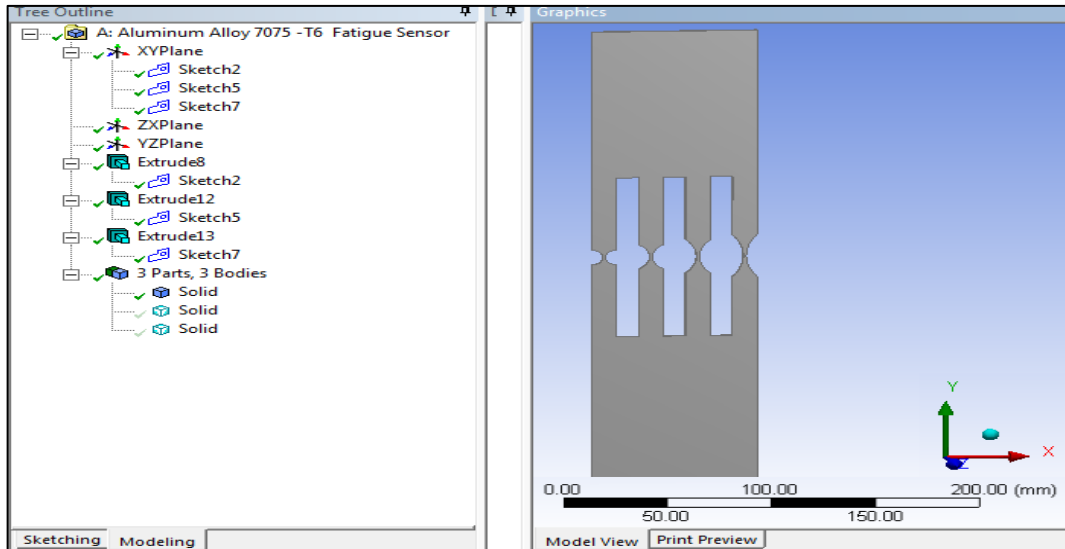


Figure 4.12. Fatigue sensor geometry in ANSYS software.

#### 4.3.3. Meshing of the Fatigue Sensor Model

Meshing is used by all FEA analysis programs to divide the model into elements. Generally, a finer mesh will increase accuracy of the results but dramatically increase simulation time. A coarser mesh will decrease accuracy but also decrease the simulation time. This is because if the number of elements is higher, there will be a high number of equilibrium equations that the program needs to solve. Finding a good balance between mesh quality and result accuracy is essential when reducing simulation time in complex analyses, such those carried out in this thesis.

In ANSYS there are several meshing methods that can be used. To achieve the desired meshing of the model, a combination of different methods was chosen. Since the model basically consists of four beams, different meshing methods would be necessary. If the meshing method is set to automatic, a mesh would be created with an uneven and overly fine mesh, which in this case, would cause the simulation time to increase drastically.

The many functions available via the Mesh Tool, including:

1. Control of smart sizes
2. Adjustment of element sizes
3. Specifying element shape(s)
4. Specifying mesh type
5. Meshing solid model entities
6. Clearing meshes
7. Refining meshes

In Figure 4.13, we see an outcome of automatic mesh generation. The mesh looks decent and uniform for this model. This, however, would make the results of a simulation inaccurate. The total number of elements in this mesh exceeds 200. It would not be advisable to run a simulation with this kind of meshing as it would be both time-consuming and inaccurate.

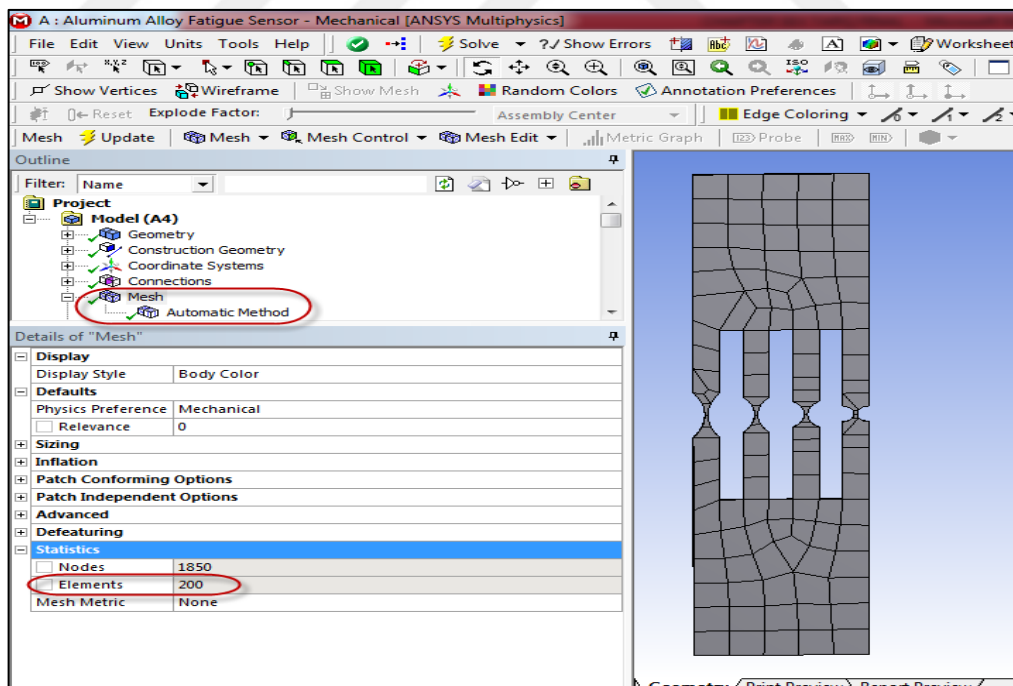


Figure 4.13. Automatic mesh method.

It shows a custom mesh, which we have defined keeping in view all aspects of the mesh. Although the mesh is slightly coarser than the auto-generated mesh, it is much

more even and uniform. Making the mesh finer than this might increase accuracy, but maintaining a good accuracy-to-simulation time ratio for this mesh was considered to be sufficiently accurate with the total number of elements in this mesh exceeding 106727 elements, as in Figure 4.14.

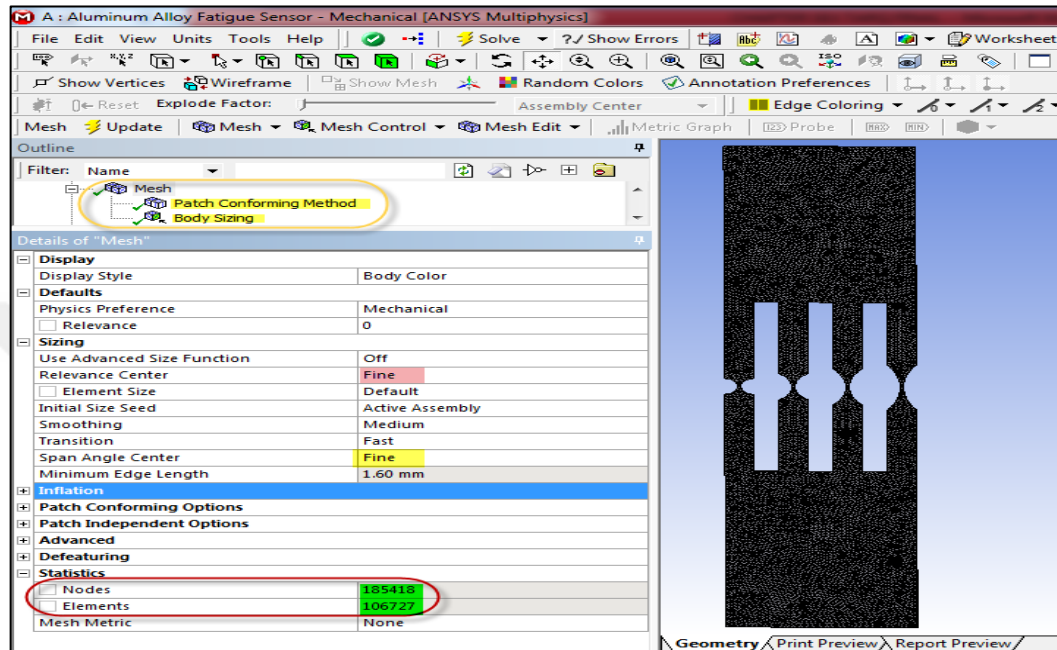


Figure 4.14. Fine mesh of the sensor model.

More elements in the critical region in the U-notch radius are required to obtain accurate results. Therefore, refining the mesh is obvious, as in Figure 4.15, and the total number of mesh elements exceeds 121561 as shown in Figure 4.16.

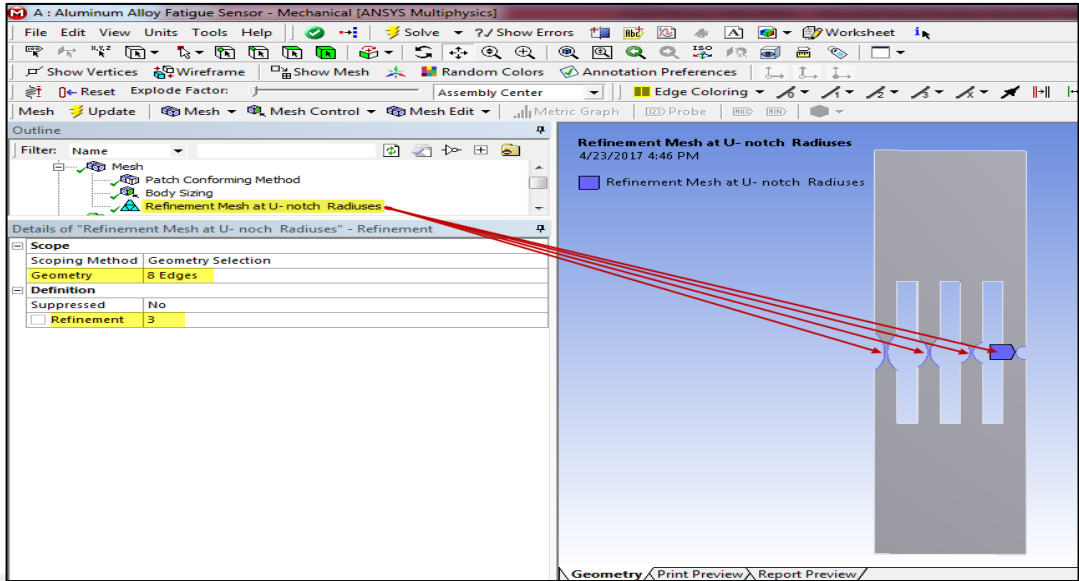


Figure 4.15. Mesh refinement steps.

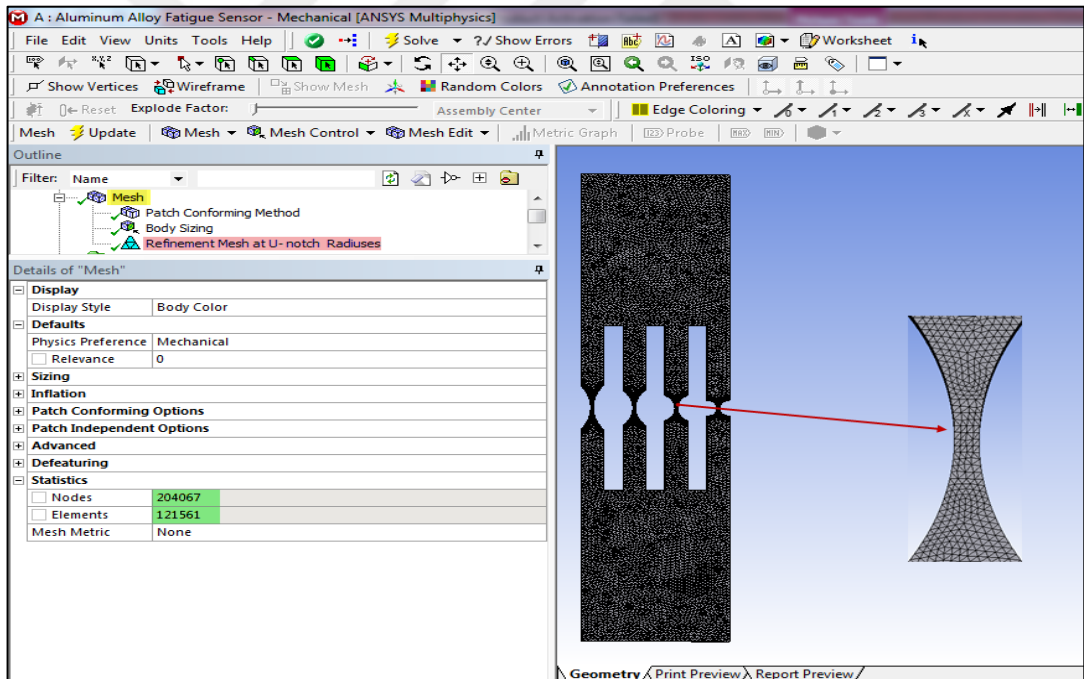


Figure 4.16. Refinement of the mesh in a sensor model.

#### 4.3.4. Applied Loads and Boundary Conditions

An objective finite element analysis examines the structure or components and its response to specific loads. Mentioning loading condition is a significant step in conducting a credible analysis. It is possible to apply a load in a model through

multiple methods using ANSYS. The load step option helps to control a load while finding a solution.

We applied boundary conditions to a fatigue sensing model. Specific non-variable boundary conditions were given for the bottom side of a fatigue sensor model disabling any movement on the  $x$ -axis,  $y$ -axis and  $z$ -axis, as shown in Figure 4.17. The displacement boundary conditions only allow movement along the  $y$ -axis (the  $x$  component and  $z$  component were zero and the  $y$  component was free), as seen in Figure 4.18.

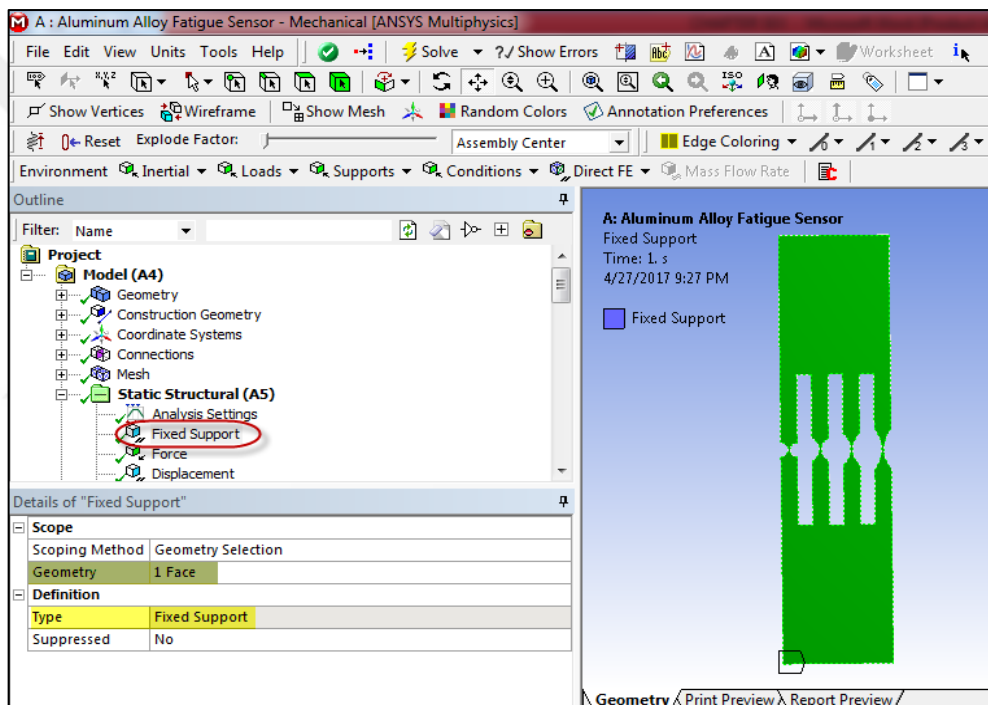


Figure 4.17. Fixed boundary condition in a fatigue sensor model.

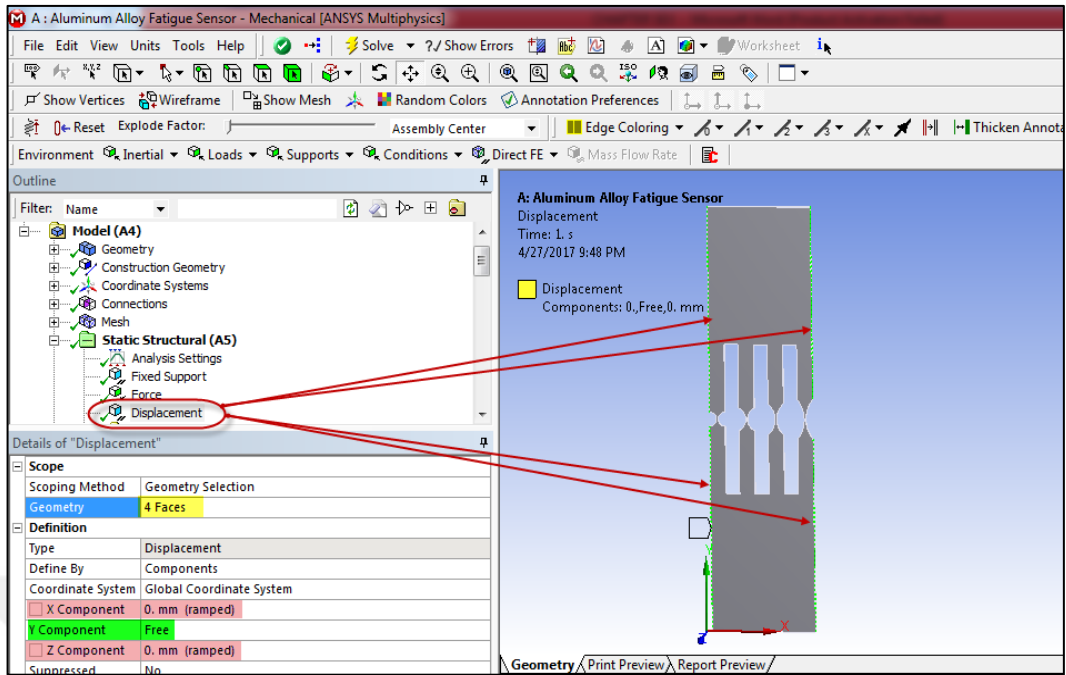


Figure 4.18. Displacement boundary conditions of the fatigue sensor model.

ANSYS developed a finite element model that estimates the nominal stresses and fatigue life under tensile loading by applying it to the top face of a fatigue sensor model, as in Figure 4.19.

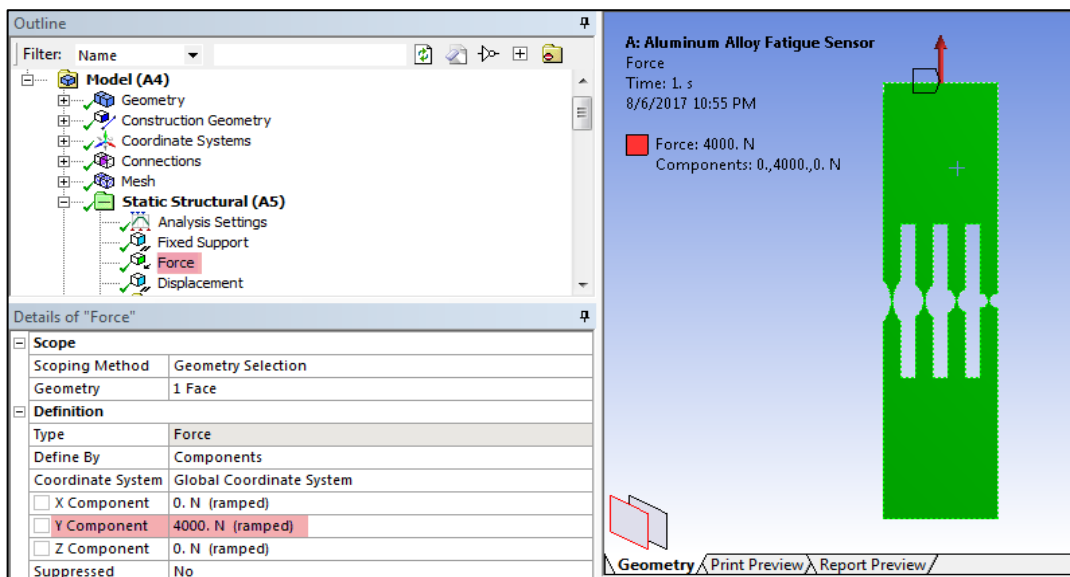


Figure 4.19. Applied load of the fatigue sensor model.

The sensor has different applied tension loads to estimate the changes to the fatigue lives of the U-notch sensor under different loads and to optimize the high loading that the sensor withstands prior to failure occurring. The magnitudes of the loads are given in Table 4.4.

Table 4.4. Magnitudes of tension loads.

Case No	Tension Load (N)
1	1000
2	2000
3	3000
4	4000

#### 4.3.5. Solving of the Fatigue Sensor Model

The solution steps analyzing the fatigue sensor model are given in Figure 4.20. It is necessary to define the stress tool, the deformation, the strain, the stress and the fatigue tools in order to use the fatigue sensor model, after which finally, the solution will be provided. Now we shift to the general post-process step to read the results following different methods as nodal or element solutions. ANSYS observes the state (transient or steady) and solves the problem.

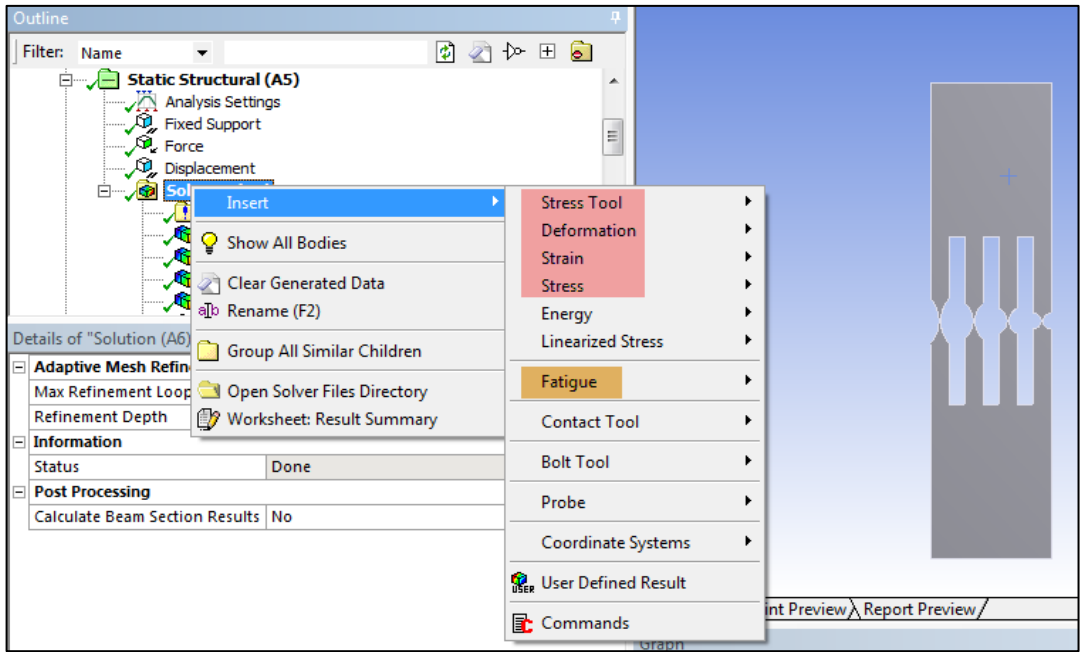


Figure 4.20. Solution steps analyzing the fatigue sensor model.



## **PART 5**

### **FINDING AND DISCUSSION**

#### **5.1. FINITE ELEMENT SOLUTION**

This chapter consists of an analytical summary based on the analytical approaches used so far and concerning simulation outcomes. Understanding deformations is an objective of numerical simulation, whereas distributions of stress and fatigue life of a sensor are among other objectives. These outcomes are compared because several aluminum alloys have been tested. In Chapter 4, we discussed the FE model and performed ANSYS processing which provided certain outcomes. When considering the outcomes of simulations obtained using ANSYS, some modifications are required in the FE approach for the refinement of results. The solver performs the analysis and finally evaluates the results. These simulations support design, analysis, and fatigue life evaluation of reverse edged U-notch sensors by using the original technique to solve this problem. When we compare the results with different types of aluminum alloy, we obtain our findings. ANSYS facilitates static, transient and buckling analyses; however, the FE static approach is suitable for loading conditions. Normally, this analysis is a series of defined events, so the FE approach provides the situation for the next step. The details of the ANSYS simulations are given in the next section.

The FE model was designed using ANSYS and it has similar boundary and loading conditions as well as properties. It is meshed using ANSYS refinement. Triangular substances suit the modeled curved structures very well. It has 204067 nodes and 121561 elements. The meshing of the model sensor is shown in Figure 5.1.

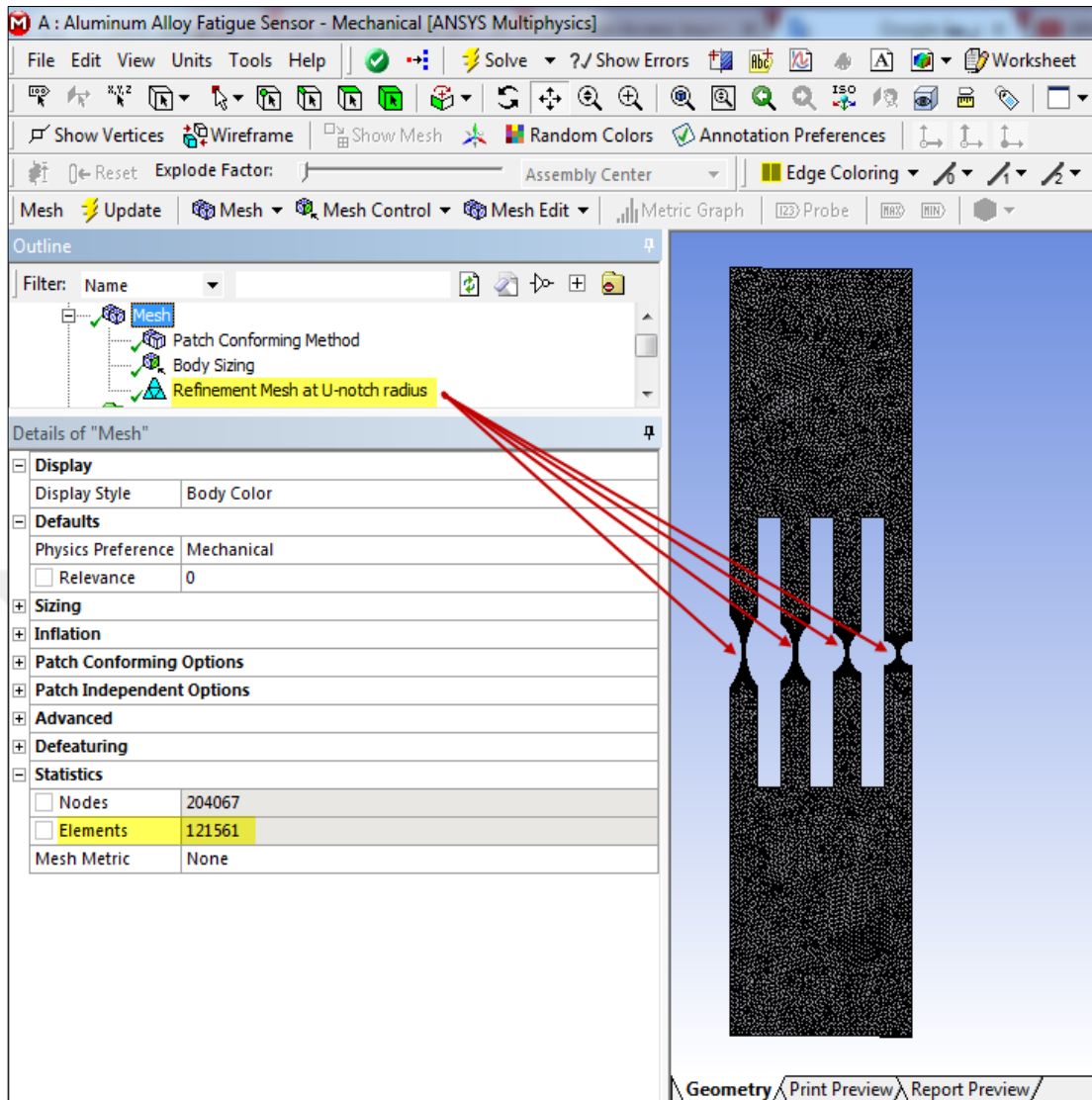


Figure 5.1. Meshing model implemented in ANSYS.

In order to achieve accurate simulation results using more elements in the critical region of the U-notch, refinement of the mesh becomes necessary, as shown in Figures 5.2 and 5.3. For this reason, 121561 mesh elements and 204067 nodes were used.

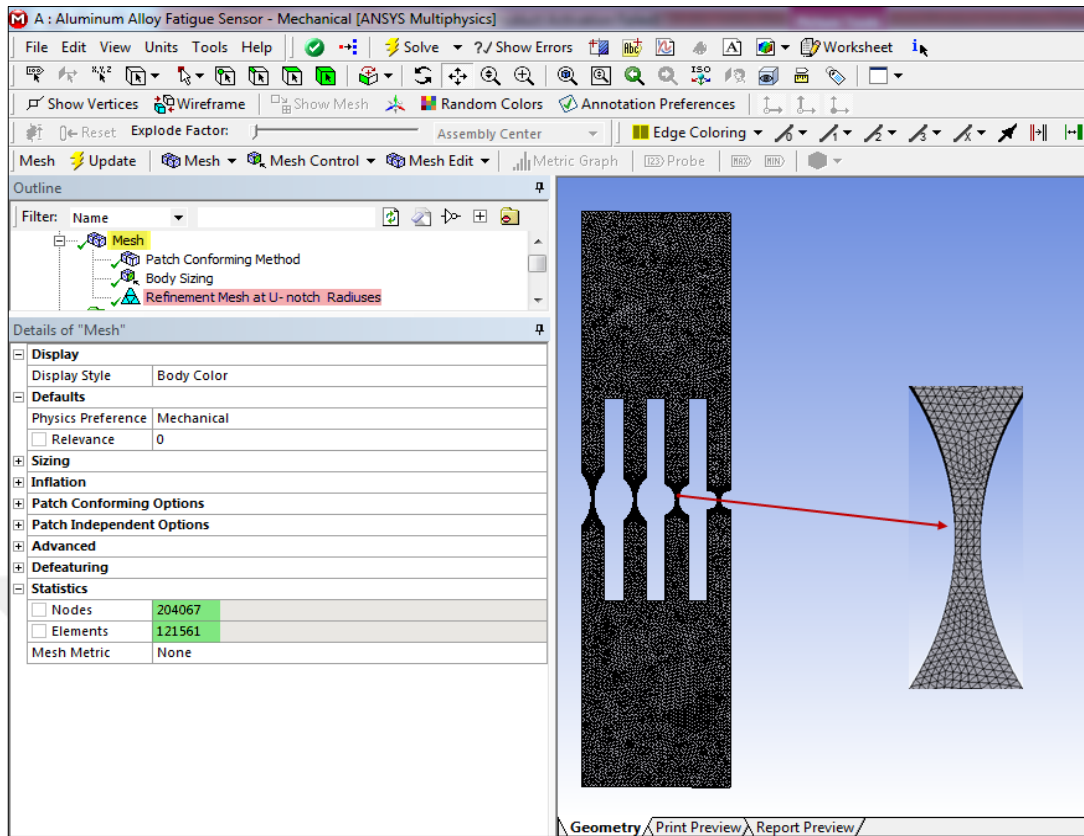


Figure 5.2. A fine mesh is used around the U-notch of the model.

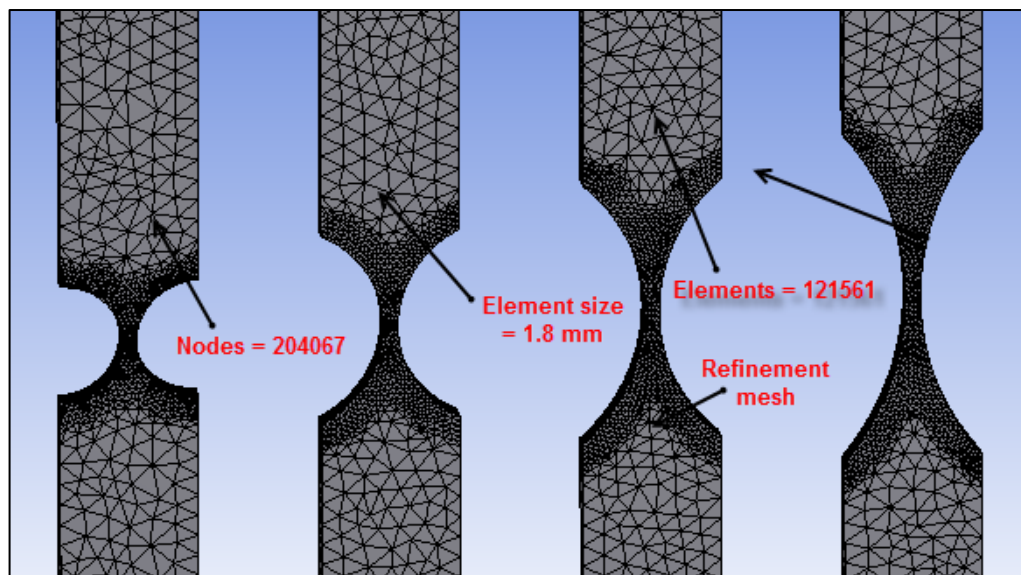


Figure 5.3. Simulation results of the fatigue sensor model.

In order to ensure that the stress concentration is independent of element size, a mesh sensitivity study is performed. Our mesh sensitivity study was carried for five ele-

ment sizes, as listed in Table 5.1. The equivalent stresses were considered for the mesh sensitivity. The mesh has to be refined globally and/or locally to improve stress prediction in the critical regions. The mesh sensitivity analysis was carried out for the critical location ( $r = 6.4$  mm) in the high stress regions obtained during the first iterative analysis of the sensor model.

Table 5.1. The mesh sensitivity analysis.

No.	No. of Elements	Equivalent stress (MPa) ( $r = 6.4$ mm)
1	11,717	93.421
2	21,095	92.023
3	39,367	91.071
4	55,222	91.023
5	121,561	90.815

Figure 5.4 shows the variation of equivalent stresses as a function of the number of elements. It is clear from the mesh sensitivity analysis that the equivalent stress is independent of the mesh size beyond 55222 elements. Although 121561 elements also yield the same results but at higher computational cost, and because the results were not changing after 121561 elements, this refined mesh became also necessary for every future analysis. Based on this result, the stress concentration was due to the notch rather than the mesh itself.

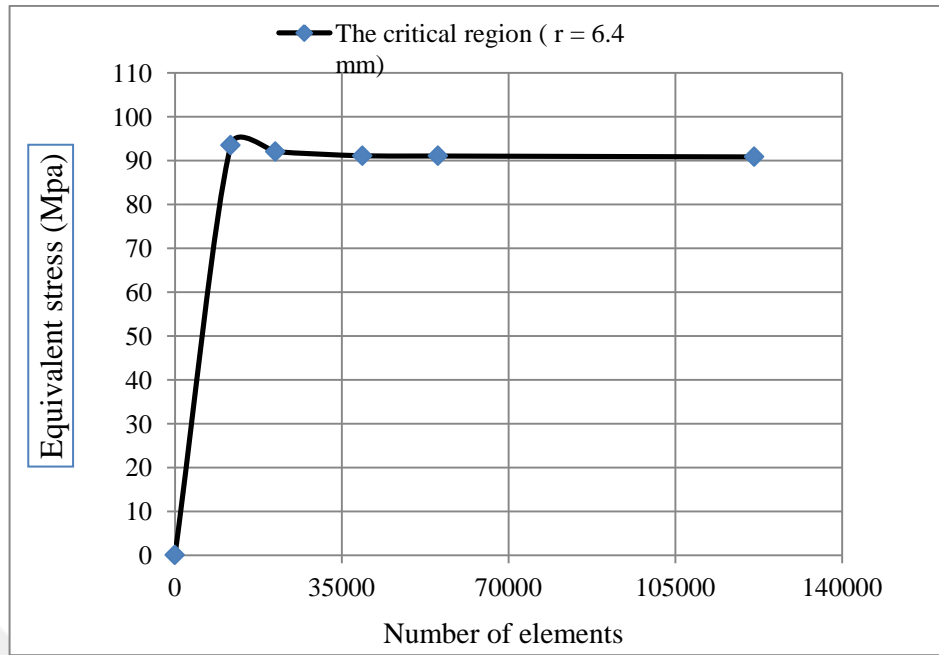


Figure 5.4. Variation of equivalent stresses as a function of the number of elements.

After accomplishment of the simulation in ANSYS, the outcomes are obtained as deformations, stress distributions and fatigue lives. These are as follows:

The fatigue notch factor ( $K_f$ ) can also be calculated according to Peterson's equation (3.18), as in Table 5.2.

Table 5.2. Magnitudes of the fatigue notch factor ( $K_f$ ).

Notch Radius (mm)	Stress Concentration Factor ( $K_t$ )	Fatigue Notch Factor ( $K_f$ )
6.4	1.06	1.056
12.7	1.03	1.028
19	1.02	1.021
25.4	1.01	1.009

## 5.2. DEFORMATION RESULTS

The ANSYS deformation result is described as follows:

### 5.2.1. Total Deformation Result

The total deformation behavior can be obtained through simulation results which show structural total deformations. These values exist within an agreeable range. The total deformation results are increasing on the right side of the model. The total deformation for the fatigue sensor model is shown in Figure 5.5. The maximum total deformation is equal 0.34379 mm and it occurs on the right side of the model. The minimum total deformation is equal to 0.0 mm, which occurs on the left side of the model as expected.

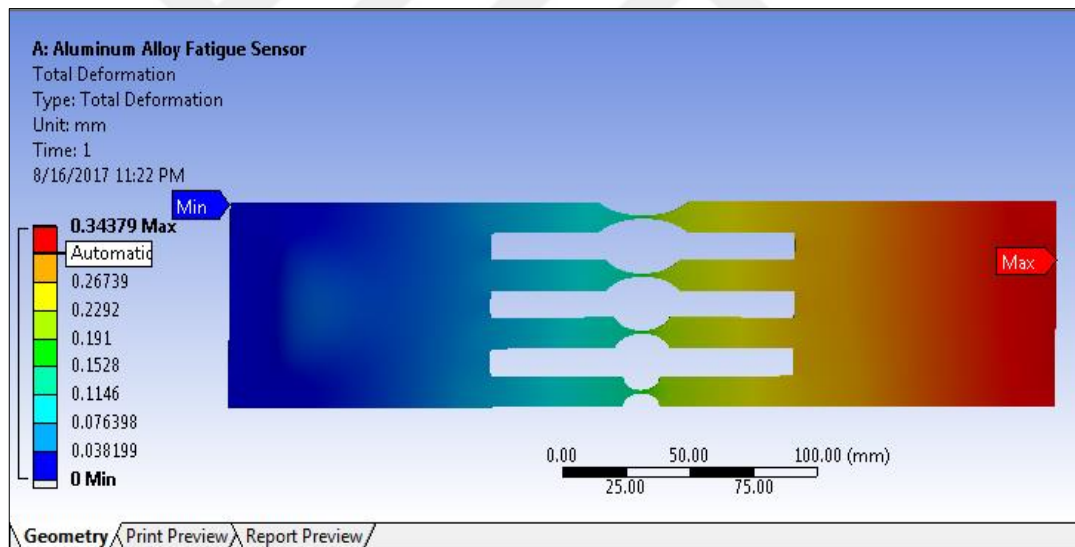


Figure 5.5. The total deformation behavior of the fatigue sensor model.

Figures 5.6 and 5.7 illustrate the total deformation in middle of the sensor (at a length of 152.5 mm) for the smallest U-notch radius ( $r = 6.4$  mm) at 0.14872 mm and for the largest U-notch radius ( $r = 25.4$  mm) at 0.15166 mm. Therefore, these data show that the strain will differ at the notch roots due to different notch geometries.

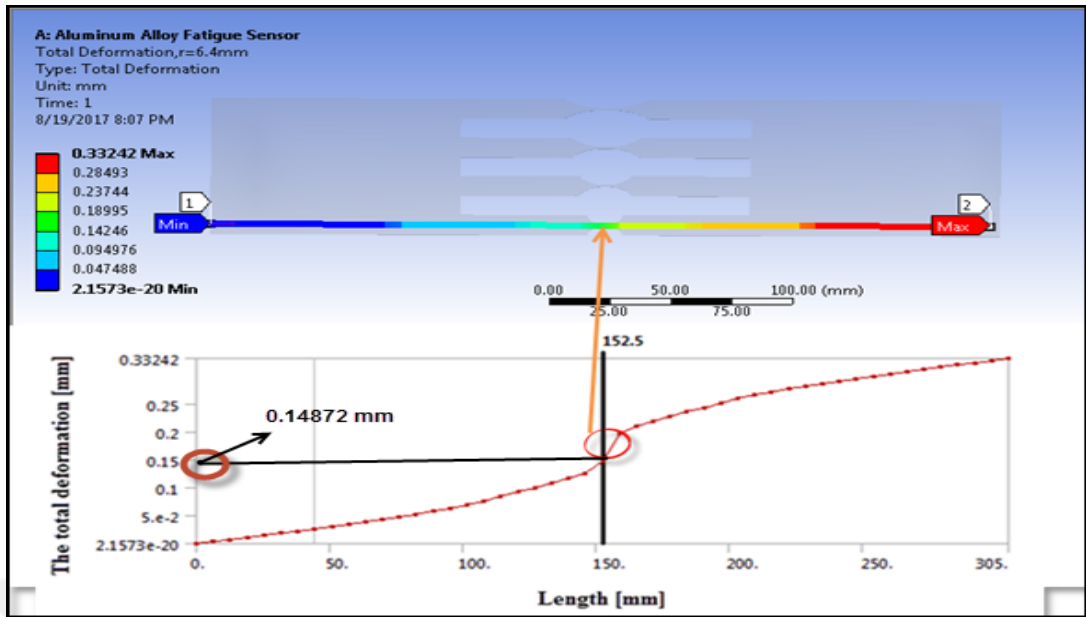


Figure 5.6. Total deformation of the fatigue sensor model at  $r = 6.4$  mm.

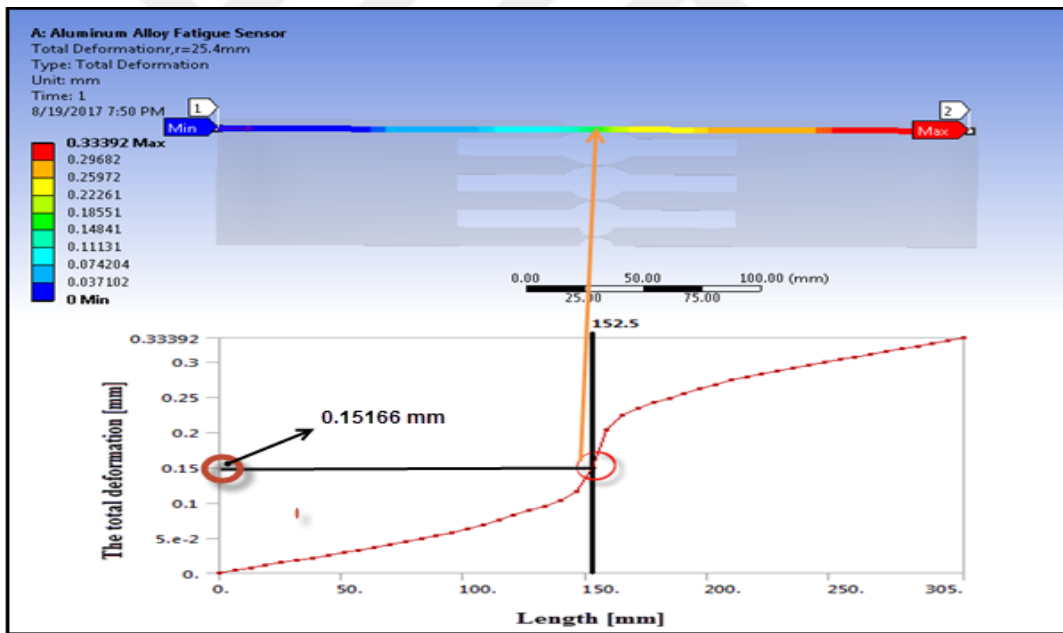


Figure 5.7. Total deformation of the fatigue sensor model at  $r = 25.4$  mm.

### 5.2.2. Directional Deformation Results

Deformations exist along the  $y$ -axis. Outcomes illustrate that deformations are symmetric, as in Figure 5.8, showing a maximum value of 0.3383 mm. It exists on the right side of the model and it is at a minimum under fixed boundary conditions related to the applied load direction. The  $x$ -direction deformations show a similar behavior and axial deformation values are smaller relative to those in the  $y$ -direction.

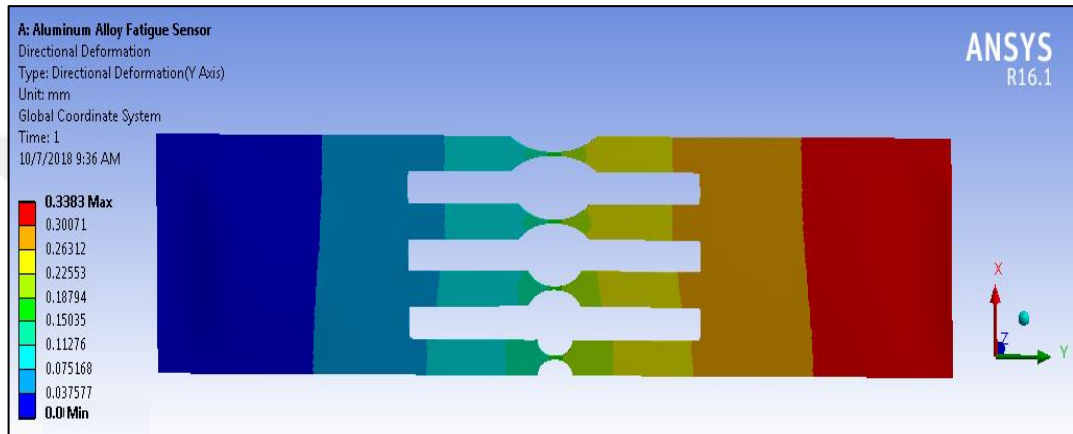


Figure 5.8. Directional deformation along the  $y$ -axis of the fatigue sensor model.

### 5.3. EQUIVALENT ELASTIC STRAIN RESULTS

Equivalent elastic strain was obtained for the fatigue sensor model using ANSYS Workbench. The critical locations were found at the U-notch holes. The maximum equivalent elastic strain was equal to 0.012791 at a U-notch radius of 6.4 mm. Figure 5.9 shows the maximum equivalent elastic strain found around the U-notch holes when the U-notch radius decreased.



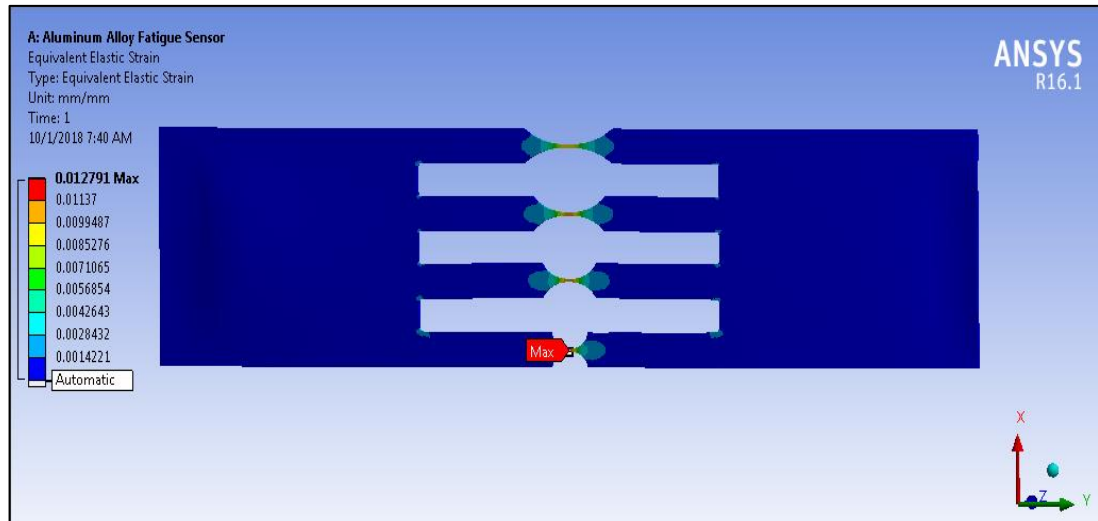


Figure 5.9. Equivalent elastic strain of the fatigue sensor model in ANSYS.

## 5.4. STRESS DISTRIBUTION RESULTS

The outcomes show stress distributions through the fatigue sensor model, which are symmetric because the loading is acting on the right side with fixed boundary conditions on the left side.

### 5.4.1. Normal Stress

When we analyze normal stress outcomes using ANSYS, we observe that normal stress behavior that has symmetry in three directions. The  $x$ -direction  $\sigma_x$  and  $z$ -direction  $\sigma_z$  stresses have the least impact in the absence of loading on the axial direction. The  $y$ -direction with the highest normal stress ( $\sigma_y$ ) was 91.296 MPa. Figure 5.10 shows normal stress distributions in the  $y$ -direction. The outcomes of the stress distribution show that  $\sigma_y$  has a dominating stress when compared with the other stresses. The maximum  $\sigma_y$  exists closer to the U-notched holes.

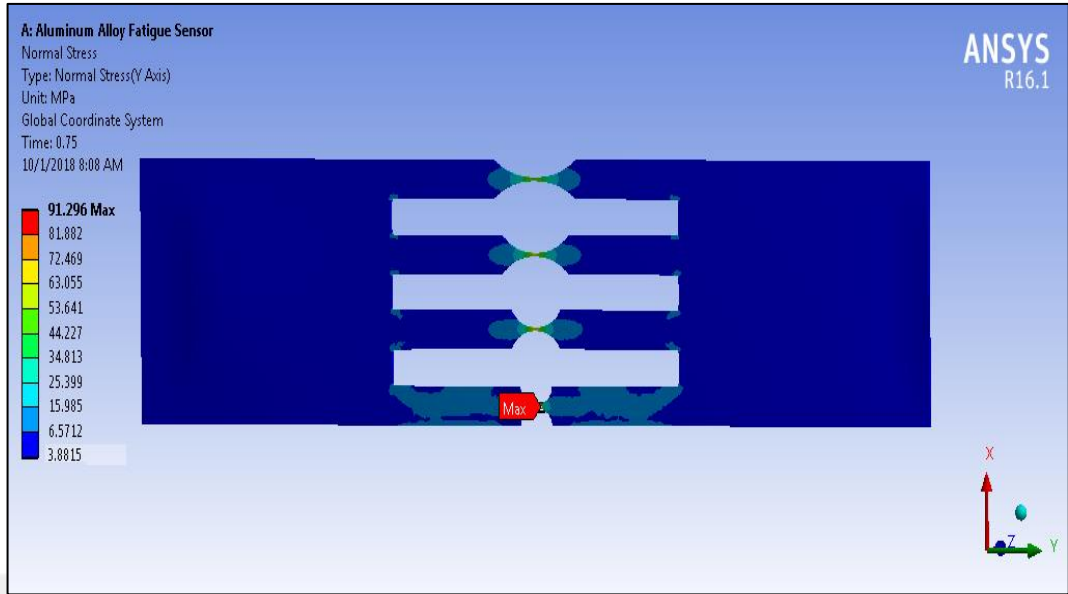


Figure 5.10. Normal stress ( $\sigma_y$ ) distribution in y-direction.

As explained in previous chapters, the investigation of the simulation showed the highest normal stress along the y-axis ( $\sigma_y$ ) near the U-notched holes, specifically at a U-notch radius of 6.4 mm, as seen in Figure 5.11. The maximum normal stress along with the corresponding U-notch radius is illustrated in Table 5.3 and Figure 5.12.

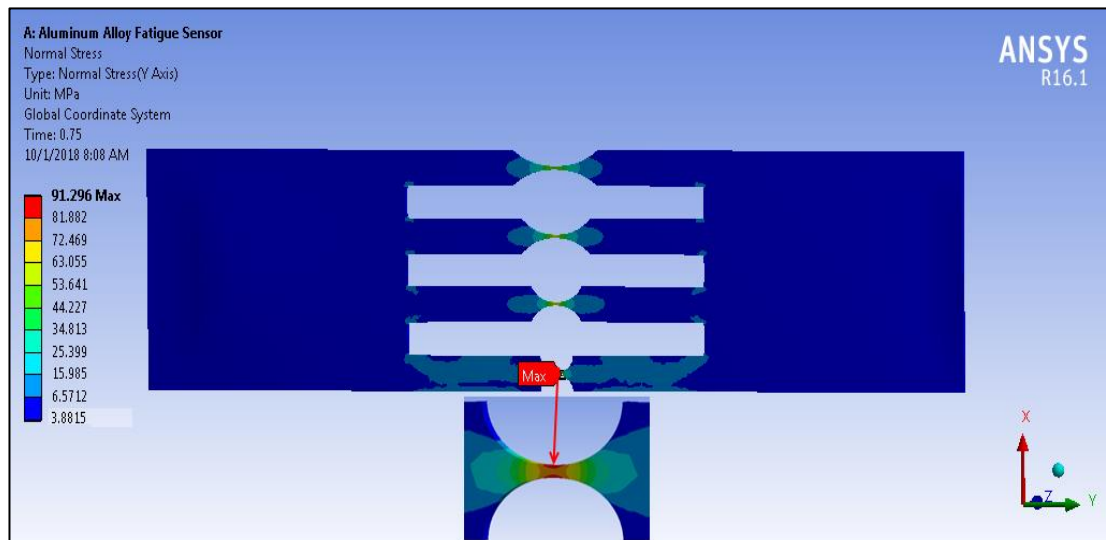


Figure 5.11. Maximum normal stress in the y direction ( $\sigma_y$ ) around the U-notch radius.

Table 5.3. Maximum normal stress with respect to U-notch radius.

U-notch radius [ mm ]	Maximum normal stress [MPa]
6.4	91.296
12.7	86.42
19	78.88
25.4	71.54

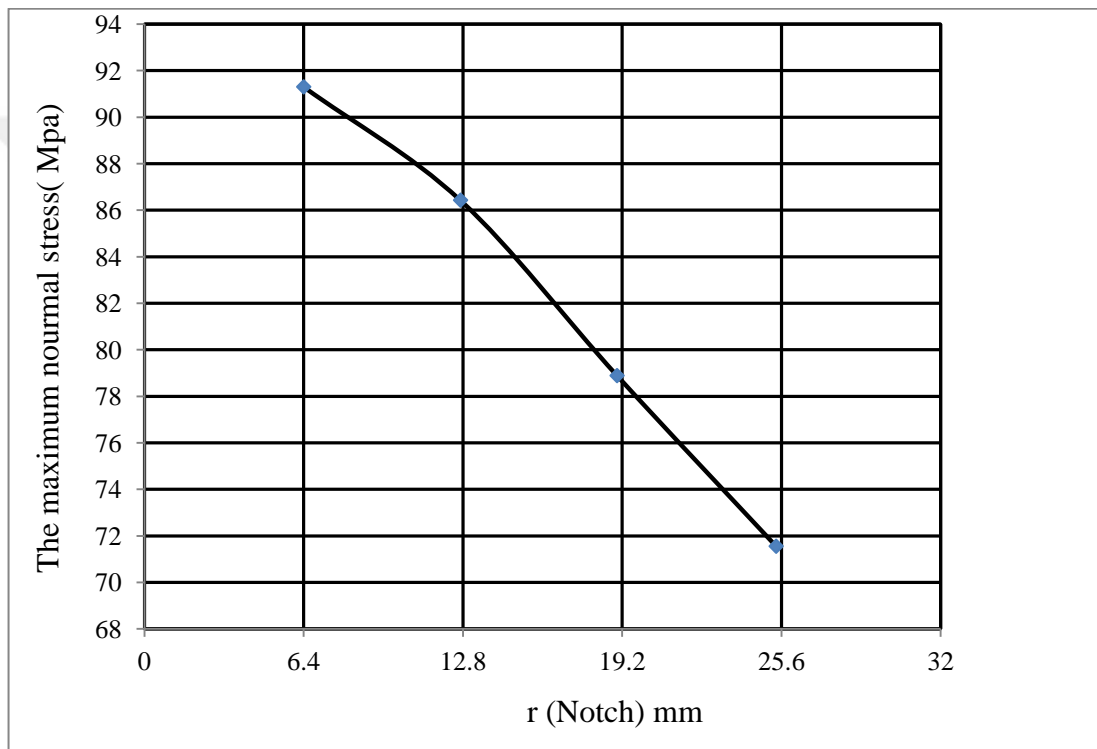


Figure 5.12. Maximum normal stresses with different U-notch radii.

#### 5.4.2. Equivalent Stress (Von- Mises)

Figure 5.13 shows the equivalent stress (Von-Mises) around a U-notch fatigue sensor. The highest equivalent stress occurred at 90.815 MPa, while it was around the U-notch when  $r = 6.4$  mm.

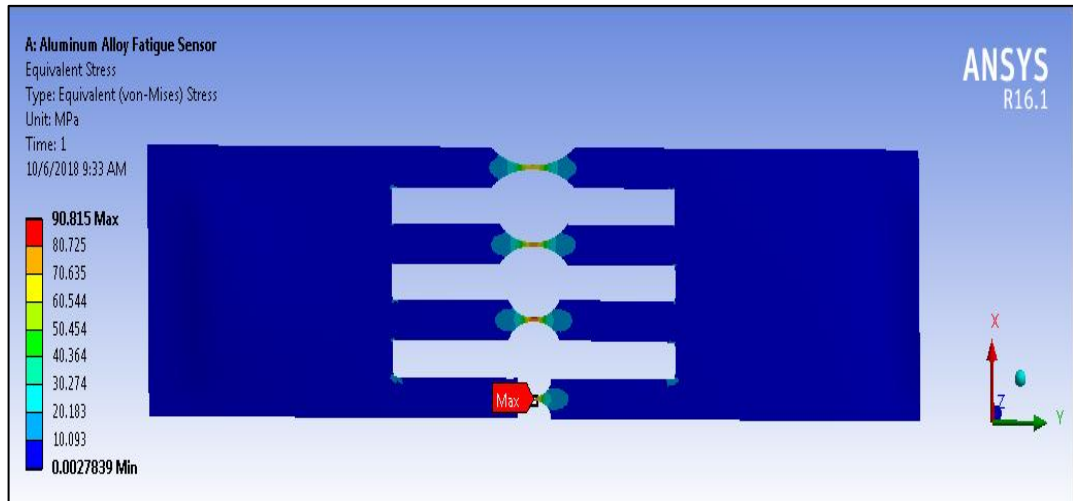


Figure 5.13. Equivalent stresses (Von Mises) distribution around the U-notch.

The equivalent stress distribution for different U-notch radii for the fatigue sensor model can be clearly observed in Figures 5.14, 5.15, 5.16 and 5.17. The equivalent stresses are increased by decreasing the U-notch radius. The simulation shows the maximum equivalent stress as 90.815 MPa at a U-notch radius of 6.4 mm. The equivalent stress decreases by increasing the U-notch radius. For example, at a U-notch radius of 12.7 mm, the equivalent stress is equal to 78.686 MPa. Moreover, for U-notch radii of 19 mm and 25.4 mm, the maximum equivalent stresses are equal to 74.41 MPa and 68.715 MPa, respectively.

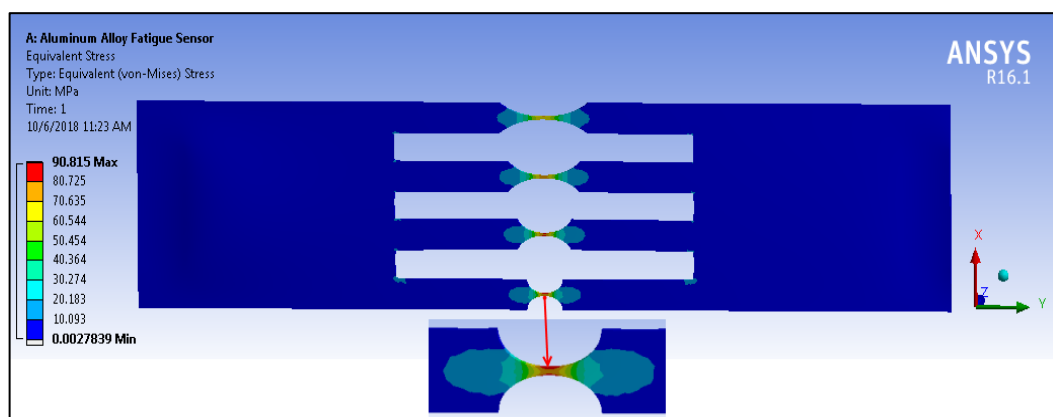


Figure 5.14. Equivalent stress distribution at  $r = 6.4$  mm.

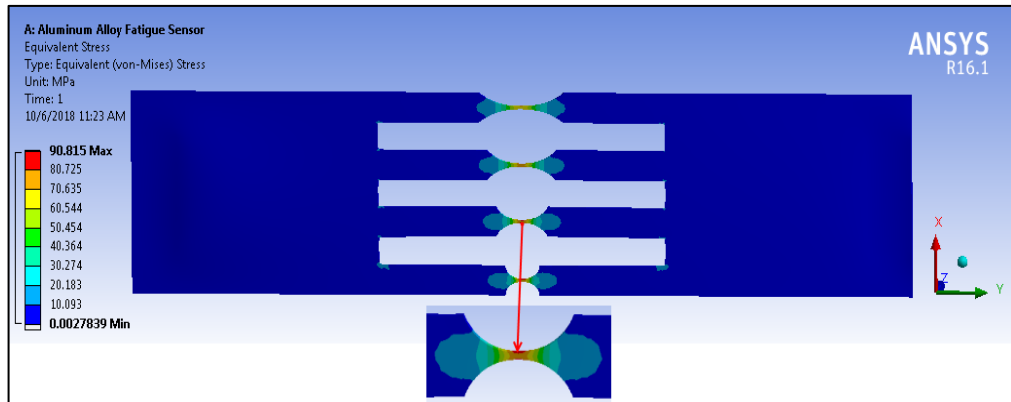


Figure 5.15. Equivalent stress distribution at  $r = 12.7$  mm.

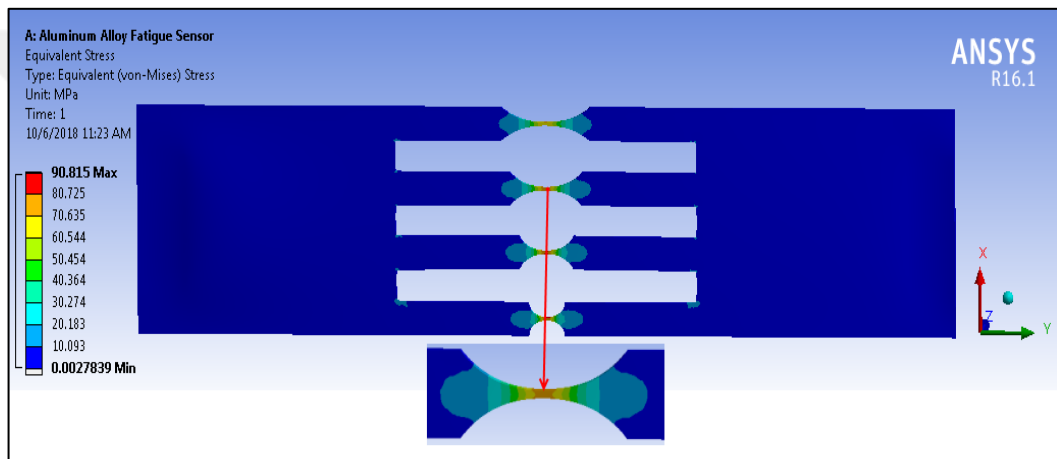


Figure 5.16. Equivalent stress distribution at  $r = 19$  mm.

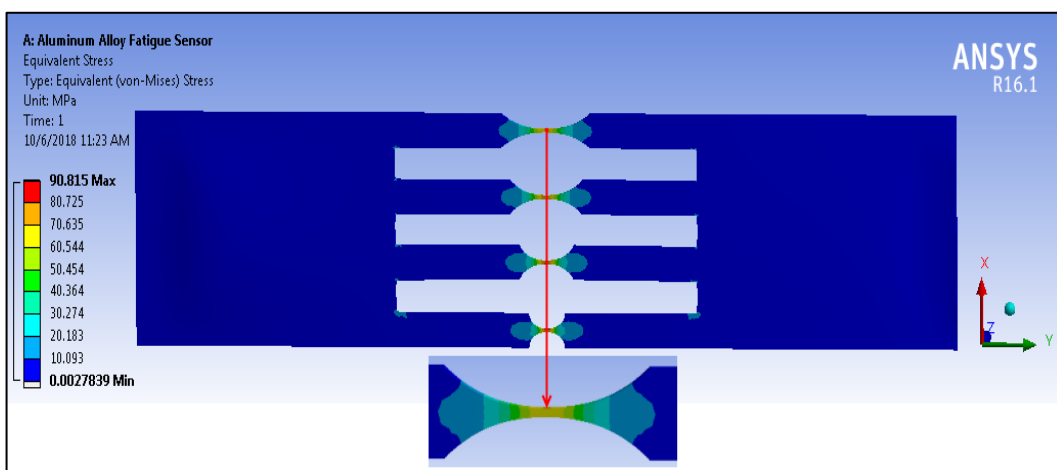


Figure 5.17. Equivalent stress distribution at  $r = 25.4$  mm.

The previous cases indicate that the equivalent stress is dependent on the U-notch radius because in all four cases, the maximum equivalent stresses are different relative to one another.

Simulation outcomes indicate the maximum equivalent stress as 90.815 MPa found at a U-notch radius of 6.4 mm when relative to the others. The highest stress around the circumference is shown in Figure 5.18.

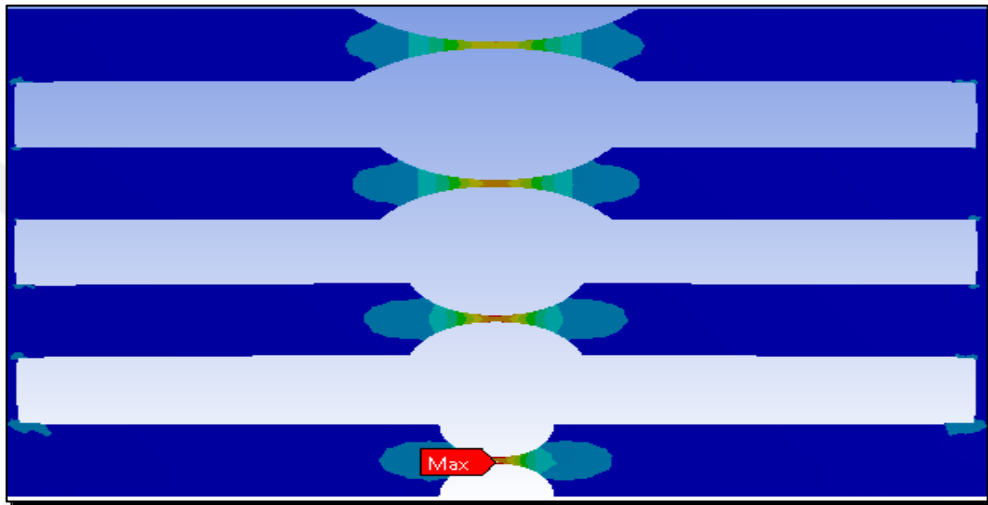


Figure 5.18. Equivalent stress distribution around the notches.

The maximum equivalent stresses with respect to U-notch radii are presented in Table 5.4 and as Figure 5.19.

Table 5.4. Maximum equivalent stress with respect to U-notch radii.

U-notch radius [ mm ]	The maximum equivalent stress [MPa]
6.4	90.815
12.7	78.686
19	74.41
25.4	68.715

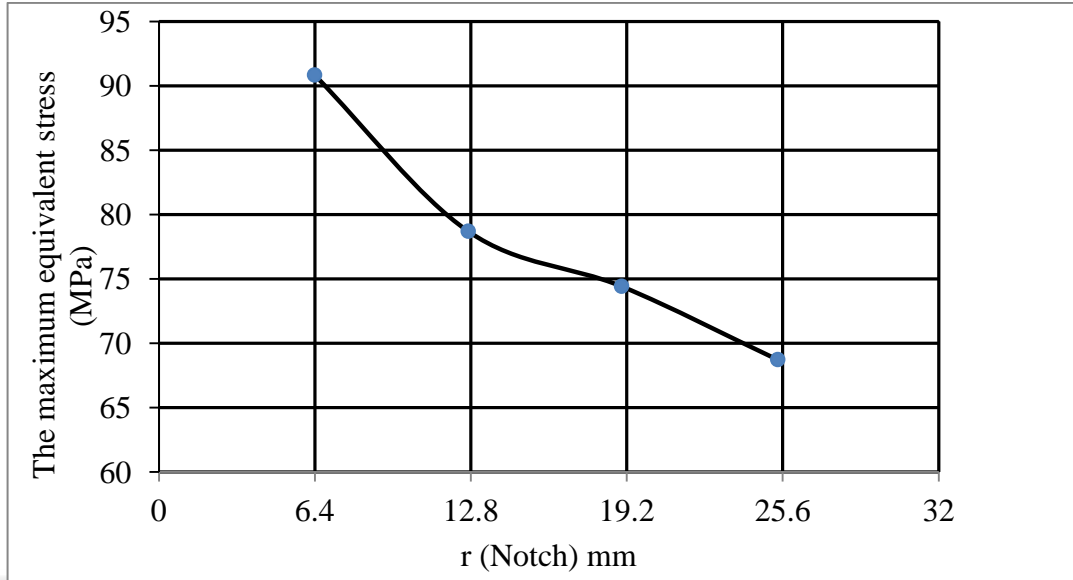


Figure 5.19. Maximum equivalent stress with different U-notch radii.

Compression between the equivalent stress distributions and sensor radius of the beams is shown in Table 5.5 and Figure 5.20. When the compression between the equivalent stress distribution and beams sensor length is sufficient, we find the maximum equivalent stress at  $r = 6.4$  mm and the minimum equivalent stress at  $r = 25.4$  mm. Moreover, the equivalent stress distribution is symmetric between the left side and the right side of the fatigue sensor model.

Table 5.5. Maximum equivalent stress with respect to the path of the beam sensor.

Path length [ mm ]	Equivalent stress (MPa)	Equivalent stress (MPa)	Equivalent stress (MPa)	Equivalent stress (MPa)
	$r = 6.4$ mm	$r = 12.7$ mm	$r = 19$ mm	$r = 25.4$ mm
97	7.61	6.6	6.12	5.61
125	8.81	8.50	8.10	7.53
152.5	90.815	78.686	74.41	68.715
185	8.81	8.50	8.10	7.53
213	7.61	6.6	6.12	5.61

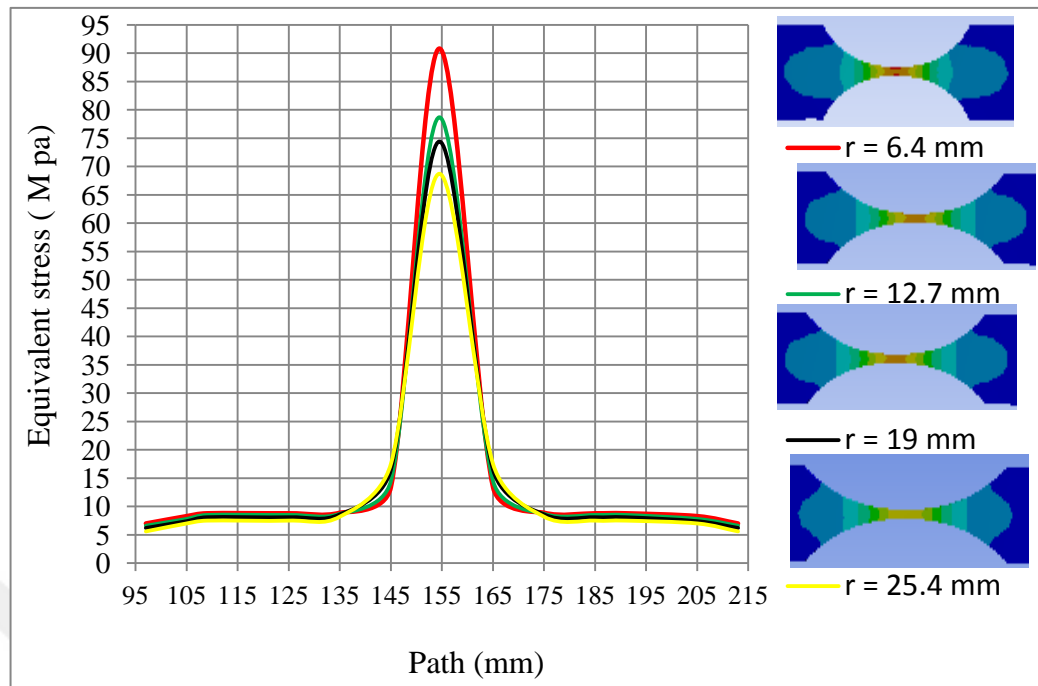


Figure 5.20. Equivalent stress distributions vs. U-notch radius sensor.

## 5.5. FATIGUE RESULTS

Stress and strain-life has been considered for the model. All cases show that the stress-life approach is better suited for evaluation of the model structure. Therefore, only stress-life results are discussed. The types of fatigue results conducted in this research are as follows:

1. Fatigue Life
2. Fatigue Damage
3. Fatigue Safety Factor

Fatigue Life means the counting of the stress cycles, which is an element under cyclic loadings that can resist before failure. Comparative results are shown using the ANSYS Workbench for the model. The resulting plots show the life of certain components. Fatigue damage is obtained by dividing the design life by the available life and if the resulting value is greater than 1, it shows an occurrence of failure before the end of useful life.



Fatigue safety is another important factor that is linked with fatigue failure. The highest safety factor can be 15, and if it is 1, it means that failure is likely to occur within the design life.

### 5.5.1 Fatigue Life

Fatigue life analyses are conducted for the model structure with different load cases. Every case examines the influence of different U-notch radii on fatigue life. Each of the notch beams shown in Figures 5.21 and 5.22 was manufactured to bear different fatigue cycles. The necessary parameters for placing the fatigue damage sensor is near a notch radius; however, the results showed that the longer fatigue life was at a U-notch radius of 25.4 mm and the short fatigue life was at a U-notch radius of 6.4 mm. This is due to the stress concentration on the notch being higher and leading to failure first due to low fatigue life, as illustrated in Figure 5.23. To design a structure, it is essential to characterize the relations between different variables to predict fatigue life.

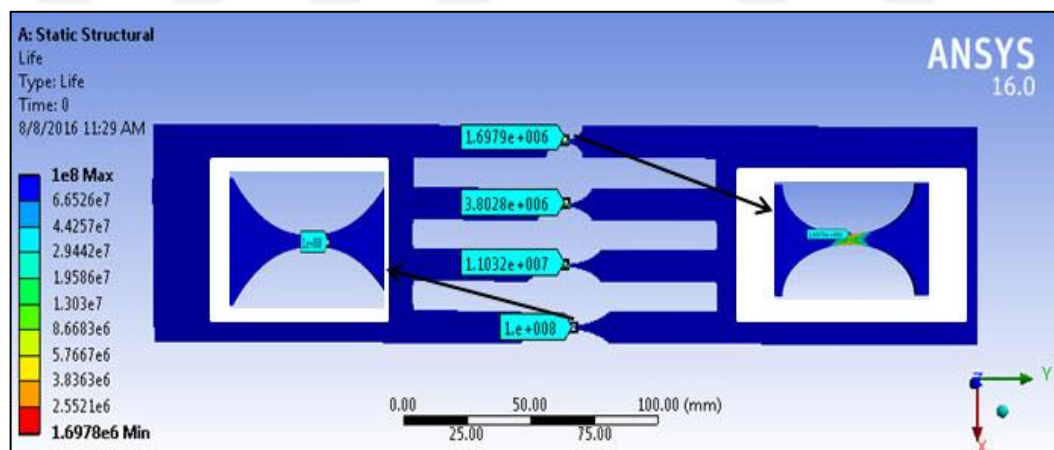


Figure 5.21. Fatigue life of the fatigue-notch sensor model.

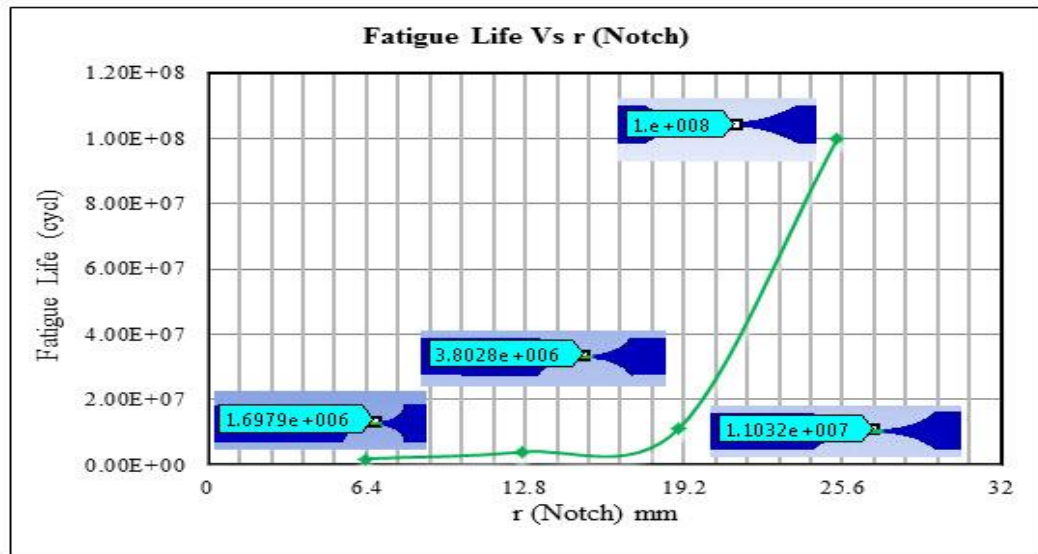


Figure 5.22. Fatigue life vs. radius for U-notch fatigue sensor model.

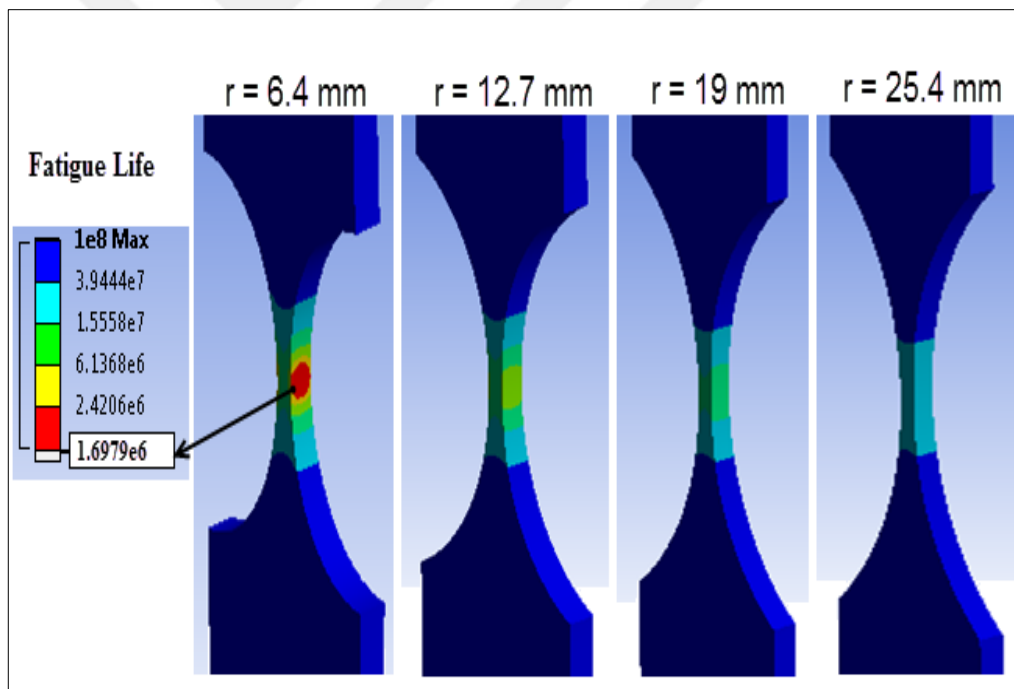


Figure 5.23. Fatigue life of fatigue sensor for different U-notch radii.

The theoretical analysis includes finding the fatigue life of the structural member using the principal stress values. They require finding the mean stress and alternating stress to find the endurance limit of the structural component at particular fatigue stresses. The actual stress values based on measured values are given. The equations were used to calculate the fatigue life in Section 3. Therefore, the number of cycles

the sensor component can withstand before failure at maximum stress is  $3.5760e+06$ . From Table 5.6, it can be observed that the theoretical fatigue life is  $3.5760e+06$  cycles, whereas the numerical fatigue life from the software analysis is  $1.6979e+06$  cycles. The numerical results agree well with the theoretical results; however, the deviation between the numerical and theoretical results are comparatively apparent at the stress levels. This is mainly because the accuracy of the predicted fatigue life from the simulation depends on the selection of appropriate material models (especially mesh parameters) and the reliability of the mechanical properties of the materials used. D. Cendon et al. (2015) worked on testing U-notched and V-notched specimens made of this material with different loading modes using the numerical method of investigation (LS-DYNA 971 software (Livermore Software Technology Corporation, Livermore, California, USA) [98]. This paper focused on the same purpose and support these results.

Table 5.6. Comparison between the theoretical and numerical fatigue life of the sensor model.

Notch radius (mm)	Fatigue life (Numerical)	Fatigue life (Theoretical)
6.4	$1.6979e+06$	$3.5760e+06$
12.7	$3.8028e+06$	$4.1057e+06$
19	$1.1032e+07$	$4.3092e+07$
25.4	$1.000e+08$	$4.5217e+07$

Figure 5.24 illustrate the relationship between alternating stresses and the number of cycles when using different U-notch radii and un-notched geometry.

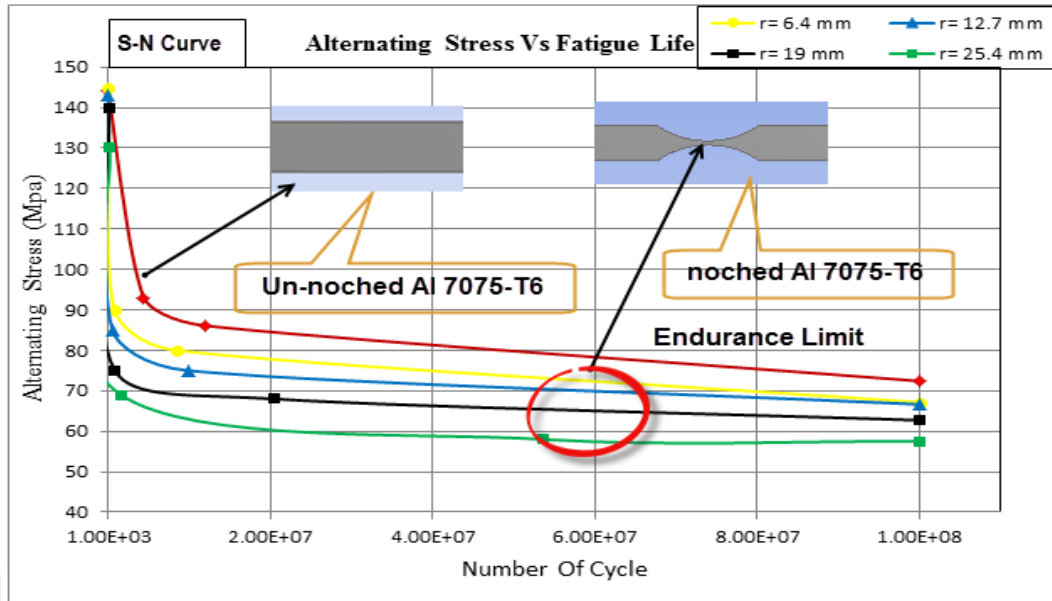


Figure 5.24. Alternating stress vs. number of cycles (S-N curve).

The results show that a longer fatigue life was observed at U-notch radius  $r = 25.4$  mm and a short fatigue life was observed at U-notch radius  $r = 6.4$  mm. The stress concentration on the notch was high, which leads to failure firstly at the notch having a low fatigue life. To design a structure, characterizing the link between different factors is critical, which affects fatigue life. A popular method for this objective is to characterize this relationship using the S-N curve. Here, S represents a cyclical stress range, and N shows the number of cycles after which a component or structure fails. The notch geometry has a profound impact on the fatigue life of materials, and this leads to the enhancement of fatigue endurance limits for every notched beam, which is part of the proposed fatigue damage sensor.

### 5.5.2. Fatigue Damage

Fatigue damage analyses are conducted in every case. The contours beside each figure indicate that damage occurs in locations where the damage contour number is greater than one. Critical locations can be found around the U-notch radius when  $r = 6.4$  mm. Additional details are presented in Figure 5.25, which shows a damage analysis shown as the maximum critical damage that occurs in a U-notch sensor of radius to 6.4 mm and minimum damage occurring in the U-notch sensor of radius

25.4 mm. In addition, fatigue damage affects a smaller area around the U-notch radius.

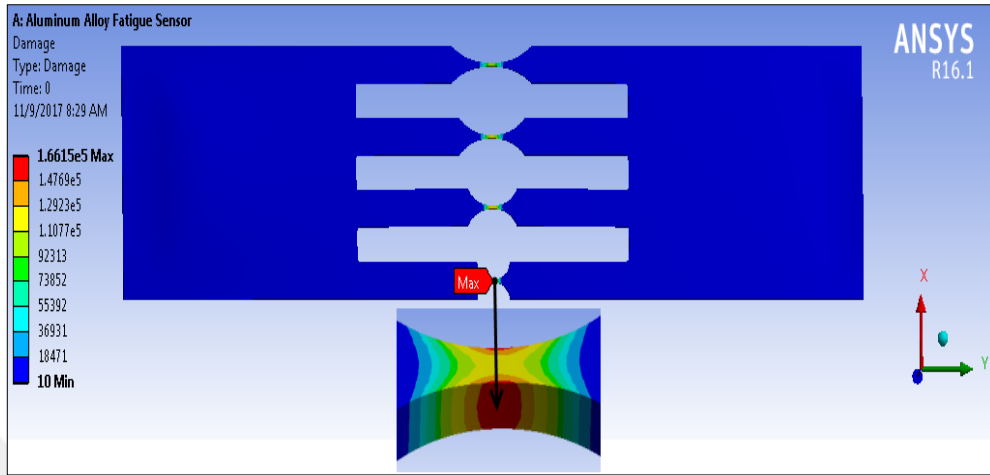


Figure 5.25. Alternating stress vs. number of cycles.

Figure 5.26 shows fatigue damage with respect to the U notch radius. Four different U-notch radii were considered for this case. The results indicate that increasing the U-notch radius from 6.4 mm to 25.4 mm decreases the amount of damage.

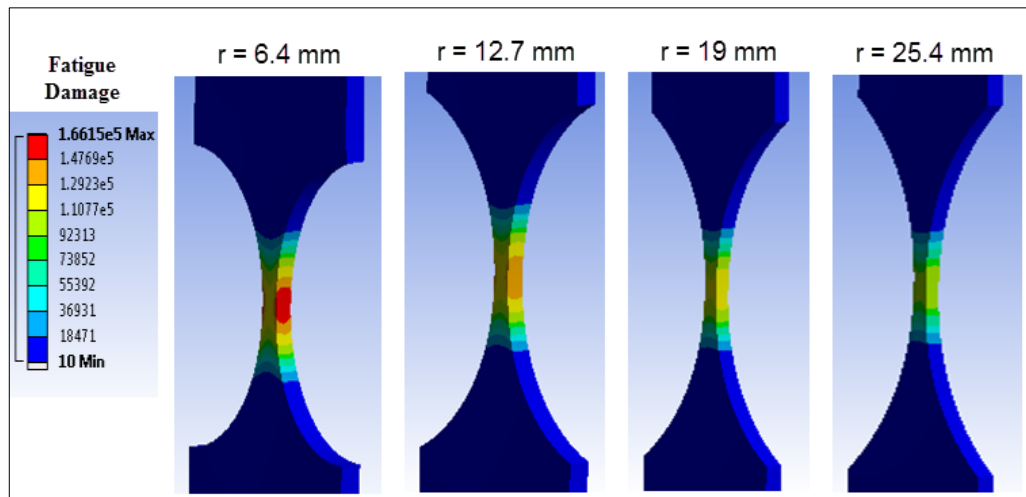


Figure 5.26. Fatigue damage for different U-notch radii.

### 5.5.3. Safety Factor

Factor of Safety analyses were carried out in the finite element models from 0 to 15. The contour numbers less than 1 show failures earlier than the end of the design life. A safety factor less than 1.0 indicates potential fatigue issues.

The parametric study results for the safety analysis in the model are shown in Figure 5.27. A factor of safety ranging from 0.94943 to 5 is recommended for the design. Moreover, it shows that for only a U-notch with radius equal to 6.4 mm, the safety factor is less than 1.0 and equal to 0.94943, providing an acceptable safety factor for the other three U-notch radii with 4000 N loading due to their being greater than 1.0. In addition, if the loading is less than 4000 N, it provides an acceptable safety factor for all U-notch radii. The effect on the safety factor of changing the U-notch is presented in Figure 5.28. It can be observed that by increasing U-notch radii and decreasing the loading, the factor of safety will increase.

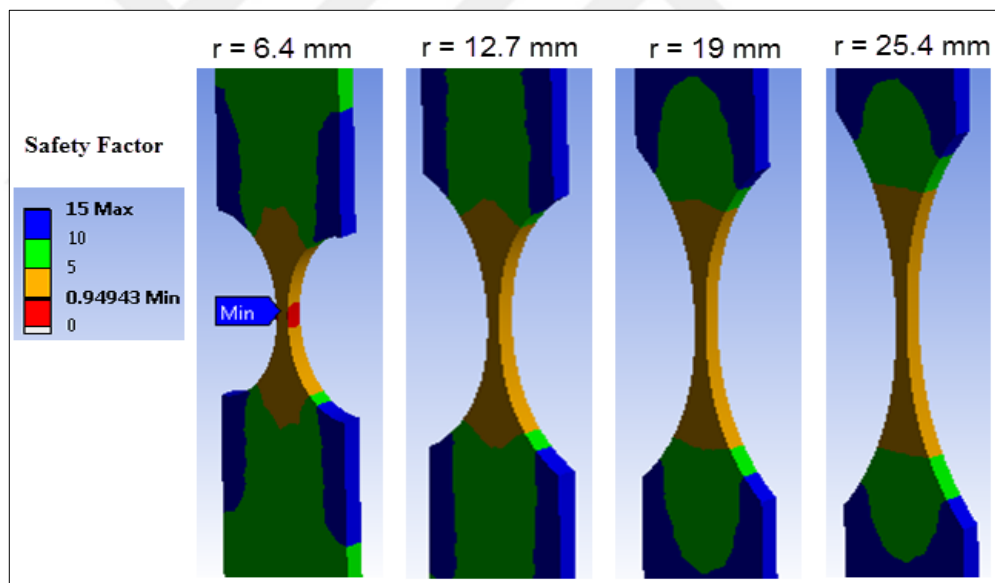


Figure 5.27. Safety factor for different U-notch radii with loading (4000 N).

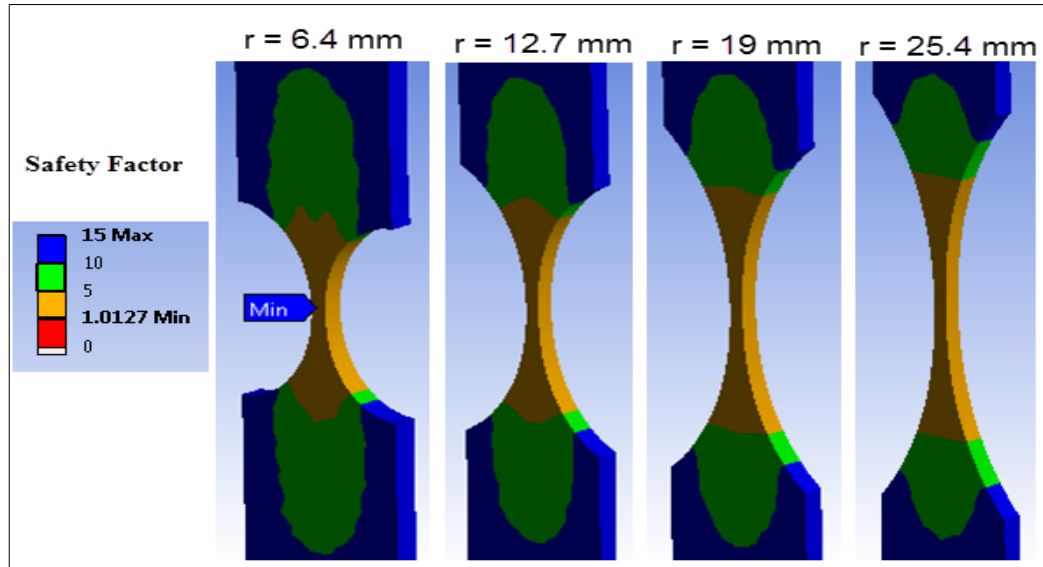


Figure 5.28. Safety factor for different U-notch radii with loading (3500 N).

## 5.6. COMPARISON BETWEEN THE FATIGUE LIFE OF AL 7075 – T6, AL 2024 – T4 AND AL 6061 – T6 SENSOR

Based on the numerical simulation using the ANSYS workbench, the fatigue life of the aluminum alloy 7075-T6 U-notch sensor is higher than the fatigue life of the aluminum alloy 2024-T4 U-notch sensor and the fatigue life of the Al-6061-T6 U-notch sensor, as shown in Figure 5.29. Moreover, the maximum fatigue life was at a U-notch radius of 25.4 mm for three types of aluminum alloy and the minimum fatigue life was at a U-notch radius of 6.4 mm for the three types of aluminum alloy. When a comparison is made between the fatigue life of the U-notches for the three types of aluminum alloy sensor, the maximum fatigue life at a high U-notch radius of 25.4 mm for AL-7075-T6, AL-2024-T4 and AL-6061-T6 were  $2.7501 \times 10^7$  cycles,  $2.3869 \times 10^7$  cycles and  $1.6691 \times 10^7$  cycles, respectively. The minimum fatigue life at the low U-notch radius of 6.4 mm for AL-7075-T6, AL-2024-T4 and AL-6061-T6 were  $1.6979 \times 10^6$  cycles,  $8.4364 \times 10^5$  cycles and  $6.0166 \times 10^5$  cycles, respectively. This indicates that the AL-7075-T6 has the best fatigue life when compared with the AL-2024-T4 and AL-6061-T6, and failure will occur firstly on AL-6061-T6 because of its low fatigue life. These details are shown in Figure 5.30 and Table 5.7, showing that the AL-7075-T6 sensor has the best fatigue life.

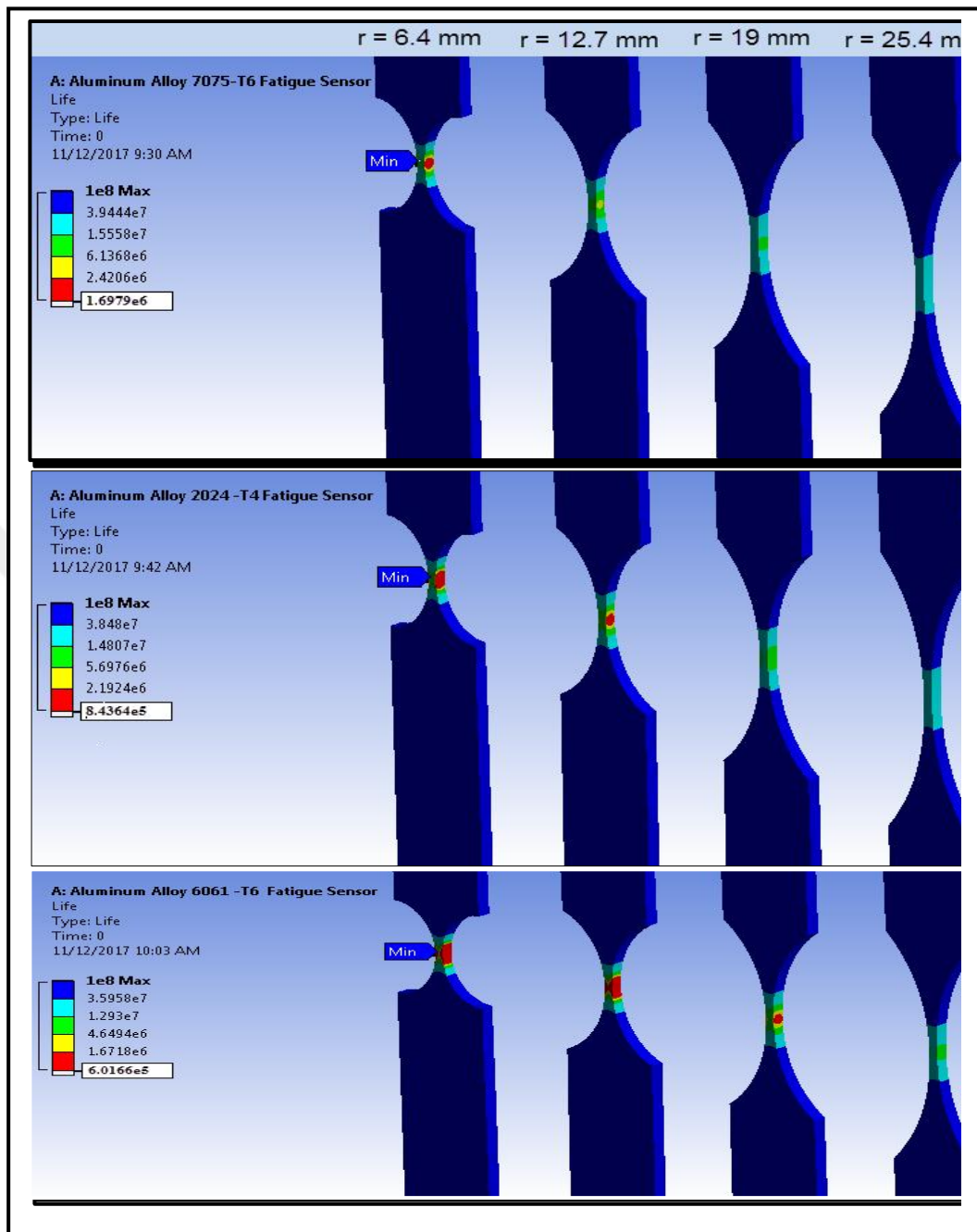


Figure 5.29. Comparison between the fatigue life of aluminum alloy 7075-T6, aluminum alloy 2024-T4 and aluminum alloy 6160-T6.



Table 5.7. Fatigue life of AL-7075-T6, AL-2024-4 and AL-6061-T6.

Type of Aluminum Alloy	Fatigue Life (cycle)			
	r = 6.4 mm	r =12.7 mm	r =19 mm	r = 25.4 mm
<b>AL 7075 – T6</b>	1.6979e+06	3.8028e+06	1.1032e+07	2.7501e+07
<b>AL 2024 – T4</b>	8.4364e+05	3.3005e+06	9.5749e+06	2.3869e+07
<b>AL 6061 – T6</b>	6.0166e+05	2.3080e+06	6.6955e+06	1.6691e+07

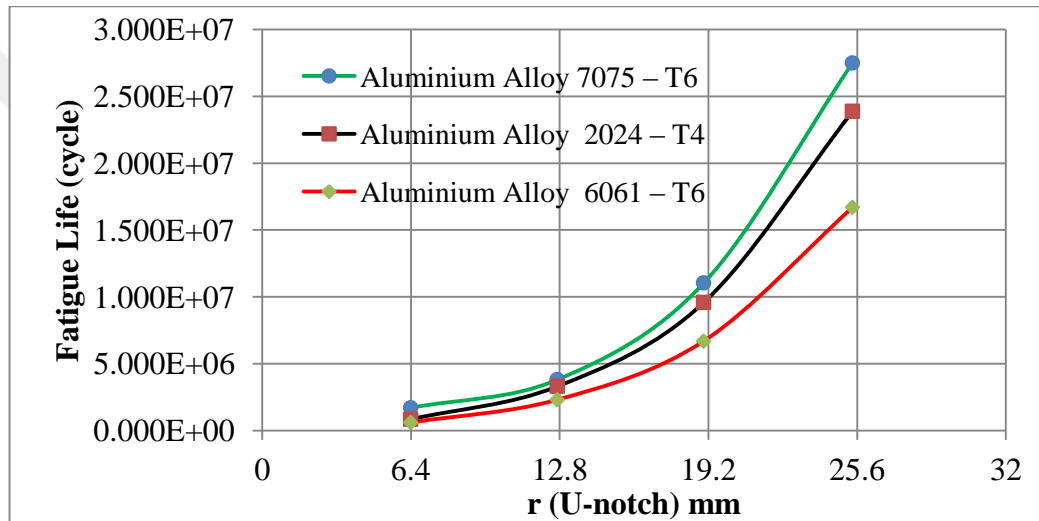


Figure 5.30. Fatigue life vs. U-notch radius of aluminum alloy 7075-T6, aluminum alloy 2024-T4 and aluminum alloy 6061-T6.

Many studies have focused on the structural parts of the bridges and they used steel as an application material. Here, we use a sensor with four beams each of which with a different U-notch radius, 7075 aluminum alloy as aircraft wing material and using ANSYS Workbench software to detect the fatigue life of the sensor to provide information to engineers. The contribution of this work to the science and technology surmised in the following items:

1. Load sensing.
2. Digitizing monitoring processes.
3. To increase efficiency, reduce costs.

## PART 6

### CONCLUSIONS AND RECOMMENDATIONS

#### 6.1. CONCLUSIONS

Failures caused by fatigue often occur around U- notch sensor structure. Many of these failures are caused by applied stress cycles. This research provides the outline of the fatigue U-notch sensor, which has been analyzed with ANSYS workbench software. The key benefits of this fatigue U-notch sensor are generally mentioned in terms of geometry, design, preparation processes, production costs, and the need to connect with recording and gauging equipment's. Moreover, we have mentioned general issues and disadvantages in terms of reliability, environmental sensitivity, stability, and repeatability. Those sensors are installed in the fatigue sensitive areas and also can be embedded within weak/delicate/vulnerable areas of dangerous mechanical parts, for example, bridge ways, aircrafts and so on. Based on this parametric study, the following results were obtained:

1. The deforming behavior can be judged using ANSYS simulations, which were symmetric. The total deformation value is 0.34379 mm.
2. The maximum equivalent elastic strain values decrease when notch radius increases. The highest elastic strain is 0.012791 according to the FE approach for the notch radius of 6.4 mm.
3. The max equivalent stress value is 90.815 MPa that decreases when the notch radius increases. This value was found with the help of FE model having notch radius 6.4 mm.
4. The life prediction precision through FEA simulations depend on choosing the right material model using accurate parameters.
5. The maximum fatigue life was observed at a large U-notch radius sensor and the minimum fatigue life at a small U-notch radius sensor.
6. The maximum fatigue life occurs at U-notch radius (25.4 mm) and the minimum fatigue life occurs at U-notch radius (6.4 mm).
7. Increasing reverse-edged U-notch radius also increases fatigue life.

8. Fatigue damage occurs around the U-notch sensor when the U-notch radius equals or less than 6.4 mm.
9. U-notches sensor with U-notch radius equal or less than 6.4mm are not recommended for this loading and geometry because safety factor is less than one.
10. This safety factor shows a value less than one around the U-notch sensor specifically for small radius.
11. The result of this study gives evidence that fatigue life depends on fatigue U-notch radius sensor, applied forces and specifically tension/stress at end of the sensor structures.
12. The fatigue endurance limits for every U-notched beam sensor was less than fatigue endurance limits for aluminum alloy 7075-T6.
13. Sensor arms as per current design should be increased for accommodating extra notches that addresses lower stress ranges with larger number of loading cycles.
14. The maximum fatigue life was at U-notch radius ( $r = 25.4$  mm) for three types of Aluminum alloy and the minimum fatigue life was at U-notch radius ( $r = 6.4$  mm) for three types of Aluminum alloy.
15. 7075-T6 Alloy has better fatigue life than 2024-T4 and 6061-T6 alloys.

## **6.2. SCOPE FOR FUTURE WORK**

Based on what is observed throughout the work of this thesis, some recommendations for further work are given in the following points:

1. This work can be extended with the modifications of the notch shape like V-notch shape and I-notch shape, and comparison of the result between V-notch shape, I-notch shape and U-notch shape.
2. Analysis can be carried out for different loads and boundary conditions.
3. Theoretical studies can be verified with the experimental studies

## REFERENCES

1. J. Schijve, *Fatigue of structures and materials: Kluwer Academic*, (2001).
2. H. Oja and K. Nordhausen, "Independent component analysis," *Encyclopedia of Environmetrics*, (2001).
3. D. S. Eddy and D. R. Sparks, "Application of MEMS technology in automotive sensors and actuators", *Proceedings of the IEEE*, vol. 86, pp. 1747-1755, (1998).
4. R. Frank, "Understanding Smart Sensors Second Edition" *Artech House, Inc.*, (2017).
5. N. R. C. C. o. N. S. "Technologies and Applications, Expanding the vision of sensor materials" *National Academies Press*, (1995).
6. D. W. Hoepfner and W. E. Krupp, "Prediction of component life by application of fatigue crack growth knowledge," *Engineering Fracture Mechanics*, vol. 6, pp. 47-70, (1974).
7. C. Boller and N. Meyendorf, "State-of-the-art in Structural Health monitoring for aeronautics," in *Proceedings of the International Symposium on NDT in Aerospace*, (2008).
8. B. M. Phares, "The Electrochemical Fatigue Sensor: A Novel Sensor for Active Fatigue Crack Detection and Characterization Material Technologies," in *International Conference on Structural Health Monitoring & Intelligent Infrastructure, Ankeny, IA USA*, , p. 126.(2007).
9. M. K. Fay and G. L. Sheffield, "Fracture detecting structural health sensor," *ed: Google Patents*, (2009).
10. J. M. Papazian, J. Nardiello, R. P. Silberstein, G. Welsh, D. Grundy, C. Craven, et al., "Sensors for monitoring early stage fatigue cracking," *International journal of fatigue*, vol. 29, pp. 1668-1680, (2007).
11. N. Goldfine, D. Grundy, A. Washabaugh, C. Craven, V. Weiss, and V. Zilberstein, "Fatigue and stress monitoring with magnetic sensor arrays," in *Annual Society for Experimental Mechanics (SEM) Conference, St. Louis, Missouri*, (2006).
12. Q. Lei, Y. Shenfang, W. Qiang, S. Yajie, and Y. Weiwei, "Design and experiment of PZT network-based structural health monitoring scanning system," *Chinese Journal of Aeronautics*, vol. 22, pp. 505-512, (2009).
13. J. D. Achenbach, "Structural health monitoring—What is the prescription" *Mechanics Research Communications*, vol. 36, pp. 137-142, (2009).

14. B. Pyttel, D. Schwerdt, and C. Berger, "Very high cycle fatigue—is there a fatigue limit" *International Journal of fatigue*, vol. 33, pp. 49-58, (2011).
15. W. Lee, L. Nguyen, and G. S. Selvaduray, "Solder joint fatigue models: review and applicability to chip scale packages" *Microelectronics reliability*, vol. 40, pp. 231-244, (2000).
16. G. Mesmacque, S. Garcia, A. Amrouche, and C. Rubio-Gonzalez, "Sequential law in multiaxial fatigue, a new damage indicator" *International Journal of Fatigue*, vol. 27, pp. 461-467, (2005).
17. W. Wu, H. Liou, and H. Tse, "Estimation of fatigue damage and fatigue life of components under random loading" *International journal of pressure vessels and piping*, vol. 72, pp. 243-249, (1997).
18. A. Wöhler, "Versuche über die Festigkeit der Eisenbahnwagenachsen" *Zeitschrift für Bauwesen*, vol. 10, pp. 160-161, (1860).
19. P. D. Okulov, "Micro electro-mechanical strain displacement sensor and usage monitoring system," *ed: Google Patents*, (2016).
20. R. Fussinger, "Apparatus for monitoring the fatigue strength of structures," *ed: Google Patents*, (1996).
21. H. W. Smith, "Fatigue damage indicator," *ed: Google Patents*, (1976).
22. C. P. Townsend and S. W. Arms, "System for remote powering and communication with a network of addressable, multichannel sensing modules," *ed: Google Patents*, (2003).
23. G. Majzoobi and N. Daemi, "The effects of notch geometry on fatigue life using notch sensitivity factor" *Transactions of the Indian Institute of Metals*, vol. 63, pp. 547-552, (2010).
24. S. Gokanakonda, M. K. Ghantasala, and D. Kujawski, "Fatigue sensor for structural health monitoring: Design, fabrication and experimental testing of a prototype sensor" *Structural Control and Health Monitoring*, vol. 23, pp. 237-251, (2016).
25. T. Ozkul, H. Kaplan, and M. Dolen, "Wireless enabled fatigue sensor for structural health monitoring" *ed: Google Patents*, (2014).
26. M. Enckell, "Lessons learned in structural health monitoring of bridges using advanced sensor technology," (2011).
27. Z. A. Chaudhry, T. Joseph, F. P. Sun, and C. A. Rogers, "Local-area health monitoring of aircraft via piezoelectric actuator/sensor patches," *in Smart Structures & Materials' 95*, pp. 268-276.(1995).

28. H. Banks, D. Inman, D. Leo, and Y. Wang, "An experimentally validated damage detection theory in smart structures," *Journal of Sound and Vibration*, vol. 191, pp. 859-880, (1996).
29. J. W. Fisher, G. L. Kulak, and I. F. Smith, "A fatigue primer for structural engineers," *National Steel Bridge Alliance, American Institute of Steel Construction*.(1998).
30. B. P. Wijesinghe, S. A. Zacharie, K. D. Mish, and J. D. Baldwin, "Design and development of in situ fatigue sensors for structural health monitoring of highway bridges," *Journal of Bridge Engineering*, vol. 18, pp. 297-307, (2011).
31. V. Giurgiutiu, J. M. Redmond, D. P. Roach, and K. Rackow, "Active sensors for health monitoring of aging aerospace structures," in *SPIE's 7th Annual International Symposium on Smart Structures and Materials*, pp. 294-305, (2000).
32. M. Aygül, M. Al-Emrani, and S. Urushadze, "Modelling and fatigue life assessment of orthotropic bridge deck details using FEM" *International Journal of Fatigue*, vol. 40, pp. 129-142, (2012).
33. R. Haghani, M. Al-Emrani, and M. Heshmati, "Fatigue-prone details in steel bridges," *Buildings*, vol. 2, pp. 456-476, (2012).
34. M. Al-Emrani and R. Klinger, "Fatigue prone details in steel bridges," in Nordic Steel Construction Conference, (2009).
35. V. Ramachandran, "Failure analysis of engineering structures: methodology and case histories" *ASM International*, (2005).
36. G. Park, C. R. Farrar, F. L. di Scalea, and S. Coccia, "Performance assessment and validation of piezoelectric active-sensors in structural health monitoring" *Smart Materials and Structures*, vol. 15, p. 1673, (2006).
37. M. Lemley and C. Chien, "Are the US Patent Priority Rules Necessary" *Boalt Working Papers in Public Law*, (2003).
38. H. Kaplan and T. Ozkul, "A novel smart fatigue damage sensor for structural health monitoring of critical components of structures," in *Industrial Informatics and Computer Systems (CIICS), 2016 International Conference on*, , pp. 1-5. (2016).
39. S. V. Kailas, "Material Science". *India*, (2004).
40. G. E. Dieter and D. J. Bacon, Mechanical metallurgy vol. 3: *McGraw-Hill New York*, (1986).
41. J. M. Naser and F. Serrano Toledano, "Analysis of vibration-induced fatigue cracking in steel bridges" (2011).

42. S. S. Manson, "Behavior of materials under conditions of thermal stress" (1954).
43. A. Wohler, "Versuche zur Ermittlung der auf die Eisenbahnwagen Achsen Einwirkenden Kräfte und der widerstandsfähigkeit der Achsen," *Zeitschrift für Bauwesen*, (1860).
44. R. L. Norton, "Machine design: an integrated approach " ed: **Prentice-Hall Inc: NJ, USA**, (1996).
45. L. Pook, Why Metal Fatigue Matters: *Springer*, (2007).
46. Y.-L. Lee, Fatigue testing and analysis: theory and practice vol. 13: *Butterworth-Heinemann*, (2005).
47. S. Gokanakonda, "Fabrication, testing and analysis of a fatigue sensor for structural health monitoring," *Doctor of Philosophy, Mechanical and Aerospace Engineering, Western Michigan University*, (2014).
48. M. Kuna, Finite elements in fracture mechanics: Springer, (2013).
49. A. Abass, "Fatigue Failure And Testing Methods" (2013).
50. [K. Miller and M. Ibrahim, "Damage accumulation during initiation and short crack growth regimes," *Fatigue & Fracture of Engineering Materials & Structures*, vol. 4, pp. 263-277, (1981).
51. G. Waddell, "A new clinical model of low back pain and disability," *The back pain revolution*, (1998).
52. J. G. Chaos. Rubber physics (Alexander Dubcek University of Trencin ed.). (1996).
53. M. Bruyneel and D. Granville, "An industrial solution to analyze delamination," *JEC Composites Magazine*, vol. 41, (2008).
54. M. A. Choudhary, "Fatigue strength analysis and end-of-life crack propagation in thin stainless steel structures by means of comparing FE-analyses and experimental results " *Master Materials Science and Strength of Materials University of Stuttgart* (2009).
55. JohnHiatt, "What is a SN-Curve" (2016).
56. K. G. RV, "Stress Analysis Of The Landing Gear-Well Beams And Damage Calculation Due To Landing Cycles," *Visvesvaraya Technological University*, (2014).
57. W. D. Callister, Materials science and engineering: an introduction: *John Wiley & Sons*, (2003).

58. R. I. Stephens, A. Fatemi, R. R. Stephens, and H. O. Fuchs, Metal fatigue in engineering: *John Wiley & Sons*, (2000).
59. A. Fatemi. ((2011)). Chapter\_7-Notches And Their Effects. Available: [https://www.efatigue.com/training/Chapter\\_7.pdf](https://www.efatigue.com/training/Chapter_7.pdf)
60. M. A. Maleque and M. S. Salit, Materials selection and design: *Springer*, (2013).
61. T. Baumeister, Avallone, E., BaumeisterIII, A., & Marks, T., "Standard handbook for mechanical engineers": *MC GraWrHill Book Company*, (1978).
62. A. Milton, "Miner: Cumulative damage in fatigue Journal of Appl," *ed: Mech*, (1945).
63. G. Ayoub, M. Nait-Abdelaziz, F. Zaïri, and J.-M. Gloaguen, "Multiaxial fatigue life prediction of rubber-like materials using the continuum damage mechanics approach," *Procedia Engineering*, vol. 2, pp. 985-993, (2010).
64. S. Bhat and R. Patibandla, "Metal fatigue and basic theoretical models: a review," *in Alloy Steel-Properties and Use, ed: InTech*, (2011).
65. C. F. Zorowski, "Design for Strength and Endurance", (2002).
66. C. Bannantine, Handrock, "Fundamentals of Metal Fatigue Analysis". *Englewood Cliffs, NJ: Prentice- Hall Inc.*, (1990).
67. S. Namata, "Structural Stability Crack Analysis of Thermoplastic Composites," *J Appl Mech Eng*, vol. 5, p. 213, (2016).
68. M. Mahmoud, M. Mousa, and N. Hasan, "Stress concentration of single and double notched plate under bi-axial state of stress," *in The 3 rd Minia International Conference for Advanced Trends in engineering, MICATE*, (2005).
69. D. F. P. Walter D. Pilkey, Peterson's Stress Concentration Factors, 3rd Edition ed. in Canada.: *John Wiley & Sons, Inc.*, (2008).
70. W. D. Pilkey and D. F. Pilkey, Peterson's stress concentration factors: *John Wiley & Sons*, (2008).
71. G. Roebroeks, "The development of a fatigue insensitive and damage tolerant aircraft material," *Delft University of Technology*, (1991).
72. G. Roebroeks, "Fibre-metal laminates: recent developments and applications," *International journal of fatigue*, vol. 16, pp. 33-42, (1994).
73. D. Grieve. Stress Concentration, (2008).



74. R. Peterson, "Stress Concentration Factors", *John Wiley & Sons, New York* (1974).
75. M. Isida, "On the tension of the strip with semi-circular notches," *Trans. Japan Soc. Mech. Engrs*, vol. 19, pp. 5-10, (1953).
76. C.-B. Ling, "On stress-concentration factor in a notched strip," *Journal of Applied Mechanics*, vol. 35, pp. 833-835, (1968).
77. P. Flynn and A. Roll, "A re-examination of stresses in a tension bar with symmetrical U-shaped grooves," *Experimental Mechanics*, vol. 6, pp. 93-98, (1966).
78. F. J. Appl and D. R. Koerner, "Stress Concentration Factors For U-Shaped, Hyperbolic, And Rounded V-Shaped, Notches," *In Mechanical Engineering*, pp. 73. (1969).
79. S. Gokanakonda, Fabrication, testing and analysis of a fatigue sensor for structural health monitoring: *Western Michigan University*, (2014).
80. E. J. Mastascusa, "Sensors", (2008).
81. G. R. Snuti Kumari, Priyanka Attri, Manee Kumar, "ypes of Sensors and Their Applications" *International Journal of Engineering Research and Development*, vol. 10, p. 14, (2014).
82. B. Kleyman.. "Top 5 Reasons Why Environment Sensors are in All Modern Data Centers". (2014).
83. H. Saalfelden, "Sensors In Engineering" *Higher college for Mechatronics*, (2016).
84. D. Adams, "different types of displacement, velocity, acceleration, strain, force, temperature, and pressure sensors ", *Journals and Conferences Dealing with Health Monitoring*, (2006).
85. J. R. Gyorki. "Strain Sensor Basics and Signal Conditioning Tips", (2005).
86. D. Williams, "Force sensors and their uses" *Machine Design*, (2013).
87. KhairiBudayawan.). "Temperature Sensor Types for Temperature Measurement". Available: <https://www.scribd.com/document/338236400/Temperature-Sensor-Types-for-Temperature-Measurement>, (2017).
88. D. P. Henkel, "Remote and powerless miniature fatigue monitor and method," *ed: Google Patents*, (1996).

89. L. Sidney, Aluminium Alloys - New Trends in Fabrication and Applications: *Scitus Academics LLC*, (2016).
90. C. Willan, "Aluminum Metallurgy," *OMEGA RESEARCH*, vol. 5, (2001).
91. Azom.. Aluminium An Introduction To Aluminium Properties, Production and Applications,Supplier Data by Aalco.,Available: <http://www.azom.com/article.aspx?ArticleID=2861>,(2005).
92. G. Silva, B. Rivolta, R. Gerosa, and U. Derudi, "Study of the SCC behavior of 7075 aluminum alloy after one-step aging at 163 C," *Journal of materials engineering and performance*, vol. 22, pp. 210-214, (2013).
93. G. Silva, B. Rivolta, R. Gerosa, and U. Derudi, "Study of new heat treatment parameters for increasing mechanical strength and stress corrosion cracking resistance of 7075 Aluminium alloy," *La Metallurgia Italiana*, (2013).
94. R. Abdullah and N. Beithou, "Burnishing Effects on Friction Stir Welding of Al-Alloy 7075 T6," *Global Journal of Research In Engineering*, (2014).
95. S. Panda, "Fatigue Life Estimation of Pre-corroded 7075 Aluminium Alloy," *Bachelor Of Technology, National Institute Of Technology, Rourkela*, (2012).
96. A. I. John Swanson. "Simulation Software Products ANSYS". Available: <http://www.swmath.org/software/44>,(2010).
97. X. C. He, "Finite Element Analysis of Adhesively Bonded Single-lap Joints," *in Advanced Materials Research*, , pp. 411-415, (2010).
98. D. Cendon, A. Torabi, and M. Elices, "Fracture assessment of graphite V-notched and U-notched specimens by using the cohesive crack model," *Fatigue & fracture of engineering materials & structures*, vol. 38, pp. 563-573, (2015).

## APPENDIX A.

### DETAILED DRAWINGS OF THE FATIGUE U-NOTCH SENSOR

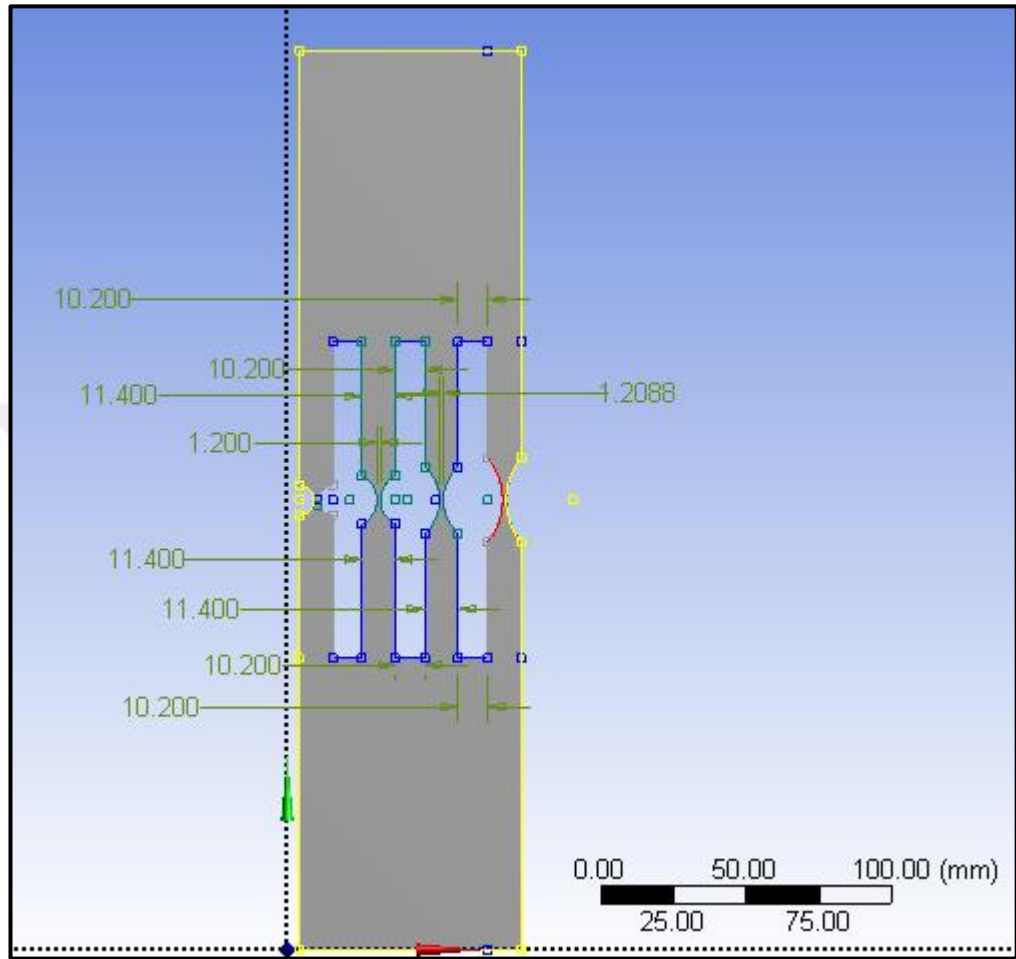


Figure A.1. Detail drawing of U-notched sensor structure.

## APPENDIX B. DEFORMATION RESULTS

Table B.1. The total deformation of the U-notch sensor

Path Length [ mm]	Total Deformation [ mm]			
	r = 6.4 mm	r = 12.7 mm	r = 19 mm	r = 25.4 mm
0.0	0.0	0.0	0.0	0.0
6.3542	3.5574e-003	2.7836e-003	2.7478e-003	3.5298e-003
12.708	7.318e-003	7.3849e-003	7.2276e-003	7.3334e-003
19.063	1.1336e-002	2.2086e-002	2.1705e-002	1.1241e-002
25.417	1.5194e-002	3.5537e-002	3.4988e-002	1.4772e-002
31.771	1.8869e-002	3.9616e-002	3.9163e-002	1.81e-002
38.125	2.263e-002	3.9322e-002	3.892e-002	2.1543e-002
44.479	2.654e-002	3.7931e-002	3.7474e-002	2.5122e-002
50.833	3.0579e-002	3.7246e-002	3.6635e-002	2.8801e-002
57.188	3.4724e-002	3.7922e-002	3.7095e-002	3.2539e-002
63.542	3.8976e-002	3.9857e-002	3.8788e-002	3.6323e-002
69.896	4.3348e-002	4.2654e-002	4.1334e-002	4.0159e-002
76.25	4.7872e-002	4.594e-002	4.4366e-002	4.4068e-002
82.604	5.2608e-002	4.9499e-002	4.7676e-002	4.8104e-002
88.958	5.769e-002	5.3389e-002	5.1323e-002	5.2406e-002
95.313	6.3372e-002	5.8148e-002	5.5828e-002	5.7226e-002
101.67	6.9606e-002	6.3935e-002	6.1309e-002	6.2536e-002
108.02	7.7033e-002	7.1249e-002	6.8175e-002	6.8745e-002
114.38	8.4919e-002	7.9012e-002	7.5455e-002	7.5297e-002
120.73	9.2817e-002	8.6752e-002	8.2709e-002	8.1857e-002
127.08	0.1007	9.4488e-002	8.9952e-002	8.8411e-002
133.44	0.10858	0.10222	9.7202e-002	9.506e-002
139.79	0.11657	0.1102	0.10507	0.10289
146.15	0.12615	0.1209	0.11668	0.11537
152.5	0.14834	0.14801	0.14814	0.14928
158.85	0.19785	0.202	0.20356	0.20282
165.21	0.2118	0.21816	0.22258	0.22453
171.56	0.22029	0.22709	0.23207	0.23436
177.92	0.2282	0.23478	0.23949	0.24143
184.27	0.23608	0.24244	0.24671	0.24801
190.63	0.24398	0.25012	0.25395	0.25456
196.98	0.25187	0.25782	0.26121	0.26112
203.33	0.25967	0.26553	0.26846	0.2676
209.69	0.26653	0.27218	0.27475	0.2734
216.04	0.27255	0.27762	0.27994	0.27855
222.4	0.27795	0.28203	0.28411	0.28313
228.75	0.28286	0.28594	0.28778	0.28731
235.1	0.28749	0.28977	0.29138	0.29129
241.46	0.29194	0.29364	0.29503	0.29518
247.81	0.29626	0.29754	0.29874	0.29902
254.17	0.30048	0.30149	0.30252	0.30283

Path Length [ mm]	Total Deformation [ mm]			
	r = 6.4 mm	r = 12.7 mm	r = 19 mm	r = 25.4 mm
260.52	0.30461	0.30547	0.30636	0.30663
266.88	0.30869	0.3095	0.31027	0.31042
273.23	0.3127	0.31359	0.31426	0.3142
279.58	0.31666	0.31777	0.31837	0.31796
285.94	0.32058	0.32212	0.32266	0.32172
292.29	0.3245	0.3258	0.32628	0.32561
298.65	0.32846	0.32777	0.3282	0.32974
305.	0.33242	0.3297	0.3301	0.34379

Table B.2. The directional deformation y- Axis of the U-notch sensor

Path Length [ mm]	The directional deformation y- Axis [ mm]			
	r = 6.4 mm	r = 12.7 mm	r = 19 mm	r = 25.4 mm
0.0	0.0	0.0	0.0	0.0
6.3542	3.5666e-003	2.7908e-003	2.755e-003	3.5389e-003
12.708	7.3369e-003	7.404e-003	7.2464e-003	7.3524e-003
19.063	1.1366e-002	2.2143e-002	2.1761e-002	1.127e-002
25.417	1.5233e-002	3.5629e-002	3.5079e-002	1.481e-002
31.771	1.8918e-002	3.9719e-002	3.9264e-002	1.8147e-002
38.125	2.2689e-002	3.9424e-002	3.902e-002	2.1598e-002
44.479	2.6609e-002	3.8029e-002	3.7572e-002	2.5187e-002
50.833	3.0658e-002	3.7343e-002	3.673e-002	2.8876e-002
57.188	3.4814e-002	3.8021e-002	3.7192e-002	3.2624e-002
63.542	3.9077e-002	3.9961e-002	3.8888e-002	3.6417e-002
69.896	4.346e-002	4.2765e-002	4.1441e-002	4.0263e-002
76.25	4.7996e-002	4.6059e-002	4.4481e-002	4.4182e-002
82.604	5.2744e-002	4.9627e-002	4.7799e-002	4.8229e-002
88.958	5.7839e-002	5.3527e-002	5.1456e-002	5.2541e-002
95.313	6.3536e-002	5.8299e-002	5.5973e-002	5.7374e-002
101.67	6.9786e-002	6.4101e-002	6.1467e-002	6.2698e-002
108.02	7.7233e-002	7.1434e-002	6.8352e-002	6.8923e-002
114.38	8.5139e-002	7.9217e-002	7.5651e-002	7.5492e-002
120.73	9.3057e-002	8.6977e-002	8.2923e-002	8.2069e-002
127.08	0.10096	9.4733e-002	9.0185e-002	8.864e-002
133.44	0.10886	0.10248	9.7454e-002	9.5306e-002
139.79	0.11688	0.11048	0.10534	0.10315
146.15	0.12648	0.12121	0.11698	0.11567
152.5	0.14873	0.1484	0.14853	0.14967
158.85	0.19836	0.20252	0.20409	0.20335
165.21	0.21235	0.21872	0.22316	0.22511
171.56	0.22087	0.22768	0.23267	0.23496
177.92	0.22878	0.23539	0.24011	0.24206
184.27	0.23668	0.24307	0.24735	0.24865
190.63	0.2446	0.25077	0.25461	0.25522
196.98	0.25252	0.25849	0.26188	0.2618

Path Length [ mm]	The directional deformation y- Axis [ mm]			
	r = 6.4 mm	r = 12.7 mm	r = 19 mm	r = 25.4 mm
203.33	0.26034	0.26622	0.26915	0.2683
209.69	0.26722	0.27289	0.27546	0.27411
216.04	0.27326	0.27834	0.28067	0.27927
222.4	0.27867	0.28276	0.28485	0.28386
228.75	0.28359	0.28668	0.28853	0.28805
235.1	0.28823	0.29052	0.29214	0.29205
241.46	0.2927	0.2944	0.2958	0.29595
247.81	0.29703	0.29832	0.29952	0.29979
254.17	0.30126	0.30227	0.3033	0.30362
260.52	0.3054	0.30627	0.30715	0.30743
266.88	0.30948	0.3103	0.31107	0.31122
273.23	0.31351	0.3144	0.31508	0.31501
279.58	0.31748	0.3186	0.3192	0.31878
285.94	0.32141	0.32296	0.3235	0.32255
292.29	0.32534	0.32665	0.32712	0.32645
298.65	0.32931	0.32862	0.32905	0.3306
305.	0.33328	0.33056	0.33096	0.33479

## **RESUME**

Tariq Salem K. Alshahbouni was born in Tripoli, Libya in 1975 where he accomplished his elementary education. He completed high school education in Grabouli High School, after that, he started the undergraduate program at Tripoli University, Department of Power Section and faculty of Engineering in 1993. In 2003, he started assignment as a Research Assistant at Tripoli University, Department of Applied Section and faculty of engineering to complete M.Sc.degree. Later, He moved to Karabük University, where he has been still working as a Ph.D. student.

In addition to his academic career, he has gained substantial experience while working for Almergeb University, Libya.

### **CONTACT INFORMATION**

Address : Karabük University

Graduate School of Natural & Applied Science

E-mail : talshahbouni@yahoo.com